Ion Mobility-Mass Spectrometry of Complex Carbohydrates

Inaugural-Dissertation

to obtain the academic degree

Doctor rerum naturalium (Dr. rer. nat.)

Submitted to the Department

of Biology, Chemistry and Pharmacy

of Freie Universität Berlin

by

Johanna Hofmann

from Berlin, Germany

2017

The work reported in this thesis was performed from November 2012 to June 2017, at the Freie Universität Berlin and the Fritz Haber Institute of the Max Planck Society in Berlin, under the supervision of Prof. Dr. Kevin Pagel.

I

Danksagung

Zu aller erst möchte ich mich bei Prof. Kevin Pagel bedanken, für all die Möglichkeiten die er mir eröffnet hat und die Überlassung dieses wunderschönen Forschungsthemas. Durch seine gute Betreuung und das Weiterreichen seines Wissens habe ich in der Zeit unglaublich viel gelernt und mehr erreicht als ich es je für möglich gehalten hätte.

Ein großer Dank geht auch an Gert von Helden, der meine Arbeit am Fritz-Haber-Institut ermöglichte und an Gerard Meijer der sie in den letzten Monaten unterstützt hat.

Prof. Christoph Schalley möchte ich für seine Tätigkeiten als Zweitgutachter danken.

Außerdem möchte ich mich bei den Leuten des Fritz-Haber-Instituts bedanken, vor allem natürlich der gesamten Abteilung Molekülphysik. Sie haben mich von Anfang an herzlich aufgenommen, mich schnell in all ihre Traditionen eingeweiht und an allen Aktivitäten beteiligt. Neben den gemeinsamen Mittagessen, diversen Filmdrehs, Weinverkostungen und der ein oder anderen Feier, war auch die wissenschaftliche Zusammenarbeit unglaublich angenehm und produktiv. Die Hilfsbereitschaft und Unterstützung von jedem einzelnen hat meine Arbeit unheimlich erleichtert und ich habe die tolle Arbeitsatmosphäre immer zu schätzen gewusst. Ich bin glücklich ein Teil dieser "Patchworkfamilie" zu sein und werde bestimmt auch in Zukunft zu dem ein oder anderen Sommerfest zu Besuch kommen.

Besonders bei den Leuten meiner Arbeitsgruppe Kevin, Gert, Alexandra, Chris, Christian, Daniel, Doo-Sik, Eike, Isabel, Jakob, Jongcheol, Leo, Mateusz, Melanie, Sebastian, Stephan und Waldemar möchte ich mich hier noch einmal besonders für die gemeinsame Zeit, die gegenseitige Unterstützung und vielen Aktivitäten bedanken. Ihr habt mich stets in den frustrierenden Phasen der Forschung aufgebaut und die erfolgreichen Momente gemeinsam mit mir gefeiert. Und auch in den letzten Wochen wart ihr jederzeit bereit noch Teile meine Arbeit zu lesen und sie mit euren Vorschläge zu verbessern. Meinen langjährigen Büromitbewohnern Waldemar und Stephan danke ich dafür, dass sie es mit mir ausgehalten haben und Stephan besonders dafür, dass er immer geduldig alle meine physikalischen und technischen Fragen beantwortet hat. Melanie möchte ich dafür danken, dass ich mich immer auf sie verlassen konnte und

sie immer ein offenes Ohr für alle Angelegenheiten hatte. Ich finde wir waren ein verdammt gutes Team und ich hätte mir zudem keinen besseren "Roomie" für die Dienstreisen vorstellen können.

Ohne meine Kooperationspartner wäre diese Arbeit nie zustande gekommen und deswegen möchte ich ihnen an dieser Stelle ebenfalls danken. Ich danke Florian Fabig, dessen Programmierkünste mir in der Anfangszeit meiner Doktorarbeit die Arbeit sehr erleichtert haben. Ich danke Prof. Peter Seeberger und seinen Mitarbeitern für die gute Zusammenarbeit und die Möglichkeit interessante synthetische Zucker untersuchen zu können. Daniel Kolarich danke ich für die Einblicke in die Welt der Glykopeptide. Besonders meinem Lieblingsprobendealer Hannes möchte ich für die tolle Zusammenarbeit danken, dass er mich stets mit neue Proben versorgt hat und immer bereit war durch weitere Experimente noch bessere Ergebnisse zu erhalten.

Furthermore, I thank Weston Struwe and David Harvey. It was fantastic to work with you and to have the possibility to absorb a little bit of your knowledge about glycans.

Unersetzbar war auch die Zusammenarbeit mit der FU Massenspektrometrie Abteilung, wobei ich insbesondere Andreas Springer danken möchte. Er hatte in Notfällen immer einen guten Rat oder die passenden Ersatzteile parat und hat ohne zu zögern jederzeit ausgeholfen.

Als letztes möchte ich die Menschen hervorheben, die mich abseits der Arbeit unterstützt haben, die mir geholfen haben auch einmal abzuschalten und neue Energie zu tanken. Ein unglaublicher Dank geht dabei an meine Mädels Esther, Jule und Yvi. Ich bin wahnsinnig froh das unsere Freundschaft nun schon so viele Jahre hält und hoffe, dass sie in Zukunft auch weiter so besteht und wir noch viel zusammen erleben. Außerdem danke ich meinen "alten" Uni-Leuten. Adlershof hat uns zusammengeschweißt und auch danach haben wir Tiefen und Höhepunkte gemeinsam erlebt. Ich habe viele schöne Erinnerungen von gemeinsamen Urlauben, Konzerten und Feiern die auch immer mit meiner Doktorandenzeit verknüpft sein werden. Auch wenn sich unsere Wege nun langsam trennen und es uns in unterschiedliche Städte verschlägt, hoffe ich das unser traditionelles Weihnachtsessen uns auch in Zukunft wieder zusammenbringt.

Als letztes möchte ich mich besonders bei meiner Familie von Herzen bedanken. Sie haben mich immer unterstützt, ermutigt diesen Weg zu gehen und dabei stets an mich geglaubt.

Zusammenfassung

Kohlenhydrate, oft auch als Glykane oder Oligosaccharide bezeichnet, sind Biomoleküle, die praktisch in allen lebenden Organismen eine wichtige Rolle spielen. Sie sind unter anderem beteiligt an der Zellerkennung, der Proteinfaltung oder der Entstehung von Krebs. Oligosaccharide bestehen aus Monosaccharid-Bausteinen, welche häufig Isomere sind und sich oft nur in der Konfiguration einzelner Kohlenstoffatome unterscheiden. Sie besitzen zudem mehrere Hydroxylgruppen, an denen glykosidische Bindungen zu weiteren Monosacchariden entstehen können. Dies kann zur Bildung von linearen sowie verzweigte Strukturen führen, welche eine komplexe Regio- und Stereochemie besitzen. Die dadurch entstehende immense strukturelle Vielfalt stellt eine große Herausforderung für fast alle Zweige der Glykowissenschaften dar.

Eine vielversprechende Methode zur Strukturanalyse von Glykanen ist die Ionenmobilitäts-Massenspektrometrie (IM-MS). Mit dieser wird sowohl das Masse-zu-Ladungs-Verhältnis (m/z) eines Ions gemessen als auch die Zeit, welche es benötigt, unter dem Einfluss eines schwachen elektrischen Feldes eine mit Inertgas gefüllte Zelle zu durchqueren. Dabei erfolgt eine Trennung der Ionen anhand ihrer Masse, Ladung, Größe und Form, welche auch die Unterscheidung von Isomeren ermöglicht. Zusätzlich kann aus einer gemessenen Driftzeit der Kollisionsquerschnitt (CCS) eines Ions berechnet werden, welcher eine Moleküleigenschaft darstellt, die universell vergleichbar ist.

In dieser Arbeit wurde das Potenzial der Ionenmobilitäts-Massenspektrometrie für die Strukturaufklärung von Kohlenhydraten untersucht. Zunächst wurden eine Reihe von N-Glykanen sowie das Polysaccharid Dextran analysiert und die CCSs ihrer intakten Ionen und Fragmente gemessen. Diese Referenzwerte konnten im Anschluss verwendet werden, um eine CCS Kalibrationsmethode für kommerziell erhältliche *traveling wave* IM-MS Instrumente zu entwickeln. Zusätzlich wurde der Einfluss des Driftgases sowie der Ladung der Ionen auf die Qualität der Kalibration betrachtet. Um das Leistungsvermögen von IM-MS zu untersuchen, wurde eine systematische Studie anhand von sechs synthetischen Oligosacchariden durchgeführt, welche alle möglichen Arten der Isomerie repräsentierten. Es zeigte sich, dass Regio- oder Stereoisomere als deprotonierte Ionen eindeutig identifiziert und getrennt werden

können. Außerdem ist die Bestimmung der relativen Konzentration eines Isomers innerhalb einer Mischung möglich.

Mit zunehmender Größe der Kohlenhydrate wird es jedoch schwieriger, kleine Strukturunterschiede zu identifizieren. In dieser Arbeit konnte gezeigt werden, dass Fragmente, welche zwei bis fünf Monosaccharide enthalten, häufig informativer sind als ihre Vorläuferionen. Dies konnte genutzt werden, um weit verbreitete Glykanmotive innerhalb von größeren Kohlenhydraten anhand von speziellen Fragmenten mit charakteristischen CCSs zu identifizieren. So konnte beispielsweise gezeigt werden, dass Blutgruppenepitope ideale Marker-Fragmente darstellen. Außerdem wurden N-Acetylneuraminsäuren, welche entweder über eine $\alpha2{\rightarrow}3$ oder $\alpha2{\rightarrow}6$ glykosidische Bindung an Glykane gebunden sind, mit diesem Ansatz identifiziert. Die beschriebene Methode lässt sich unabhängig von der Art der zu analysierenden Probe verwenden und eine Anwendung bei N-Glykanen, Milch-Oligosacchariden sowie Glykoproteinen wurde hier gezeigt.

Die Analyse mittels IM-MS ermöglicht es somit, einen dualen Datensatz aus m/z und CCS Informationen zu erstellen, welcher für jedes Molekül eine einzigartige Signatur ergibt. Dies ermöglicht eine schnelle und verlässliche Identifizierung von Glykanen. Die Daten sind zudem ideal geeignet, um in Datenbanken implementiert zu werden, und sie bilden somit die Grundlage für die zukünftige Entwicklung automatisierter Hochdurchsatz-Analysen.

Abstract

Carbohydrates, also referred to as glycans or oligosaccharides, are biomolecules that play an important role in all living organisms. They are, for example, involved in cell-cell recognition, protein folding or the development of cancer. Oligosaccharides consist of monosaccharide building blocks, which are often isomers that only differ in the stereochemistry at individual carbons. Additionally, they contain several hydroxyl groups that can be connected to other monosaccharides via the formation of a glycosidic bond. This often results in branched structures with a complex regio- and stereochemistry. The high structural diversity of glycans provides an enormous challenge for almost all areas of the glycosciences.

A promising technique for the structural investigation of carbohydrates is ion mobility-mass spectrometry (IM-MS). IM-MS measures the mass-to-charge ratio (m/z) of ions as well as the time they need to traverse a cell, filled with inert gas, under the influence of a weak electric field. Ions are separated according to their mass, charge, size, and shape, which enables the differentiation of isomers. In addition, an obtained drift time can be converted into a collision cross section (CCS), which is a molecular property that can be universally compared.

In this thesis, the potential of IM-MS for the structural analysis of glycans was investigated. First, a variety of N-glycans and the polysaccharide dextran were examined and the absolute CCSs of their intact ions and fragments reported. Subsequently, these reference values were used to establish a CCS calibration procedure for commercial traveling wave IM-MS instruments. In addition, the influence of the utilized drift gas and the ion's charge on the quality of a calibration were investigated. To assess the capability of IM-MS, a systematic study was performed using a set of six synthetic carbohydrates that represent all possible types of isomerism. It was shown that regio- and stereoisomers can be identified and separated when analyzed as deprotonated ions. Furthermore, the relative concentration of an isomer in a mixture was determined. With the increasing size of glycans it becomes exceedingly more difficult to identify small structural differences. In this thesis, it was shown that fragments, which contain two to five monosaccharides, are often more informative than their precursor ions. This can be exploited to identify common glycan motifs within larger glycans, based on characteristic fragments with unique CCSs. It was,

for example, shown that blood group epitopes can function as such marker fragments. In addition, N-acetylneuraminic acids, linked either via an $\alpha2\rightarrow3$ or $\alpha2\rightarrow6$ glycosidic bond to larger glycans, were identified using characteristic fragments. The application of this approach is independent of the type of precursor and was successfully applied to N-glycans, milk sugars and glycopeptides.

Overall, IM-MS can be used to generate dual sets of m/z and CCS information, which form unique signatures that enable a fast and accurate identification of glycans. The data are ideally suited to be implemented into databases and provide the basis for the future development of automated, high-throughput glycan analysis.

This work is based on the following publications

Estimating collision cross sections of negatively charged N-glycans using traveling wave ion mobility-mass spectrometry
J. Hofmann, W. B. Struwe, C. A. Scarff, J. H. Scrivens, D. J. Harvey, K. Pagel, *Anal. Chem.* **2014**, *86*, 10789-10795.
doi: 10.1021/ac5028353

Identification of carbohydrate anomers using ion mobility-mass spectrometry
J. Hofmann, H. S. Hahm, P. H. Seeberger, K. Pagel, *Nature* **2015**, *526*, 241-244.
doi: 10.1038/nature15388

Distinguishing N-acetylneuraminic acid linkage isomers on glycopeptides by ion mobility-mass spectrometry
H. Hinneburg, J. Hofmann, W. B. Struwe, A. Thader, F. Altmann, D. Varón Silva, P. H. Seeberger, K. Pagel, D. Kolarich, *Chem. Commun.* **2016**, *52*, 4381-4384.
doi: 10.1039/C6CC01114D

Identification of Lewis and blood group carbohydrate epitopes by ion mobility-tandem-mass spectrometry fingerprinting
J. Hofmann, A. Stuckmann, D. J. Harvey, K. Pagel, W. B. Struwe, *Anal. Chem.* **2017**, *89*, 2318-2325.
doi: 10.1021/acs.analchem.6b03853

Glycan analysis by ion mobility-mass spectrometry
J. Hofmann and K. Pagel, *Angew. Chem. Int. Ed.* **2017**, *56*, 8342-8349.
doi: 10.1002/anie.201701309

Contents

1 Introduction

When people talk about carbohydrates, they mostly discuss their diet and think about how to avoid eating too much of them. What they usually do not know is that they are surrounded by them all the time and can, luckily, never completely escape them. Carbohydrates are more than a food category that supposedly should be avoided by all means, they are foremost one of the main classes of biomolecules and have many vital functions and properties not widely known. These molecules define for example our blood groups, they are the reason we do not get directly infected by bird flu and indeed provide us with energy to get through the day. They functionalize proteins and cover most of our cells, where they regulate their interaction and communication. Researchers have unraveled many of their secrets, however, carbohydrates are still far less understood than proteins or DNA. A long time ago scientists have learned to "read" the DNA, which provides the blueprint for the synthesis of proteins.[1] For a long time DNA and proteins were considered as the most important components for understanding life. Lipids and carbohydrates were given only minor considerations and occasionally even seen as mere decorations. However, they are essential for the construction of cells and organisms, and necessary to understand biological processes.[2–6]

Scientists undertook great efforts to investigate carbohydrates, also referred to as glycans, and revealed a large variety of functions and their involvement in many processes. By the time of the 90s a new picture of the importance of carbohydrates had formed.[3] Yet, the field of glycobiology receives still less attention compared to other areas of biochemistry.

One reason for this is that conversely to proteins their biosynthesis is not directly encoded in the DNA, which makes their identification and study difficult. In addition, the molecular structure of carbohydrates is very complex and their building blocks can be connected to branched assemblies. Many glycans also possess an identical molecular formula, but differ in their chemical structures. This presents a massive challenge for the identification and differentiation of these molecules and the monitoring in biological systems. Furthermore, the complexity of carbohydrates is problematic for their chemical synthesis. Synthetic model compounds are essential to study the influence of individual molecules to biological processes, which in turn increases our

understanding of nature. This knowledge can especially be applied in medicine to improve treatment of diseases and the development of better medications or vaccines, which themselves can also be glycans. Research in this field is therefore immensely important so that in the future glycans are naturally considered as important as proteins and the DNA, outside and within the scientific community.

1.1 Motivation

The increased awareness of the importance of glycans in health, disease, and drug discovery [4,7,8] has raised the demand for better analytical methods for their characterization. The complex structure of glycans, however, makes this task one of the major challenges in current analytical chemistry. [9] Glycans consist of monosaccharide building blocks, which are often isomeric, and carry many functional groups. Unlike proteins and nucleic acids, they form complex, branched structures that can differ in their monosaccharide composition, connectivity, or configuration.

Nuclear magnetic resonance spectroscopy (NMR) [10] and X-ray crystallography are used to obtain a precise structure of individual molecules. Intrinsic limits arise, however, from sample amount and purity requirements and they are not suitable for the analysis of complex samples and high-throughput screenings. Among the most commonly used techniques for glycan analysis are mass spectrometry (MS), [11–15] capillary electrophoresis (CE), [16–19] high performance liquid chromatography (HPLC), [20] and liquid chromatography coupled to mass spectrometry (LC-MS). CE and HPLC experiments can be automated, but are time consuming and often lack in resolution to discriminate glycans in complex mixtures. In all cases, the ability to detect and analyze structural isomers still remains a problem. In general, there is no universal tool that enables a reliable routine and high-throughput analysis of synthetic and biological samples.

A technique that has the potential to overcome these limitations is ion mobility-mass spectrometry (IM-MS), a method which has the ability to separate ions according to their mass, charge, size, and shape. [21–26] This technique provides an additional identification parameter, the collision cross section (CCS), which is a molecular property independent of utilized instrument parameters. As a result, CCSs are

universally comparable values with a high potential for a faster and more reliable glycan assignment.[27,28]

1.2 Outline

This thesis is dedicated to evaluate the potential and the utility of ion mobility-mass spectrometry for carbohydrate analysis. The first part of **Chapter 2** introduces the general structure and function of carbohydrates together with nomenclatures for their representation. In the second part of that chapter an introduction to ion mobility-mass spectrometry is given.

The main parameter that is obtained from such measurements is the collision cross section (CCS), which is a molecular property that can be used to identify carbohydrates and differentiate between isomers. However, not all IM-MS instrument types are capable of measuring the CCS directly, but instead rely on a calibration procedure to provide this information. In **Chapter 3** a calibration method for traveling wave IM-MS instruments is described and a large number of carbohydrate CCS reference values is obtained. In addition, the influence of the ion's charge and utilized drift gas on the quality of a calibration are evaluated.

IM-MS is then applied in the following chapters to analyze different synthetic and biological carbohydrates. In **Chapter 4** six synthetic carbohydrate isomers are investigated to systematically examine which structural elements of carbohydrates can be differentiated. Furthermore, the limits for qualitative and quantitative separations are studied and general experimental aspects that need to be considered during an analysis are discussed.

Chapter 5 introduces the concept of fragment-based analyses. Dual information sets of CCS and m/z of intact ions and their fragments are used to generate individual molecular fingerprints. This allows a reliable and fast identification of common carbohydrate motifs.

In **Chapter 6** the by then established concepts will be applied to larger bio-molecules such as glycopeptides and -proteins. Here, different sialic acid motifs are differentiated based on the CCS of a characteristic marker fragment. Such fragments can be directly obtained from synthetic glycopeptides as well as products of a tryptic

digestion of a glycoprotein. This shows the robustness of this approach and that ion mobility-mass spectrometry is a versatile and highly valuable analytical tool.

2 Fundamentals

2.1 Carbohydrates

Carbohydrates are one of the main classes of biomacromolecules and are essential for a variety of biological processes. Historically the term carbohydrates evolved because many molecules of this class possess the formula $(CH_2O)_n$ and were thus believed to be hydrates of carbons. Today, this class also contains molecules that deviate from this form such as molecules containing additional elements and carbohydrate derivatives (Figure 2.1). This includes among others deoxysaccharides such as 2-deoxyribose, which is part of the DNA, amines or sialic acids, which are acidic sugars containing nine carbon atoms. Thus, other terms such as saccharides or glycans arose, which are generally used synonymously today. Saccharides are often divided according to their size into either oligosaccharides, to describe molecules containing up to nine monosaccharides, or polysaccharides, starting with ten monosaccharides.

β-Galactose   β-N-Acetylglucosamine   β-2-Deoxyribose   α-N-Acetylneuraminic Acid
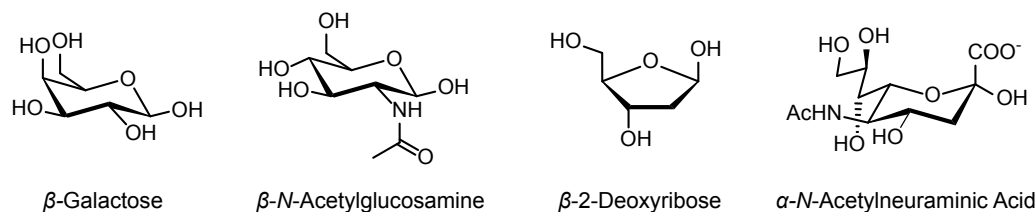
Figure 2.1: Examples of monosaccharides. The hexose galactose is a classic representative of the chemical formular $(CH_2O)_n$ ($n = 6$). *N*-acetlyglucosamine (GlcNAc), 2-desoxyribose and *N*-acetylneuraminic acid (NeuAc, a representative of the sialic acid family) are further examples of common and fundamental carbohydrate building blocks in nature.

Glycans are defined as compounds "consisting of a large number of monosaccharide residues joined to each other by glycosidic linkages".[29] Monosaccharides can be categorized by the number of containing carbon atoms, for example tetroses, pentoses and hexoses contain four, five and six carbons, respectively. In addition, each class comprises a variety of different molecules, which only differ in the arrangement of the hydroxyl groups. In the case of $C_6H_{12}O_6$ already 16 possible isomers exist including glucose (Glc), mannose (Man) and galactose (Gal), when just aldoses are considered.

Furthermore, all monosaccharides exist in a variety of configurations. For example, each saccharide has a mirror image (enantiomers), which for carbohydrates are termed

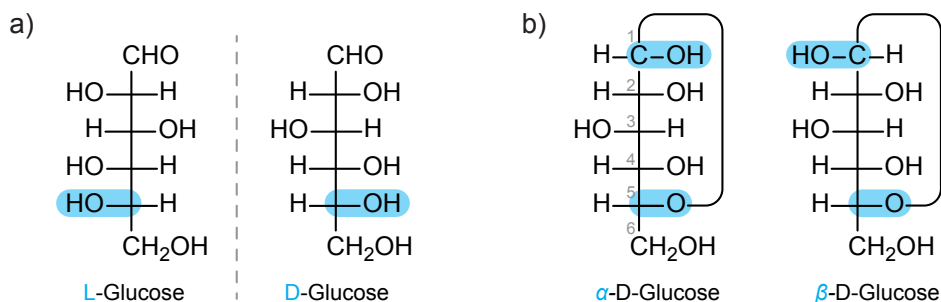**Figure 2.2:** Configurations of monosaccharides shown for glucose in the Fischer projection. a) L- and D-glucose are mirror images and are defined based on the orientation of the hydroxyl group at the penultimate carbon, depending on whether it is displayed on the left or right side, respectively. b) The configuration of a monosaccharide is determined by the orientation of hydroxyl group at the anomeric carbon (C1) compared to an oxygen of a reference carbon (here C5). The α-anomer is present if they are *cis*, the β-anomer if they are *trans* to each other.

L- and D-configurations (Figure 2.2a). The terminology results from monosaccharides written in the Fischer projection. Here, the carbon with the highest oxidation state is written on the top, whereas the longest carbon chain follows below in a vertical line. The position of the hydroxyl group at the penultimate carbon defines if a L- or D-configuration is present, depending on whether it is situated on the right or left side of the carbon, respectively. In solution monosaccharides are predominantly present in a ring structure. Here, the just mentioned hydroxyl group at the penultimate carbon forms a bond with the C1 atom. As the C1 carbon is prochiral, the formation of the ring results in a new stereocenter, the so called anomeric center. This gives rise to two possible configuration, called anomers, (Figure 2.2b) labeled with α and β. In the α anomer, the hydroxyl group of the anomeric carbon is *cis* compared to the oxygen at a reference atom (Figure 2.2b).[29] If these groups are *trans* to each other the β-anomer is present.[29]

This already provides a first glimpse into the immense structural variety of carbohydrates, but becomes even more prominent when oligosaccharides are considered. The general structure of glycans is probably best described by their composition, connectivity and configuration (Figure 2.3). The composition of a carbohydrate is defined by the identity of its individual monosaccharide building blocks. As previously mentioned these building blocks are often stereoisomers that differ only in the stereochemistry at one particular carbon atom (Figure 2.3 I).
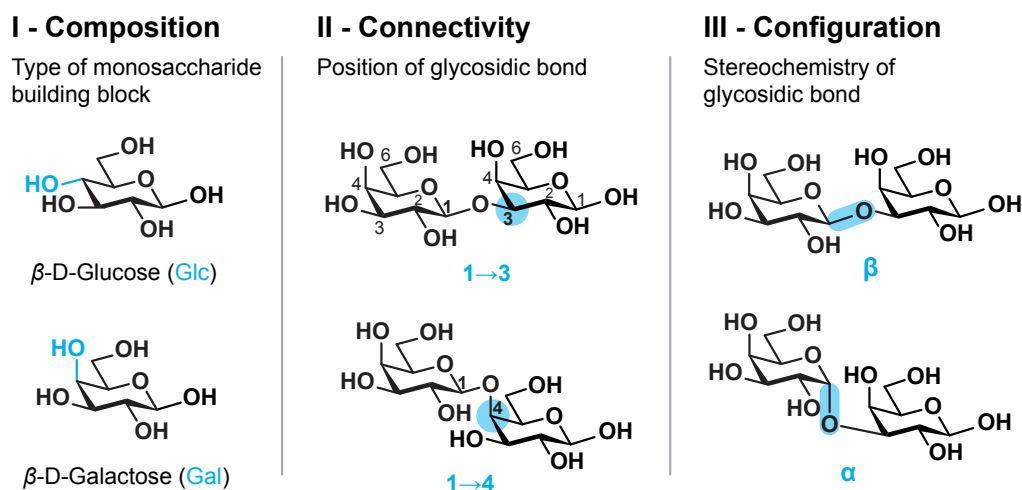
I - Composition

Type of monosaccharide
building block

β-D-Glucose (Glc)

β-D-Galactose (Gal)

II - Connectivity

Position of glycosidic bond

1→3

1→4

III - Configuration

Stereochemistry of
glycosidic bond

β

α

Figure 2.3: Structural features of carbohydrates. The composition (I) of a carbohydrate is defined by its monosaccharides. Monosaccharide building blocks are often isomers, as shown for glucose (Glc) and galactose (Gal), which differ only in their C4 stereochemistry. Because of the many possible functional groups, the formation of a new glycosidic bond can occur at several positions, resulting in different connectivities (II), such as those shown here. Each glycosidic linkage is a new stereocenter that can have either *α*- or *β*-configuration (III).

Each monosaccharide contains multiple hydroxyl groups and the position at which two monosaccharides are linked by a glycosidic bond determines their connectivity. Thus, unlike oligonucleotides and proteins, carbohydrates are not necessarily linear, but can be branched with a diverse regiochemistry (Figure 2.3 II). When a glycosidic bond is formed, the anomeric center can adopt an *α*- or *β*-configuration (Figure 2.3 III). It is noteworthy that in monosaccharides or at the reducing end of an oligosaccharide an equilibrium between the open chain and ring form exists and thus equilibrium between the configurations. However, once a glycoside is formed, the configuration at the anomeric carbon is fixed.

2.1.1 Symbol Nomenclature for Glycans

The immense structural diversity of carbohydrates represents one of the greatest challenges for almost all aspects of the glycosciences. They also have consequences for how glycans can be depicted. Using the precise chemical structure is certainly the most accurate way, however, minute structural differences can be easily overlooked, and for larger, more complex glycans this is often not practical. To solve this problem,

shorter notations were developed by individual scientific groups. Until the 1970s mostly three or one letter abbreviations were used for the monosaccharides that were connected by lines to indicate connectivities. In 1978 Kornfeld et al. were the first to represent monosaccharides with symbols in order to be able to draw complex glycans, and write biosynthetic pathways and chemical reaction mechanism in a concise way.[30] It further provided a distinction from the one-letter code used for amino acids, which was developed in the 60s and approved by IUPAC in 1968.[31] However, for carbohydrates there was no agreement to a uniform system and many scientific groups developed their own notations.

The first proposal for a standardized nomenclature for glycans was introduced 1999 in the book *Essentials of Glycobiology* and further refined in its second edition 2009.[32,33] This system was adopted by an increasing amount of scientist over the following years including those of the Consortium for Functional Glycomics (CFG), an international research initiative. Their support and involvement in the dissemination of the system is also the reason why it is commonly referred to as CFG notation.

In parallel, scientists from the University of Oxford proposed an alternative nomenclature (UOXF) which only uses black and white symbols, the so called UOXF notation.[34] While today color Figures are a standard for journals and are used in every form of digital presentation, this nomenclature also allows an easy drawing of structures by hand, independent of colour. In addition, they proposed an elegant way to incorporate the regio- and stereochemistry of glycosidic bonds. Different connectivities can be shown depending on the angle of the line which links the monosaccaride symbols. The configuration is further indicated by the type of the lines. An alpha anomericity is indicated by using a solid line, and a dashed line represents a beta anomericity.

To reach a consensus, groups of leading scientists in the field worked towards the introduction of a uniform system for the representation of carbohydrates. In 2015 the symbol nomenclature for glycans (SNFG) was presented.[33] Here, the widely distributed symbols of the CFG nomenclature were combined with the notation of the glycosidic bonds of the UOXF nomenclature (Figure 2.4). Although this system is still not able to represent all glycans, such as cyclic structures or non-reducing
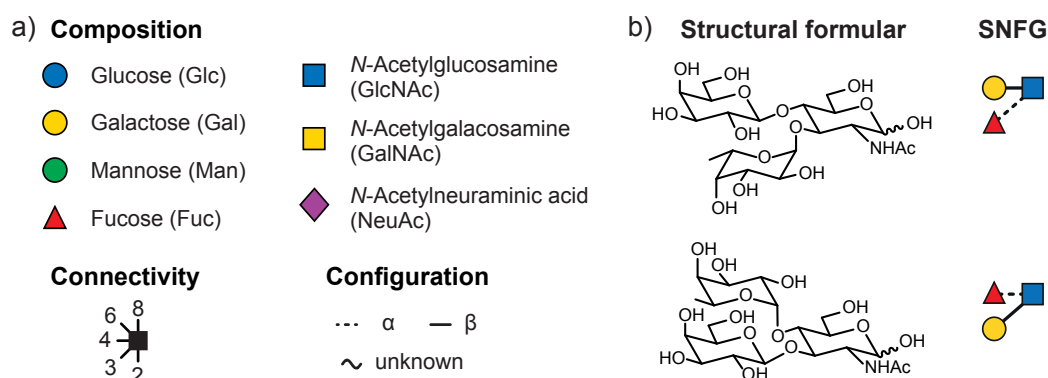
Figure 2.4: Symbol nomenclature for glycans (SNFG). a) To depict glycans in a simplified manner the SNFG was established. Monosaccharides are illustrated using symbols, whereas the glycosidic bond regio- and stereochemistry is described by the angle and type of the connecting line, respectively. b) Example how oligosaccharides can be depicted using the SNFG system in a concise and clear way.

saccharides, it is an important step towards establishing a common language for the presentation of carbohydrates as it was achieved for other scientific areas.

To follow these standards, the SNFG is used throughout this thesis to represent glycan structures.

2.1.2 Biological Roles of Glycans

Glycans play vital roles in virtually all living organisms and their functions are as diverse as their structures.[3–6] They exist as either free molecules or as glycoconjugates, connected to proteins or lipids. An example for the former are milk oligosaccharides, which are usually composed of two to ten monosaccharides and, next to lipids and proteins, are a main component in milk. They are important for nutrition, postnatal brain development and development of the immune system of infants, and as such of high interest for medicine and food formulation.[35,36] Also larger polysaccharides exist, which are best known to function as structural components in plants. In addition, they act as signal molecules that are involved in cellular processes such as plant growth and development or defense against pathogens.[37,38]

Most glycans, however, are present in the form of glycoconjugates.[6] The main classes found in or on eukaryotic cells are shown in Figure 2.5 and include glycosphingolipids, proteoglycans and glycoproteins.[2] The attachment of glycans to proteins is
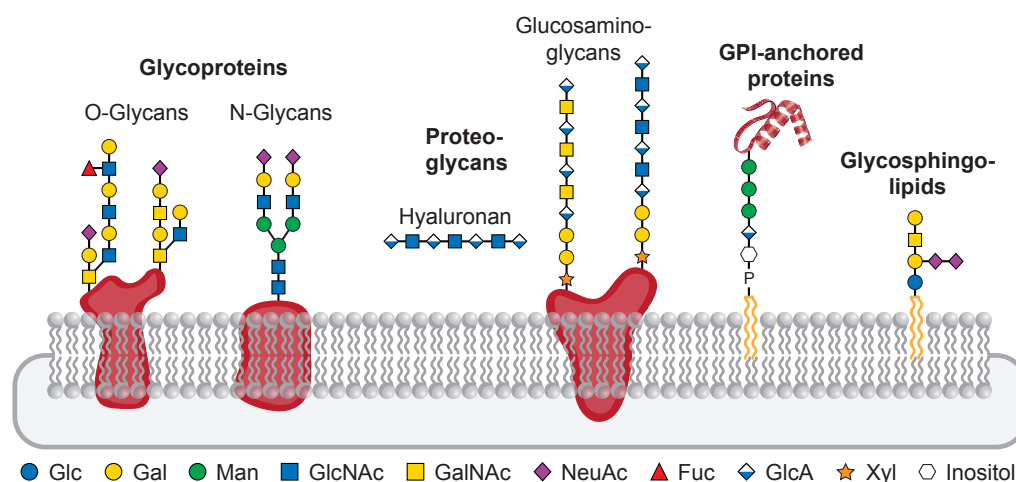
9

Figure 2.5: Schematic representation of common glycans and glycoconjugate classes. Glycoconjugates can be found as part of cellular membranes or be present in cells and the extracellular matrix. Glycans are depicted using the symbols of the SNFG, however, their regio- and steochemistry is not indicated for the sake of simplicity.

the most common form of post-translational protein modification, where they among others influence protein folding and are involved in degradation mechanisms.[7] Due to their high relevance, especially as main analytical targets addressed in this thesis, they will be discussed in more detail in Chapter 2.1.3.

A special form of glycoproteins are proteoglycans. They contain long chained glycosaminoglycans (GAGs) that are connected via xylose (Xyl) to a serine side chain of a protein (Figure 2.5). These GAGs are built up of repeating disaccharide motifs consisting of an aminosaccharide, and a uronic acid or galactose. The roles of proteoglycans range from mechanical functions to regulation of cell processes and the involvement in cell development and specification.[2,39,40] Hyaluronan, also known as hyaluronic acid, is structurally similar, however, exists as a free molecule. It is involved in cell development and migration, plays a role in wound healing and has a high hydrodynamic volume, which influences water movement.[2,41,42] Due to these properties it is also widely used in cosmetic products.

Another interesting group of glycoconjugates are glycosylphosphatidylinositol (GPI) anchors. They are glycolipids that are post-translational modifications of proteins and allow an "attachement" to cell membranes.[43,44] All GPI contain a tetrasaccharide core, which contains several modifications, and is attached to a

phosphatidylinositol lipid that differs in the length and degree of saturation of the attached fatty acids.[45] The glycan is connected to the protein, whereas the lipid domain can insert into the phospholipid bilayer of a membrane and thus anchors the protein. A specialty of this linker is its resistance towards most proteases and lipases, which ensures a stable connection of the protein to the membrane.[44] The function of GPIs, however, go beyond just linking a protein to a cell surface. There is evidence that the glycan part influences the folding and function of the attached protein.[46] Nevertheless, several properties and structure-functions-relationships of GPI anchors are still not fully understood.[44,47]

In general, the presence of glycans on the surface of cells result in their involvement in many cell recognition and cell-cell communication processes[48,49] that are essential for the function of multicellular organisms.[2] The glycans allow intrinsic and extrinsic recognition and can either function as shield against degradation and pathogens or act as their recognition site. Thus, they play major roles in several diseases and the immune response.[3–5,8,50] A prominent example is the human immunodeficiency virus (HIV), which has an envelop glycoprotein (Env) that is involved in the binding mechanism to host cells. About 50% of its mass results from glycans, which, beside ensuring a correct protein folding, shield the underlying protein from antibody recognition.[51,52] As such they can be targets for antibodies and are of interest for the development of HIV vaccines.[53] Similarly, the avian influenza A (bird flue) virus contains the surface protein hemagglutinin that specifically binds to a glycan motif consisting of a terminal sialic acid link via an $\alpha2{\to}3$ glycosidic bond. Because the sialic acid motif present on most human cell membranes are different ($\alpha2{\to}6$ linked sialic acids) the virus cannot infect humans.[8]

2.1.3 N- and O-Glycans

The attachment of oligosaccharides to proteins is the most common form of protein post-translational modification and can occur on the side chains of amino acids. They are categorized into N-glycans, linked to the amine group of asparagine, and O-glycans, which are connected to the hydroxyl group of either serine or threonine. N-Glycosylations can only occur when a protein contains the sequence motif Asn-X-Ser/Thr (X$\neq$Pro). N-Glycans have a core of $Man_3GlcNAc_2$ to which further
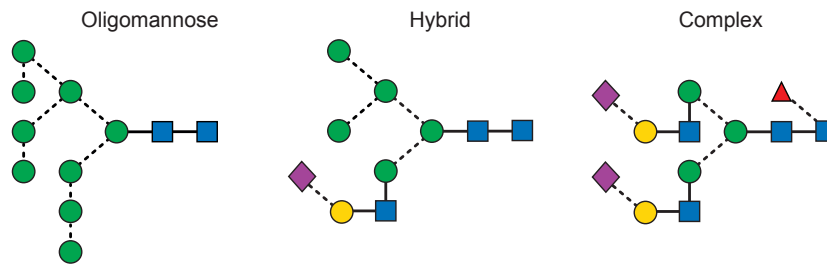
Figure 2.6: Types of N-glycans. N-Glycans are divided into three subtypes called oligomannose, hybrid and complex type, depending on the monosaccharides attached to the common $Man_3GlcNAc_2$ core.

monosaccharides are attached.[2,9] This divides them into the oligomannose, complex and hybrid type as shown in Figure 2.6. Glycans of the complex and hybrid type can also contain a *bisecting* GlcNAc, which is attached via a $\beta1{\rightarrow}4$ glycosidic bond to the central β-Man of the core.

The biosynthesis of N-glycans takes place in the endoplasmic reticulum (ER) and the Golgi (Figure 2.7). It starts with the synthesis of a $Glc_3Man_9GlcNAc_2$ glycan precursor from which all N-glycans originate, that is synthesized at the ER and then transferred to a protein.[4,8] Subsequently, a stepwise processing, in both the ER and Golgi, leads to the formation of the different glycan types (Figure 2.7). In the first steps, the glucose units are removed and the resulting glycans mediate the folding of the protein.[7,54] Afterwards, a mannose is cleaved from the central glycan arm and the glycoprotein is checked for misfolding. This results in the protein either becoming a target for degradation or being further transported to the Golgi.[55] In the *cis*-Golgi, further mannose residues are trimmed to generate different oligomannose glycans and additional modifications result in hybrid- and complex-type glycans.[2] Maturing of the glycans in the *trans*-Golgi gives rise to the final diverse structures.

O-Glycans on the other hand are structurally more diverse than N-glycans. The most prevalent types in eukaryotes are so called mucin O-glycans, which feature a GalNAc as the first building block that is attached to the serine or threonine side chain via an α-glycosidic bond.[56] Mucins are glycoproteins, which are are found in mucous secretions and in body fluids, that contain a very high number of these O-glycans.[2] However, mucin-type glycans also occur on other glycoproteins.
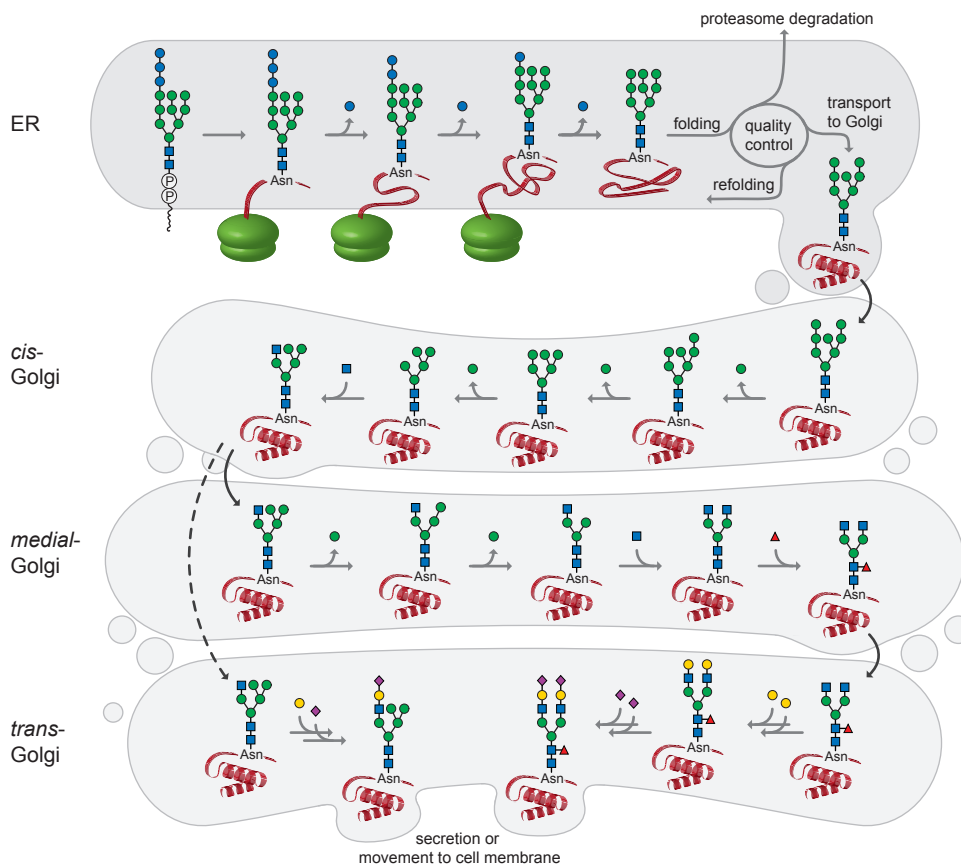
Figure 2.7: Scheme of the biosynthesis of N-glycans. The N-glycan $Glc_3Man_9GlcNAc_2$ precursor is synthesized in the ER and subsequently transferred to a protein during its synthesis. Afterwards, glucose and mannose units are stepwise removed enzymatically, which results in glycans that mediate the folding protein. The fully folded glycoprotein is then transferred to the Golgi, where the maturing of the oligosaccharides gives rise to a large variety of different N-glycans. Glycans are depicted using the symbols of the SNFG, however, their regio- and steochemistry is not indicated for the sake of simplicity.

There are eight different core structures known for mucin-type O-glycans (Figure 2.8).[2,9] These cores can then contain further monosaccharide modifications, repeating N-acetyllactosamine units (Gal-α-(1→4)-GlcNAc) and epitopes, of which the most common are presented in Figure 2.8.[2,57] Among them are the blood group epitopes, which as the name indicates are a main factor in the classification of blood groups.[57] The blood groups were first classified in 1900 by Karl Landsteiner, but it was not until the 1950s that it was discovered that the antigens consisted of carbohydrates.[57–59] Since then they are probably one of the most studied carbo-
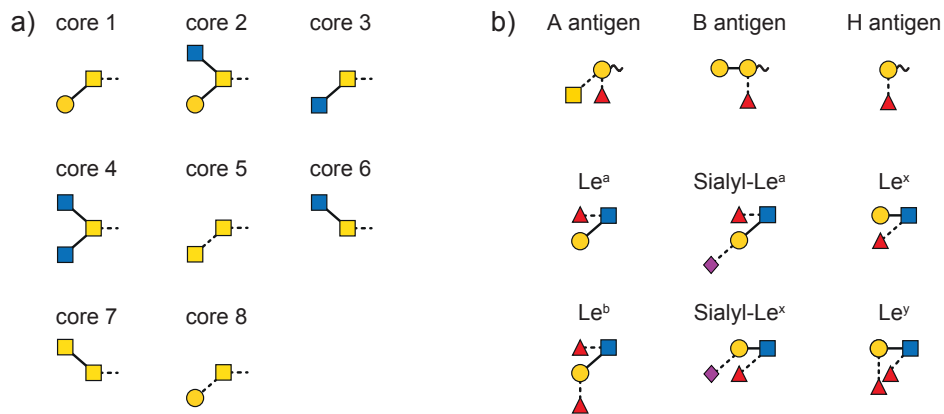
Figure 2.8: Structural features of O-glycans. a) Eight different core structures are reported for mucin O-glycans. b) Antigens of the ABO and Lewis (Le) blood group families are common structures found in O- and N-glycans.

hydrates due to their high relevance for blood transfusions and transplantation. In the early years, the antigens A and B were identified, leading to the groups A, B, AB, and O where either antigen A, B, both, or neither are present, respectively. But it soon turned out that blood group O contained a precursor of A and B the so called antigen H (Figure 2.8).[58] Another important set of structurally related antigens belong to the Lewis blood group family.[2] Blood group antigens are not only relevant for transfusion but are also associated with cancer.[60–69] In general, ABO and Lewis antigens are terminal modification on glycoproteins and glycolipids, which are predominantly present on the surface of red blood cells, but can also be found on tissue cells or in secreted forms.[2] The only exception are Le^y and Le^x which are only found on epithelial cells.[67] These antigen systems are also the focus of the investigations presented in Chapter 5 (page 59).

The biosynthesis of O-glycans occurs entirely on the fully folded protein as post-translational event within the Golgi.[2,4,70] In contrast to N-glycans, O-glycans are synthesized sequentially on the protein and the biosynthesis starts with the transfer of a GalNAc building block. This step can be performed by several polypeptide-*N*-acetyl-galactosaminyltransferases (ppGalNAcT) which differ depending on the cell type and peptide that is to be glycosylated.[71] Further synthesis of the core and terminal structures follow stepwise by the corresponding enzymes. Overall, the

biosynthesis is a highly regulated process that depends on the expression and activity of the glycosyltransferases as well as the acceptor specificity. [2,71,72]

The complexity of protein glycosylations is not only a result of the diverse glycan structures, but also stems from the fact that the same protein can show differences in the coverage of glycans. The presence of a potential glycosylation site does not necessarily result in the actual presence of a glycan. This presence or absence of glycans leads to a macroheterogeneity of a glycoprotein. In addition, one glycosylation site can feature different glycans, which defines the microheterogeneity of glycoproteins. Changes in the glycan occupancy or the type of attached glycans often indicates different disease states or are used as markers for the diagnosis for several diseases such as cancer. [60–69,73–75]

2.2 Carbohydrate Analysis

Owing to the branched structure of glycans and the presence of stereogenic centers at each anomeric carbon, carbohydrates are harder to characterize than proteins and oligonucleotides. [47] In addition, the synthesis of glycans is non-template derived and therefore no structural information can be obtained by genome sequencing. However, it was possible to identify enzymes and their genes, that are involved in glycan biosynthesis and degradation processes. Today, a variety of human and bacterial glycosidases and glycosyltransferases are known. [2] Because these enzymes are encoded in the DNA they can be produced by recombinant protein expression in cells and are a valuable tool to investigate glycans.

Endoglycosidases are able to release glycans from glycoconjugates. One of the most commonly used endoglycosidases is peptide-*N*-glycosidase F (PNGase F), which releases N-glycans by cleaving the glycosidic bond between the core GlcNAc and the asparagine of a glycoprotein. Exoglycosidases on the other hand cleave individual terminal monosaccharides specifically linked to glycans. A sequential treatment of a sample with different exoglycosidases can be used to determine the glycan sequence and the monosaccharide connectivity. [76] The drawbacks of this approach are that it is extremely time consuming, expensive, and strongly dependent on the availability of the required enzymes. [77] In addition, some types of glycans cannot be cleaved enzymatically, which is a particular problem for O-glycans. Therefore, chemical

reactions are often employed. Hydrazinolysis is used to release N-glycans, whereas β-eliminations are performed to cleave O-glycans from glycoconjugates.[2,77,78] Nevertheless, the release of O-glycans remains difficult, because the chemical reagents are not specific and can induce N-glycan release as well as unwanted glycan degradation.[78,79]

For the detection of glycans a variety of tools are available from biotechnology and instrumental analytics. It can for example be performed by using either simple staining approaches or specific antibodies or lectins (glycan-binding proteins).[2,77] The latter are used in methods such as microarray analysis, where antibodies or lectins that are immobilized on a surface can bind glycans or glycoconjugates. Their detection is subsequently carried out by using fluorescent tags that are either attached to the glycans themselves or to a second antibody or lectin that again can bind to the now immobilized carbohydrates.[77]

For the structural analysis of glycans, mostly the methods and instrumentation of proteomics and genomics are available. However, the unique structural and physical properties of carbohydrates do not necessarily allow a direct method transfer. Nuclear magnetic resonance (NMR)[10] spectroscopy is used to obtain detailed structural information, including the anomeric configurations within a glycan. Though, the analysis is time consuming, requires large amounts of sample and is neither suitable for the analysis of complex samples nor for high-throughput screenings. Instrumentation using capillary electrophoresis (CE)[16–19] and high-performance liquid chromatography (HPLC)[20,80,81] are currently the methods of choice for glycan profiling. They are capable of separating complex glycan and glycoconjugate samples and in some cases can even differentiate between isomers. Classical reversed-phase HPLC separation can be employed to analyze glycopeptides, but is not suitable for native, underivatized glycans, because of their high polarity. Instead, ion exchange chromatography, porous graphitized carbon (PGC) chromatography and hydrophilic interaction liquid chromatography (HILIC) are the preferred methods.[77,82,83]

HILIC is a variant of normal-phase chromatography and features a polar stationary phase that is coated with a thin water layer. For the mobile phase usually aqueous acetonitrile solutions are used as eluents with high percentages of the organic solvent. The separation of the analytes is predominantly based on the molecules partition

between the liquid stationary phase and the eluent. In addition, dipole-dipole and electrostatic interactions may contribute to the separation. [83] As a result high contents of organic solvent lead to increased retention times of glycans.

The subsequent detection of glycans after CE or HPLC separation is typically performed by either mass spectrometry (MS) or fluorescence detection. For the latter, the glycans need to be derivatized with fluorescence labels, [84] because they contain no natural fluorophore. In some cases the addition of markers can also have a positive effect on other analytical aspects such as an improved separation or a higher ionization efficiency in the case of MS analysis. [77,83] CE and HPLC offer a high-throughput capability, but are time consuming and often lack resolution to discriminate glycans in complex mixtures. More importantly, the ability to detect and analyze structural isomers still remains a major problem in all cases.

2.2.1 Mass Spectrometry of Glycans

Mass spectrometry based techniques are amongst the most widely utilized tools in glycan analysis. [11–15,85–87] It is not only used in hyphenated techniques, but is also as standalone method for the structural elucidation of glycans. However, the frequent presence of isomers, which naturally have identical masses, presents a great challenge for structural analyses. MS fragmentation techniques are regularly applied in MS workflows to obtain more information about an investigated molecule by studying its fragment ions.

To better assign carbohydrate fragments Domon and Costello introduced a nomenclature in 1988. [88] The glycan fragment annotation is based on a nomenclature used for peptides, where letters indicate the position of the cleaved bond. The fragments are thereby classified in two series, depending on whether the charge remains on a fragment containing the reducing end (X, Y, Z) or the terminal end (A, B, C) of the glycan. Cleavages of the glycosidic bonds are indicated using the letters B, C, Y, and Z, whereas cross-ring fragments are labeled with A and X (Figure 2.9). To specify the exact type of cross-ring fragment, the numbers of the broken bonds (red number in Figure 2.9) are indicated as superscript numbers prior to the letter. The monosaccharide building block at which the individual cleavage occurs is additionally assigned with a subscript number after the letter. It is counted
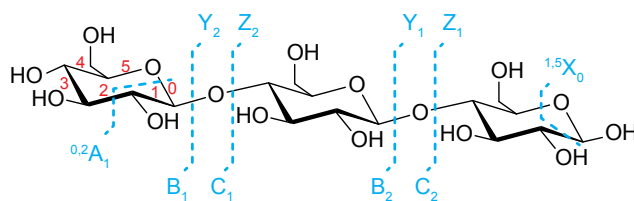
Figure 2.9: Fragmentation nomenclature for glycans according to Domon and Costello. [88] Fragments containing the reducing end are labeled X, Y, Z depending on the position of the cleavage. Fragments containing the terminal end are assigned with the letters A, B, C. Subscript numbers indicate the monosaccharide building block at which the individual cleavage occurs, counted from the terminal end of the glycan for ABC fragments and from the reducing end for XYZ fragments. The bonds within a ring that are cleaved during a cross-ring fragmentation are indicated in red and are written in superscript prior to the letter.

from the terminal end of the glycan for ABC fragments and from the reducing end for XYZ fragments.

To differentiate between peptide and oligosaccharide fragments, small and capital letters are used, respectively. This is especially important for the analysis of glycopeptides, where cleavages at the glycan and the peptide can occur. In this context, it is of great advantage that different MS fragmentation techniques provide complementary information. Collision-induced dissociation (CID) for example predominantly produces glycan fragments, whereas high-energy collisional dissociation (HCD) and electron transfer dissociation (ETD) can be applied to fragment the peptide backbone. [81,89]

In addition, the ion mode has an influence on the observed glycan fragments. For CID, which is exclusively used for the experiments in this thesis, it has been shown that negative ions yield highly informative fragmentation spectra. [87,90–94] In positive-ion mode mainly glycosidic bonds are cleaved, whereas a multitude of cross-ring cleavages are observed when negatively charged ions are analyzed. [90–93,95] The latter often provide more structural information of a carbohydrate and can be used to determine the regiochemistry and branching of oligosaccharides. In this regard, it is assumed that the charge carrier and the charge location have an influence on the formation of different fragments. [95] When positively charged glycan-metal-adducts, such as sodium adducts, are investigated the charge is localized at the metal ion, which does not especially promote cross-ring fragmentation. Instead, the formation

of fragments follows the general CID mechanism, where conversion of kinetic energy to internal energy occurs resulting in the cleavage of the weakest bonds. Therefore, cleavages of the glycosidic bonds are the preferred fragmentation pathway. Fragments of protonated molecules are presumed to result from ions where the additional proton is located at the glycosidic bond,[88] which facilitates a cleavage at this position. It is also reported that protonated ions fragment more easily and less cross-ring fragments are observed compared to metal adducts supporting the previous assumption.[95,96]

For negatively charged adduct ions, such as halogens, the first fragmentation pathway is always the loss of the corresponding acid. This results in the formation of the deprotonated ion, which then further dissociates.[90,91] Thus the fragment spectra of deprotonated carbohydrate ions and ion adducts are often very similar.[90,91] Deprotonations can occur at any of several hydroxyl groups of a carbohydrate. Recently, *ab initio* molecular dynamics simulations showed that such a deprotonation site migrates within a glycan molecule and is not localized.[97] Consequently, fragmentation is more likely to occur at different positions of the molecule, which increases the probability of the formation of different cross-ring fragments.

Even when sophisticated tandem MS[93,98,99] or MS^n [11,13] techniques are used, it is often not possible to fully disentangle the structure of a given glycan. A widely used approach to improve the structural assignment is the derivatization of glycans, for example by permethylation.[13,94,100–102] This allows an easier assignment of fragments and determination of the monosaccharide sequence. However, it also requires an additional sample preparation step, which might not be feasible if only small sample amounts are available.[95]

Overall, there is currently no universal method that answers every analytical question for glycans. In general, there is a lack of fundamental tools, which enable a reliable routine and high-throughput analysis of synthetic and biological samples.

2.3   Ion Mobility-Mass Spectrometry

To overcome the above mentioned limitations, an additional gas-phase separation step can be added using ion mobility spectrometry (IMS).[21,22,25,103–105] In IMS ions traverse a cell, filled with an inert neutral buffer gas, under the influence of an electric field, where they are separated according to their mobility (Figure 2.10). Compact
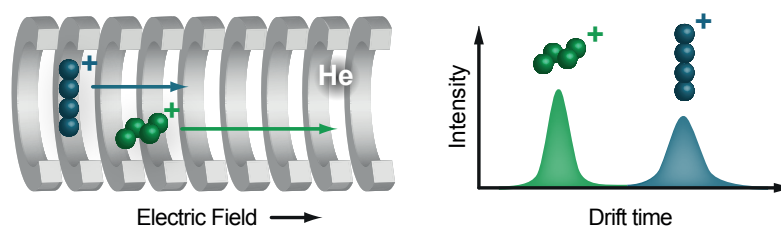
Figure 2.10: Scheme of an ion mobility separation. Ions travel through a drift cell, filled with inert neutral gas, guided by a weak electric field. The time ions need to traverse the cell is dependent on the amount of collisions with the drift gas, which is influenced by the ion's mass, charge and shape. Thus isomers with the same m/z but different structure can be separated.

ions interact less with the drift gas molecules than more extended ions and therefore traverse the cell faster. This principle allows to differentiate molecules with identical mass and charge, but different structure.

Already around 1900 the first ion mobility experiments were performed and the basic principles behind IMS were theoretically described by Langevin.[103,106] A classic instrument consists of an ionization source, a drift tube (DT) cell, to which a constant, weak electric field is applied and a detector. Since many decades now ion mobility is used as a standalone techniques predominantly to detect small molecules such as explosives or drugs. The compact design of most instruments make them portable and versatile in their application. Today, IMS is used for example by the military for the detection of chemical warfare agents, is routinely applied in airport security and can also be used for medical purposes such as breath analysis.[103,107,108]

In the 1960s and 1970s the first coupled ion mobility and mass spectrometry instruments (IM-MS) were built that provided a better detection and identification of mobility separated ions.[103,106] The coupling of these methods is facilitated, because both gas-phase techniques use similar instrumentation and operate on compatible time scales. An IMS separation takes place in milliseconds, whereas mass spectra can be recorded within micro- to nanoseconds. Thus, many mass spectra can be recorded within one ion mobility separation cycle.

The development of soft ionization techniques such as electrospray ionization (ESI) and matrix-assisted laser desorption/ionization (MALDI) in the 80s, enabled the extension of gas-phase analysis techniques to a wide range of molecules. This paved the way for the developed of modern IM-MS instruments by several groups in

the 90s and its application to all classes of biomolecules. [21,22,109–113] The sample and time requirements of IM-MS are similar to those of a conventional mass spectrometry experiment, so that the additional separation and drift time information is obtained at no extra cost. The drift times of ions that are measured in an IM-MS experiment are dependent on a variety of instrument parameters similar to retention times obtained in liquid chromatography. However, drift times can be converted into an instrument-independent parameter, the so called collision cross section (CCS).

2.3.1 Collision Cross Section

The collision cross section of an ion is related to its conformation and describes the rotationally-averaged area that can collide with a drift gas molecule. It is thus a molecular property only dependent on the shape of the ion and the utilized drift gas. Therefore, the CCS is an ideal identification parameter, because it can be universally compared. In addition, CCSs can be calculated theoretically from structural candidates using established techniques. [109,114,115]

In general, the motion of an ion through a buffer gas can be described theoretically when a constant, weak electric field is considered, as in the case of drift tube IMS. The electric field is termed *weak*, if the directed motion of an ion, induced by the electric field, is slower than its thermal motion. [116,117] Under these conditions, and at constant temperature (T) and pressure (p), the ion velocity (v) is constant and can be determined by measuring the time (t) the ion needs to traverse an IMS cell with length L. Furthermore, the velocity is directly proportional to the ion's mobility (K) and the applied electric field (E).

$$v = \frac{L}{t} = KE \tag{1}$$

The mobility K is usually normalized for standard pressure P_0 and temperature T_0

$$K_0 = \frac{P}{P_0}\frac{T_0}{T}K \tag{2}$$

21

and used to calculate the absolute CCS (Ω) using the Mason-Schamp[116,117] equation

$$\Omega = \frac{3q}{16N}\sqrt{\frac{2\pi}{\mu k_B T}}\frac{1}{K_0},\tag{3}$$

where $q = ez$ is the total charge of the ion, N the drift gas number density, μ the reduced mass of the ion and the drift gas, k_B the Boltzmann constant, and T the temperature.

To determine a CCS from an IM-MS experiment, the temperature, the drift cell pressure and the drift time of an ion need to be measured. The measured drift time t_D consists thereby of two parts

$$t_D = t + t_0,\tag{4}$$

where t is the time needed by the ion to traverse the IMS cell and t_0 being an offset resulting from the time the ion needs from the exit of the IMS cell to the detector. t_0 cannot be determined directly, however, applying eq. 1, eq. 4 can be written as

$$t_D = \frac{L}{KE} + t_0.\tag{5}$$

The resulting linear equation shows that the drift time is proportional to the inverse mobility $(1/K)$ as well as the inverse electric field $(1/E)$. The electric field is further defined by $E = V_d/L$, where V_d is the drift voltage applied to the ion mobility cell:

$$t_D = \underbrace{\frac{L^2}{K}}_{slope}\frac{1}{V_d} + \underbrace{t_0}_{intercept}.\tag{6}$$

The drift time of an ion can be measured at different drift voltages and plotted according to eq. 6 as shown in Figure 2.11. From the slope of the resulting linear regression the mobility K is determined, which in turn is used to calculate the CCS using eq. 2 and eq. 3.

There are several parameters that influence the quality of an ion mobility separation. The main factors are the type of used buffer gas and its pressure, the applied electric field, the temperature, and the length of the drift region. Different
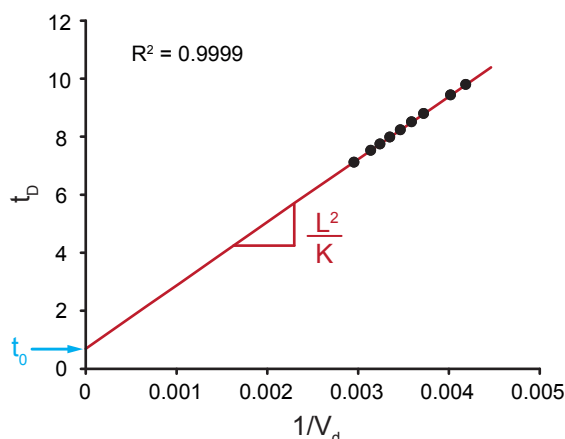
Figure 2.11: Determination of the mobility K of an ion from drift tube measurements. The drift time t_D is plotted against the inverse drift voltage V_d. The resulting linear regressing follows eq. 6 and can be used to obtain the mobility K from the slope.

buffer gases have been used, which differ in their mass and polarizability.[118–121] The most commonly used drift gases are nitrogen and helium. Nitrogen is a cheap gas that provides very good ion separation and is thus used in most commercial instruments. In addition, its larger polarizability compared to helium can lead to charge-induced dipole interactions with the ions, which can be relevant especially for small molecules.[122] On the other hand, experiments that are performed using helium buffer gas are typically used for comparisons to theoretical calculations. Helium can be easily described and is consequently the preferred choice to calculate theoretical CCSs.

An increase of the drift gas pressure from a couple of millibars to atmospheric pressure significantly improves IM resolution, as shown for example by the Hill group.[123] Thereby, increased drift voltages are applied to facilitate the ion transmission through the cell, which additionally improves a separation. However, the low electric field conditions should not be exceeded and higher voltages also increase the probability of electric discharges. Decreasing of the temperature is of high value for several reasons. On the one hand, an increased ion mobility resolution can be achieved and on the other hand low energy conformers can be investigated, which is of special interest for example for proteins. An experimental realization, however, is difficult because water condensation needs to be avoided. Recently a first IMS design was presented, which enables measurements at temperatures between 150 to 520 K.[124] Lastly, increasing the length of the drift region can be utilized to obtain better IMS separations. Clemmer and co-workers for example extended the length of

the IM cell up to three meters.[22] The limiting factors are hereby the loss in intensity due to reduced transmission and spatial limits. The former can be reduces by the addition of focusing funnels, while the latter can be circumvented by using designs such as the cyclotron IM-MS.[22,125]

2.3.2 Types of Ion Mobility-Mass Spectrometry Instruments

Through the years, a variety of IM-MS instruments were developed, which also include different designs of the ion mobility cells. Besides the drift tube (DT) technology several other ion mobility types exist, which mainly differ in the nature of the electric field that is used to propel the ions through the IM cell (Figure 2.12), namely: differential ion mobility (DIMS),[126,127] high-field asymmetric wave form ion mobility spectrometry (FAIMS),[128,129] traveling wave (TW),[130–132] and trapped ion mobility spectrometry (TIMS).[133–135]

In FAIMS ions move with a gas flow between two electrodes to which alternating high and low electric fields are perpendicularly applied (Figure 2.12b). At high and low electric fields ions have different mobilities and the difference between both is used to guide ions through the drift cell. The ions oscillate between the electrodes, but only move on a stable trajectory at defined conditions, which allows them to reach the detector. By varying a compensation voltage different ions are guided through the cell and can thus be analyzed separately.[128,129] FAIMS was one of the first commercially available techniques and has the advantage that it can be easily coupled to existing MS instruments. However, it does not provide CCS information and can only be used for qualitative sample separations.

A related design is used in differential ion mobility (DIMS) (Figure 2.12c), where ions are separated based on their spatial displacement. While the ions are carried by a fast gas flow an electric field is orthogonally applied, which transmits ions of a defined mobility into an outlet slit leading to the detector or mass spectrometer.[126,127] Scanning a range of voltages again leads to the transmission of different ions.

In contrast to DT instruments in TW IMS a non-uniform electric field is utilized. The IM cell consists thereby of ring electrodes to which a direct current potential is superimposed on the confining radio-frequency of an electrode and then transferring it to the adjacent electrodes (Figure 2.12d). This creates a traveling wave that
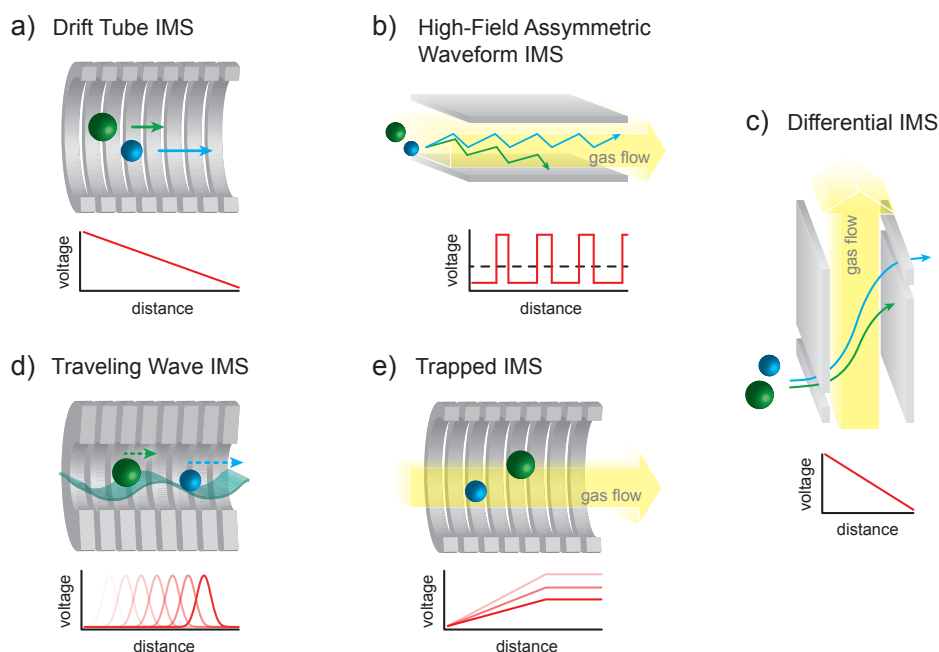
Figure 2.12: Scheme of different types of ion mobility cells and their separation principle. The ion mobility cells of a) drift tube IMS (DT IMS), b) high-field asymmetric wave form ion mobility spectrometry (FAIMS), c) differential IMS (DIMS), d) traveling wave IMS (TW IMS), e) trapped IMS (TIMS) and the potential diagrams of the utilized electric fields are schematically shown.

transports the ions through the IM cell.[130,132] The complex motion that ions undergo in TW IMS results in a better separation, so that TW cells with a length of about 20 cm show a similar resolution to a 80 cm long DT cell. A disadvantage of this technique is that it no longer allows a direct measurement of CCSs, because the theoretical correlation between drift time and CCS is not yet understood. However, it is possible to calibrate the instruments with reference substances of known CCS values to estimate a CCS.[136–139] An instrument that uses this technique is the so-called Synapt (Waters Corporation), which became commercially available in 2006 (Figure 2.13).[131,140] For a long time TW instruments were the only commercially available IM-MS instruments that were able to provide CCS information. In 2014 two DT instruments became available.[26,141]

Another technique, which became commercially available very recently in 2016, is trapped IMS (TIMS) (Figure 2.12e).[133–135] Here, ions are guided with a gas flow through an IM cell to which an increasing axial electric field gradient is applied,
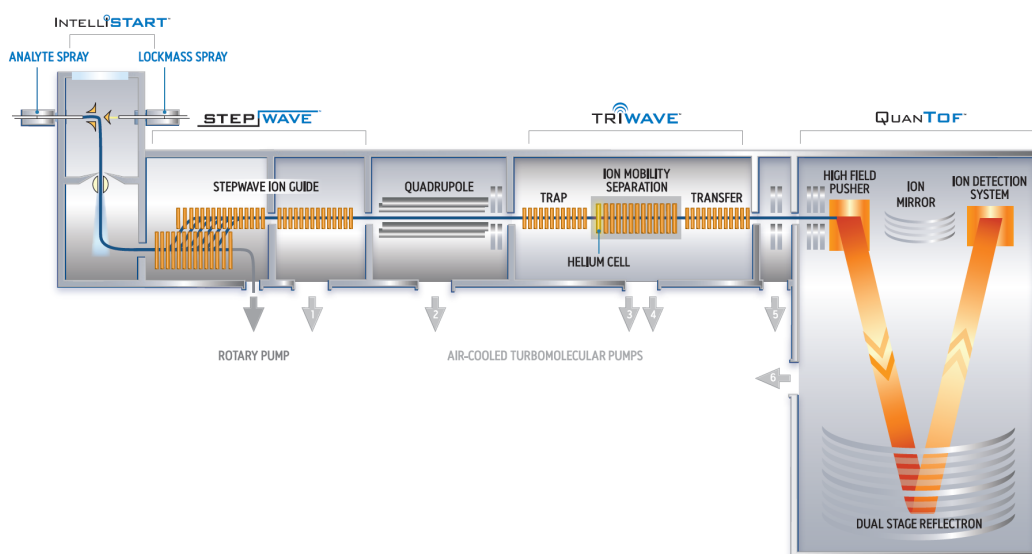
Figure 2.13: Schematic setup of a Waters Synapt G2-S traveling wave ion mobility-mass spectrometer. Illustration provided by Waters Corporation.

which traps the ions along the cell. Ions of different mobility are thus separated and held stationary against the gas flow. By lowering the strength of the applied electric field trapped ions can be gradually released and analyzed. [133–135] This technique enables high mobility resolutions because the trap time can be varied and an increase leads to a better separation of the molecules. Also for this technique a calibration procedure needs to be applied to obtain CCSs.

In this thesis, a commercial traveling wave Synapt G2-S (Waters, Manchester) instrument is mainly used for the investigations (Figure 2.13). [131,140] The instrument is equipped with a nano-electrospray ionization source (nESI) that produces the ions. nESI is a soft ionization technique that allows the intact transfer of fragile biomolecules and non-covalent complexes into the gas phase. [142] In this thesis an offline source is utilized, where the sample is ionized from metal coated glass capillaries. [143,144] The opening of the needle is about 1-10 µm in diameter and natural flow rates of 20 nL/min and lower are achieved by applying a high voltage. This has the advantage that only very small sample amounts are required for a measurement, which is of essence for the analysis of biological substances. In addition, sample
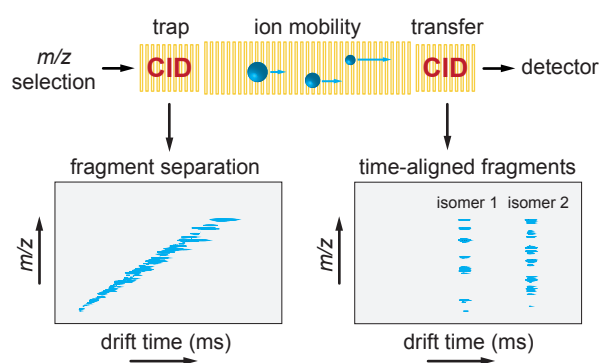
Figure 2.14: Scheme of the different fragmentation modes of a TW IM-MS instrument. CID of m/z selected ions can occur either before the IM cell in the trap cell or afterward in the transfer cell. Trap fragmentation allows to separate fragments and obtain their CCS. Transfer fragmentation produces time-aligned fragments, which can be assigned to their precursor, as shown for two isomers.

cross contamination is avoided, conversely to approaches that use capillaries and syringes, because a new needle is used for each analysis. After ionization the ions are transported to a step-wave ion guide where they are guided in an s-shaped motion further into the instrument. This separates them from remaining neutral particles, which increases the signal-to-noise ratio of the later recorded spectra. Afterwards, the ions are guided through a quadrupole, where they can be separated according to their m/z, towards a set of three collision cells. This so-called tri-wave contains the ion mobility cell and a trap and transfer cell, which are located before and after the IM cell, respectively. As the name already indicates the ions are trapped in the trap cell and then pulsed into the IM cell, where the separation according to their mobility takes place. The IM cell is usually filled with nitrogen buffer gas at about 3 mbar. To allow an easy transfer of ions from the high vacuum stages at the beginning of the instrument to the medium vacuum of the ion mobility cell an additional small helium cell is located prior to the IM cell. This leads to an increased transmission and prevents fragmentation of the ions. Following the mobility separation the ions are guided through the transfer cell to the adjacent time-of-flight analyzer where they are detected.

A unique feature of this instrument is that CID fragmentation of m/z selected ions can be performed in the trap and transfer region (Figure 2.14). Fragments produced in the trap cell are separated in the IM cell and thus their CCSs can be obtained. Fragmentation after the ion mobility cell produces fragments with aligned drift times with respect to their precursor. This can be useful to assign fragments to isomers that have different drift times.

Overall, IM-MS is a fast and sensitive technique that provides information about the mass, charge and shape of ions. In addition, the gas-phase environment allows the isolation and investigation of ions with a specific m/z even in complex mixtures. The additional CCS information is thereby obtained without any additional cost regarding time or sample consumption.

2.4   Ion Mobility-Mass Spectrometry of Carbohydrates

IM-MS is especially interesting for the field of glycomics, because isomers are regularly observed, and several analytical challenges remain. The first IM-MS experiments on carbohydrates were performed in the late 1990s using home-built DT instruments.[111,112] Using a series of small oligosaccharides it was demonstrated for the first time that isomers can exhibit different drift times, which enable their differentiation. However, after these proof-of-principle experiments, it took several years until glycans were investigated more systematically. In 2003, Gabryelski and Froese were the first to look at different isomeric oligosaccharide mixtures using FAIMS.[145] In particular, disaccharides differing in their regio- or stereochemistry or exhibiting site-specific derivatizations were analyzed. The data revealed that isomeric mixtures can be separated in positive as well as negative-ion mode and that the attachment of different ions can significantly influence the quality of the separation. The first promising results and the introduction of commercial instruments[131] fueled the interest in using IM-MS more systematically for oligosaccharide analysis. Several studies reported different examples of carbohydrate analyses, but few of them went beyond the proof-of-principle level and were instead often focused on technical aspects.[22–24,123,125,146–152]

The true potential of IM-MS for glycan analysis remained therefore unclear. Very few examples for glycobiological applications and no universal approaches and workflows existed.

3 Calibration of Traveling Wave Ion Mobility Instruments[*]

3.1 Introduction

Traveling wave (TW) IM-MS became readily available in 2006 [131] with the introduction of commercial instrumentation. In the following years it was applied to study small molecules as well as large intact protein complexes. [103,153,154] However, due to the non-uniform electric field utilized in TW IM-MS, it is not possible to directly obtain absolute CCSs from recorded drift times. Nevertheless, it has been demonstrated by several groups that the estimation of CCSs is possible using calibration approaches. [136,137,155,156] In this context, a careful choice of calibrants was shown to be essential for a successful CCS estimation. Generally, the best results are obtained when calibrants of the same molecular identity as the analytes and with comparable charge states are used.

Since there were only limited amounts of CCS reference data available for complex carbohydrates, [26,148] Pagel and Harvey reported an extensive set of CCSs for positively charged, sodiated N-glycans released from commercially available glycoproteins. [139] To complement these experiments, the investigations were extended to include negatively charged glycans, and the results are presented in this chapter. These data are of special interest for carbohydrate analysis via IM-MS because it has been shown that negative ions yield highly informative fragmentation spectra. [90–93] Compared to positive-ion mode, where mainly glycosidic bonds are cleaved upon collision-induced dissociation (CID), a multitude of cross-ring cleavages are observed when negatively charged ions are used. Those ions often provide more detailed information on the underlying structure of a carbohydrate and can, therefore, help to unambiguously identify and assign a particular structure. Additionally, it is investigated whether dextran, a readily available carbohydrate polymer that is used widely as a reference substance in chromatography, can also be used as a calibrant

---

[*]This chapter is based on the publication "Estimating collision cross sections of negatively charged N-glycans using traveling wave ion mobility-mass spectrometry" J. Hofmann, W. B. Struwe, C. A. Scarff, J. H. Scrivens, D. J. Harvey, K. Pagel, *Anal. Chem.* **2014**, *86*, 10789-10795, http://dx.doi.org/10.1021/ac5028353. Figures and content adapted with permission. Copyright 2014 American Chemical Society.

for CCS estimations on TW IM-MS instruments. Furthermore, the influence of the ion charge and the use of reference data from different drift gases is evaluated.

To differentiate between CCSs measured on DT instruments and CCSs obtained from a calibration, they are referred to as *absolute* and *estimated* CCSs, respectively, throughout this thesis. Furthermore, the type of CCS values are written in the form of $^{\text{technique}}\text{CCS}_{\text{driftgas}}$ in which the utilized technique and drift gas used to obtain a CCS is indicated. For example $^{\text{DT}}\text{CCS}_{\text{He}}$ values were obtained from a DT instrument using helium as a drift gas, whereas $^{\text{TW}}\text{CCS}_{\text{He}}$ values result from a TW instrument which was calibrated using helium reference values. Theoretical values can in principle also be indicated using this nomenclature by either using general abbreviations such as "calc" or by naming the exact type of method used for the calculation: projection approximation (PA),[109] exact hard-sphere scattering (EHSS)[114] or trajectory method (TJ).[115]

3.2 Experimental Details

N-Linked glycans were released by hydrazinolysis[157,158] from the well-characterized glycoproteins ribonuclease B,[159] bovine fetuin,[160] porcine thyroglobulin,[161,162] and chicken ovalbumin[163,164] obtained from Sigma Chemical Co. Ltd. (Poole, Dorset, U.K.). Subsequently, the glycans were re-N-acetylated using acetic anhydride in saturated $NaHCO_3$ and stored at -20 °C until required. Sialic acids were removed from the thyroglobulin and fetuin samples by heating with 1 % acetic acid for 1 h at 70 °C. For the purpose of distinguishing the samples, the original samples will be further refer to as *sialylated* whereas the samples with additional sialic acid cleavage will be called *desialylated*. The samples were dissolved in water/methanol (1:1, *v/v*) at about 1 mg/mL with the addition of 0.5 M ammonium phosphate to form stable adducts that mimic those normally found in biological samples. In this context it is important to mention that other solvents were not assessed systematically here. Therefore, it cannot be fully excluded that other solvent mixtures may lead to slightly altered CCSs.

Dextran from *Leuconostoc mesenteroides* was purchased from Fluka and Sigma-Aldrich (two fractions: MW = 1000 and MW = 5000) and used without further purification. Dextran samples were analyzed individually at a concentration of

0.1 mg/mL with 1 mM NaH_2PO_4 or as a mixture consisting of 0.1 mg/mL dextran1000, 0.5 mg/mL dextran5000, and 1 mM NaH_2PO_4 in water/methanol (1:1, *v/v*).

Absolute CCSs

Measurements of absolute ^{DT}CCSs were performed with a modified Synapt G1 HDMS (Waters Co., Manchester, U.K.) instrument, described previously.[137,139] Here, the TW ion mobility cell was replaced by an rf-confining drift tube allowing the determination of absolute CCSs in both helium and nitrogen buffer gas. Typically, 5 µL of sample was ionized using a nano-electrospray source (nESI) from platinum-palladium-coated borosilicate capillaries prepared in-house.[143]

Settings for N-glycan and dextran measurements were: capillary voltage, 1.0-1.5 kV; sample cone, 50 V, extractor cone, 10 V; cone gas, 40 L/h; trap collision voltage, 10 V; trap DC bias, 25 V; IMS drift voltage, 50-150 V; backing pressure, 2-3 mbar; trap pressure, 5.2×10^{-2} mbar (He), 2.6×10^{-2} mbar (N_2); ion mobility gas, He or N_2; ion mobility cell pressure, 3.5 mbar (He), 0.87 mbar (N_2); time-of-flight analyzer pressure, 1.8-2.2$\times 10^{-6}$ mbar.

Data were processed using MassLynx software (Version 4.1, Waters, Manchester, UK) and OriginPro 8.5 (OriginLab Corporation, Northampton). In addition a python script (written by Florian Fabig) was used to extract the arrival-time distributions (ATDs) of the relevant signals and to determine the drift times by fitting the ATDs with a Gauss distribution function. Each sample was measured twice at eight different drift voltages (50, 55, 60, 70, 80, 100, 125, and 150 V). Absolute CCSs were determined using the procedure described in Chapter 2.3.1, (page 21) and are presented in the Appendix (Table 7.1-7.6, page 107 *ff.*). The reported CCSs represent the averages of two replicates acquired in independent measurements and the corresponding error results from their relative standard deviation.

Estimated CCSs

Estimated ^{TW}CCSs were obtained from measurements on a traveling wave quadrupole/IMS/oa-ToF MS instrument, Synapt G2-S HDMS (Waters Corporation, Manchester, U.K.) using a previously described protocol.[137–139] Here again, sam-

ples were ionized from in-house-prepared platinum-palladium-coated borosilicate capillaries using nESI.

Typical instrument settings were: capillary voltage, 0.8-1.0 kV; sample cone, 125 V; source offset, 100 V, source temperature, 60 °C; trap collision voltage, 50 V; trap collision voltage, 2 V; helium cell gas flow, 180 mL/min; IMS gas flow, 90 mL/min; wave velocity, 500, 550, 600, 650, and 700 m/s; wave height, 40 V; backing pressure, 3.8 mbar; trap pressure, 2.3×10^{-2} mbar; ion mobility gas, N_2; ion mobility cell pressure, 3.4 mbar; time-of-flight analyzer pressure, 1.1×10^{-6} mbar. The instrument was mass-calibrated using a solution of caesium iodide (100 mg/mL) and the data were processed with MassLynx 4.1 software (Waters, Manchester, UK). ATDs of the relevant signals were manually extracted from raw data using DriftScope and MassLynx and fitted with a Gaussian distribution function using OriginPro 8.5.

For the calibration, a calibrant sample with known CCSs was measured under the same conditions as the analyte samples. Measured drift times (t_D) were corrected for m/z dependent delay time in the instrument

$$t'_D = t_D - c\sqrt{m/z} \tag{7}$$

with c being an empirically determined instrument constant ($c = 0.001 \times$ *EDC delay coefficient*). Furthermore, absolute CCSs ($^{DT}CCSs$) of the calibrants were corrected for charge and the reduced mass of the ion and the drift gas.

$$^{DT}CCS' = \frac{^{DT}CCS}{z}\sqrt{\frac{1}{m_{ion}} + \frac{1}{m_{gas}}} \tag{8}$$

The plot of $ln(^{DT}CCS')$ against $ln(t'_D)$ can be fitted with a linear regression

$$\ln(^{DT}CCS') = x\ln(t'_D) + \ln A \tag{9}$$

with x being the slope and lnA the intercept, and used as a calibration curve as shown in Figure 3.1.

To obtain an estimated CCS from a measured drift time of an analyte eq. 10 is used, which is obtained by substituting $^{DT}CCS'$ in eq. 9 with eq. 8 and solving it for ^{DT}CCS (^{DT}CCS now replaced with ^{TW}CCS). The values for x and A are
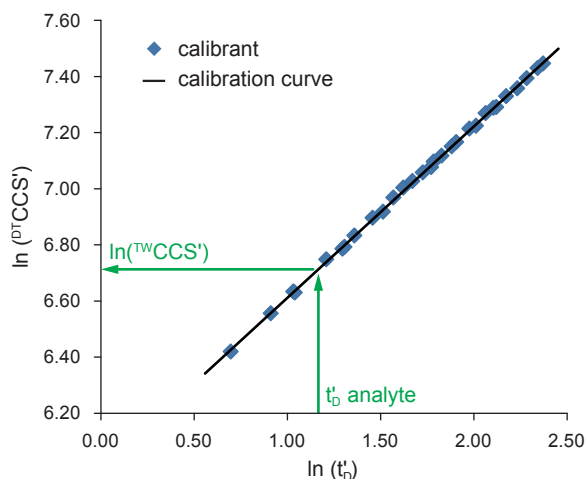
Figure 3.1: Exemplary calibration curve used to obtain estimated CCSs (^{TW}CCS). Calibrants are measured on a TW instrument and their drift times (t_D) corrected for their m/z dependent flight time. A logarithmic plot of their corrected known CCS ($^{DT}CCS'$) against corrected drift time (t'_D) can be fitted with a linear regression and used to estimate CCSs from the drift time of analytes.

ontained from the calibration curve.

$$^{TW}CCS = A \cdot z \cdot (t'_D)^x \sqrt{\frac{1}{m_{ion}} + \frac{1}{m_{gas}}} \qquad (10)$$

Absolute ^{DT}CCSs measured in nitrogen or helium drift gas are used to estimate N$_2$ and pseudo-He ^{TW}CCSs from data measurements in nitrogen, respectively. To estimate CCSs, each sample was measured at five wave velocities on a Synapt G2-S instrument. For each wave velocity one calibration curve was generated, and the resulting five estimated CCSs of one ion were averaged with a typical standard deviation of 1 %.

3.3 Results and Discussion

3.3.1 N-Glycans

Four different N-glycan mixtures that were released from the commercially available glycoproteins ribonuclease B, fetuin, thyroglobulin, and ovalbumin were analyzed by IM-MS in the negative-ion mode using helium and then nitrogen as the drift gas. On ribonuclease B, typically high mannose structures are populated. Thyroglobulin carries both high mannose and complex glycans, whereas fetuin mainly carries sialylated complex-type glycans. Ovalbumin provides the most diverse carbohydrate sample with high mannose and complex and hybrid-type glycan structures.[4,9]
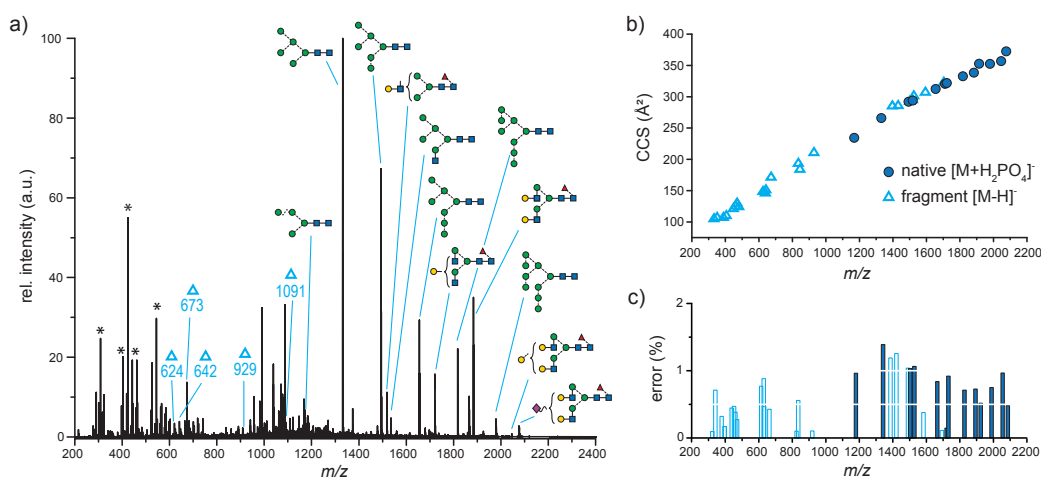
Figure 3.2: IM-MS data of desialylated glycans released from thyroglobulin. a) Mass spectrum of the glycan sample at in-source activation conditions measured at a Synapt G2-S. The most abundant singly charged fragments are labeled with triangles, and the structures of the native glycans are depicted using the SNFG.[33] The asterisks indicate background signals resulting from polydimethylsiloxane. b) Absolute helium CCSs (obtained from measurements on a modified Synapt G1) of the native glycans as phosphate adducts (circle) and the deprotonated fragments (triangle) for all singly charged ions. The corresponding relative errors c) do not exceed 2 %.

A typical mass spectrum of the glycans released from thyroglobulin is shown in Figure 3.2a. In order to simultaneously acquire data for the intact glycans as well as their fragments, spectra were recorded at in-source fragmentation conditions with an increased cone voltage between 50 and 150 V. As a result, the signals cover a broad m/z and CCSs range within one single measurement. In order to exclude that these rather harsh conditions influence the CCSs of the investigated molecules or their fragments, the arrival-time distributions (ATDs) of selected species were monitored at increasing trap collision energy after isolation in the quadruple. No significant changes in drift time were observed, which indicates that no or only minor rearrangements take place before dissociation. Besides the signals corresponding to the intact, native glycans, which (due to the added phosphate) mainly occur as phosphate adducts, a large variety of deprotonated fragment ions were observed, which are a result of glycosidic bond or cross-ring cleavages. This observation is in good agreement with previous MS/MS measurements of these glycans in negative ion polarity, which yielded a characteristic mixture of glycosidic bond and cross-ring cleavages.[90–92] For all identified peaks, ^{DT}CCSs were determined for the two drift

gases helium and nitrogen (see Table 7.2 in the Appendix, page 107). Parts b and c of Figure 3.2 show the helium CCSs and their corresponding relative errors of the singly charged ions obtained from the thyroglobulin sample. As apparent from the data, a m/z range from 332 to 2076 and a CCS range from 105 to 372 Å^2 for helium and 170 to 462 Å^2 for nitrogen is covered for the singly-charged ions. The average CCS errors observed, rarely exceed 2 %, which is the expected error associated with these measurements. In total, more than 450 ^{DT}CCSs of native glycans and their fragments were determined from the four investigated N-glycan samples (see Appendix, page 107 *ff.*).

3.3.2 Calibration with Dextran

Although N-glycans released from commercially available glycoproteins have been shown to be good calibrants in previous investigations, their spectra can be quite complex and difficult to interpret. In addition, the cleavage and sample preparation procedure for these glycans can be time-consuming, and a complete removal of protein is often difficult, resulting in additional peptide signals in the mass spectrum. Therefore, the next step was to assess whether partially hydrolyzed polysaccharides can potentially be used to simplify the calibration procedure.[165] In particular, dextran, a well-defined carbohydrate polymer consisting of $\alpha1{\rightarrow}6$-linked glucose units, was chosen as a potential calibrant. Dextran is widely used as a carbohydrate calibration standard in chromatographic experiments where a so-called dextran ladder is used to convert carbohydrate retention times into comparable glucose unit (GU) values.[20] Consequently, partially hydrolyzed dextran fractions of varying length are likely to be already available in the majority of glycomics laboratories.

Generally, the MS spectra of dextran in positive and negative-ion mode are easy to interpret and provide well-distributed signals in an m/z range similar to those of the N-glycan mixtures (Figure 3.3). In positive-ion mode mainly sodiated ions are observed, whereas the most dominant signals in negative ion polarity are phosphate adducts (when phosphate is added as in this study), deprotonated molecules, and the ^{0,4}A$_x$ fragment [M‑120‑H]$^-$, which was previously characterized by Čmelík et al.[166] The corresponding absolute CCSs of these ions and their respective errors were measured using the modified Synapt G1 instrument and are shown in Figure 3.3
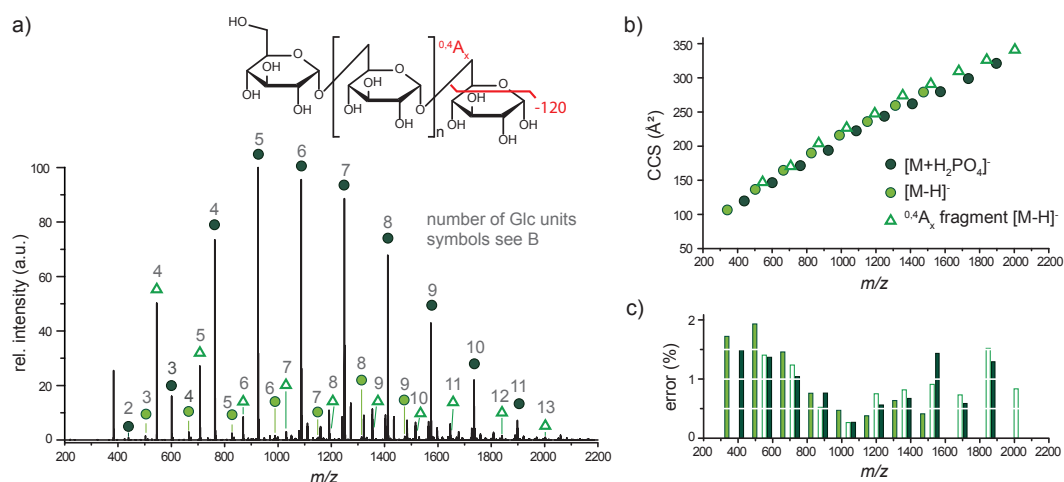
Figure 3.3: IM-MS data of partially hydrolyzed dextran. a) Mass spectrum of dextran measured in negative-ion mode on a Synapt G2-S. All singly charged ions are labeled according to their type and number of glucose units with dark green circles indicating phosphate adducts, light green circles being deprotonated species, and triangles representing fragment ions. The structure of dextran is shown, and the cleavage site of the most prominent cross-ring fragment $^{0,4}A_x$ $[M_n\text{-}120]^-$ is indicated in red. b) The corresponding absolute helium CCSs obtained from measurements on a modified Synapt G1 and c) their associated relative errors. The covered CCS range and the errors are similar to those of N-glycans.

and Table 3.1 (for full table see Table 7.5 and 7.6 in the Appentix, page 112 *ff.*). The covered CCS range for singly charged ions in the negative-ion mode is 106-341 Å^2 for helium and 174-429 Å^2 for nitrogen and therefore is comparable to those of the above-described N-glycans. Moreover, for dextran, far more doubly charged ions were observed, covering a m/z range of 596-2082 and a helium CCS range of 239-531 Å^2, which is much larger compared to N-glycans. For thyroglobulin, for example, only signals in the m/z range from 780 to 1183 (doubly charged) are observed with helium CCSs between 274 and 374 Å^2.

3.3.3 CCS Estimation

The utility of the reported ^{DT}CCS values for a CCS estimation was assessed by performing test calibrations on a Synapt G2-S (TW IM-MS), using a previously described procedure.[137,139,155] To do so, one carbohydrate mixture was used as a calibrant, whereas the other samples were treated as "unknown". This approach

Table 3.1: Helium and nitrogen ^{DT}CCSs of dextran (Glc$_n$). n = number of glucose units of the respective ions; RSTD = relative standard deviation of two or three independent measurements in percent.

n	He CCS in Å^2 ($\pm$ RSTD)			N$_2$ CCS in Å^2 ($\pm$ RSTD)		
	[M - H]$^-$	[M + H$_2$PO$_4$]$^-$	[M + Na]$^+$	[M - H]$^-$	[M + H$_2$PO$_4$]$^-$	[M + Na]$^+$
2	106.6 $\pm$ 1.7 %	119.6 $\pm$ 1.5 %	104.1 $\pm$ 0.3 %	174.6 $\pm$ 0.2 %	182.6 $\pm$ 0.1 %	179.5 $\pm$ 0.0 %
3	136.6 $\pm$ 1.9 %	146.4 $\pm$ 1.4 %	137.1 $\pm$ 1.1 %	202.3 $\pm$ 0.0 %	212.2 $\pm$ 0.2 %	215.0 $\pm$ 0.0 %
4	164.5 $\pm$ 1.5 %	171.5 $\pm$ 1.0 %	165.1 $\pm$ 0.8 %	233.9 $\pm$ 0.2 %	243.8 $\pm$ 0.6 %	243.4 $\pm$ 0.2 %
5	189.9 $\pm$ 0.8 %	193.8 $\pm$ 0.8 %	194.0 $\pm$ 0.8 %	265.4 $\pm$ 0.5 %	271.2 $\pm$ 0.3 %	273.8 $\pm$ 0.3 %
6	215.9 $\pm$ 0.5 %	222.4 $\pm$ 0.3 %	218.9 $\pm$ 0.7 %	296.7 $\pm$ 0.3 %	304.8 $\pm$ 0.2 %	302.1 $\pm$ 0.2 %
7	235.9 $\pm$ 0.4 %	243.7 $\pm$ 0.6 %	243.9 $\pm$ 0.7 %	319.2 $\pm$ 0.3 %	327.9 $\pm$ 0.3 %	330.9 $\pm$ 0.1 %
8	259.6 $\pm$ 0.6 %	262.0 $\pm$ 0.7 %	266.2 $\pm$ 0.6 %	343.6 $\pm$ 0.4 %	347.8 $\pm$ 0.4 %	355.8 $\pm$ 0.0 %
9	279.1 $\pm$ 0.4 %	279.6 $\pm$ 1.4 %	286.0 $\pm$ 0.4 %	365.2 $\pm$ 0.0 %	365.9 $\pm$ 0.1 %	377.1 $\pm$ 0.0 %
10		298.8 $\pm$ 0.6 %	305.9 $\pm$ 0.4 %		386.5 $\pm$ 0.1 %	397.8 $\pm$ 0.7 %
11		321.1 $\pm$ 1.3 %	318.0 $\pm$ 0.4 %		408.7 $\pm$ 0.1 %	412.6 $\pm$ 1.2 %
12			334.8 $\pm$ 0.6 %			425.5 $\pm$ 1.4 %

allows a direct comparison of the obtained estimated ^{TW}CCSs with the absolute ^{DT}CCSs reported above.

As shown previously for the calibration in positive-ion mode, one glycan sample usually provides enough signals to achieve a calibration of sufficient quality.[139] This trend is also observed here, and in principle, all reported glycan samples can serve as calibrants in negative-ion mode. However, samples released from fetuin, thyroglobulin, or ovalbumin are especially recommended. The structurally diverse high-mannose glycans populated on ribonuclease B on the other hand can be an inherent source of error, since isomeric CID fragments may overlay and broaden the ATD of the native glycans.[139] Regardless of the carbohydrate mixture, different calibration curves should be used for each charge state to achieve the best CCS estimation.[139]

For the calibration, each calibrant sample (thyroglobulin and dextran) was measured under the same conditions as the analyte samples, and the obtained drift times were corrected for their m/z dependent flight time and correlated to the corrected CCSs. Each estimated CCS (^{TW}CCS) is the average value of five independent measurements at different wave velocities, with a typical standard deviation of about 1 %. To evaluate the quality of the calibrants, the ^{TW}CCSs for the
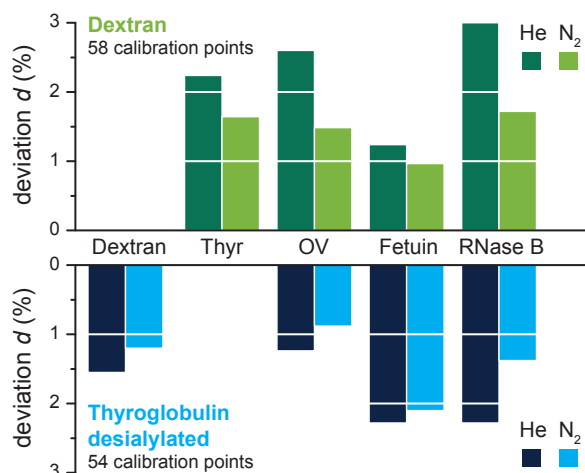
Figure 3.4: Average deviations d of estimated ^{TW}CCSs from absolute ^{DT}CCSs for dextran, and N-glycans from thyroglobulin (Thyr), ovalbumin (OV), desialylated fetuin, and ribonuclease B (RNase B). The average relative errors d (eq. 11) of He and N_2 ^{TW}CCSs obtained from a calibration with either dextran (green) or thyroglobulin glycans (blue) are shown. Both calibrations are associated with similar deviations, but larger errors are generally observed for ^{TW}CCS$_{He}$ than for ^{TW}CCS$_{N2}$.

"unknown" samples were determined and compared to their absolute CCSs (^{DT}CCSs), by calculating their relative deviation (d).

$$d = \frac{^{TW}CCS - {}^{DT}CCS}{^{DT}CCS} \times 100 \qquad (11)$$

When absolute values of d from all CCSs of one sample are averaged and compared (Figure 3.4), it immediately becomes apparent that both investigated calibrants yield comparable errors between 1 and 2 % for ^{TW}CCS$_{N2}$. This is in good agreement with values obtained for a calibration with peptides,[138] proteins,[137] and positively charged glycans.[139] In addition, these data also indicate that dextran is a highly suitable calibrant for the CCS estimation of carbohydrates on TW IM-MS instruments because the observed errors are similar to those obtained for a native N-glycan calibration. For practicality reasons, however, dextran is a far superior calibrant, since it can be purchased off the shelf without the need of a time-consuming cleavage and workup procedure that is required for native glycans.

3.3.4 Helium vs. Nitrogen CCS

Another aspect that becomes apparent from Figure 3.4 is the inherently larger error of the estimated helium CCSs. Measurements on a Synapt instrument are typically performed using nitrogen as drift gas. Conversely, the majority of data reported in the literature and all theoretical calculated CCSs are helium values.[109,114] It has
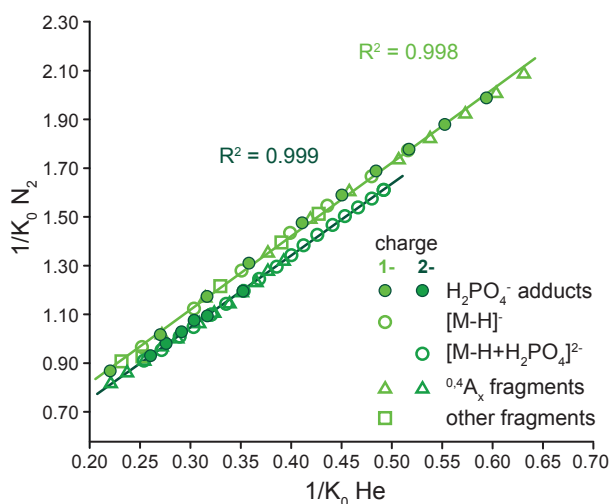
Figure 3.5: Correlation between inverse mobilities of dextran measured in helium and nitrogen. A linear correlation can be observed by comparing the inverse mobilities in two drift gases. Since they are proportional to the CCS, a conversion of He into N_2 values, and vice versa, is generally possible. The observation of two distinct trend lines highlights the necessity to use individual calibrations for each charge state.

been shown, however, that it is generally possible to use data measured in nitrogen to estimate helium CCSs.[137–139] This is possible when the inverse mobilities of ions in helium and nitrogen are linearly correlated, as shown exemplarily in Figure 3.5 for singly and doubly charged dextran ions. According to the Mason-Schamp equation (eq. 3), the inverse mobility is proportional to the CCS, and as a result, the CCSs in both drift gases should as well be proportional. Recently, however, there has been increasing evidence that estimated helium CCSs obtained from measurements in nitrogen are associated with a larger experimental error.[26]

To investigate the influence of the drift gas more closely, TW IM-MS data recorded in nitrogen were used to estimate nitrogen CCSs (using N_2 values for calibration) as well as pseudo-He CCSs (using He values for calibration). For all calibrants, larger errors were observed for estimated pseudo-He CCSs (Figure 3.4). Nitrogen CCSs are associated with errors of about 2 %, whereas pseudo-He CCSs differed up to 3.5 % from the expected values. A possible explanation for these consistently higher errors is the changed interaction potential of the analyte with the drift gas. In general, the interaction potential depends on three different parameters: (I) the polarizability of the drift gas, (II) the atoms exposed on the exterior of a molecule, and (III) the temperature of the ions.[119] The difference in polarizability between helium and nitrogen should not significantly contribute to any errors, when the inverse mobilities are linearly correlated (Figure 3.5). However, it is still not fully understood how far

the polarizability has an impact on the rather complex movement of ions in a TW field. The differences in the type of atoms exposed to the exterior, on the other hand, can be compensated for when calibrants and analyte of the same molecular identity (i.e., peptides to calibrate for peptides, carbohydrates to calibrate for carbohydrates, etc.) are used. The largest uncertainty is the ion temperature. It has been previously shown that the injection of ions into the TW IM-MS cell in Synapt instruments can lead to a significant increase in the effective ion temperature.[132,167,168] The extent of this "heating" depends on a variety of parameters, such as mass, charge, and drift gas, and it is very likely that ions measured in nitrogen have a considerably different temperature than those ions used during measurement of the reference helium CCSs. As a result of this varying temperature, the correlation between the inverse mobilities in He and N_2 is not necessarily linear over a broad range of CCSs any longer, which, in turn, can lead to a significant increase in the error of the estimated CCS. Therefore, it is recommended calibrating carbohydrate TW IM-MS data with reference CCSs measured in the same drift gas. It is nevertheless possible to estimate pseudo-He CCSs from data measured in nitrogen, for example, when the data should be compared with theoretical CCSs obtained for model structures. However, for carbohydrates a considerably larger error needs to be taken into account in this case.

3.3.5 Influence of Ion Polarity

In combination with previously published data on sodiated glycans,[139] the CCSs reported here form a data set that cannot only be used to calibrate TW IM-MS instruments, but also provide a starting point for further investigations on the gas-phase behavior of carbohydrates. Dextran CCSs in positive and negative polarity, for example, can be used to obtain information on the influence of the ion mode and the adduct ion on the underlying gas-phase structure. Per definition, the CCS of any ion is dependent on the charge but independent of the polarity. Recent investigations revealed that large, native-like protein complexes exhibit almost identical CCSs in positive and negative ion polarity, which points to a very similar gas-phase structure.[169] The carbohydrates investigated here, however, are small in comparison
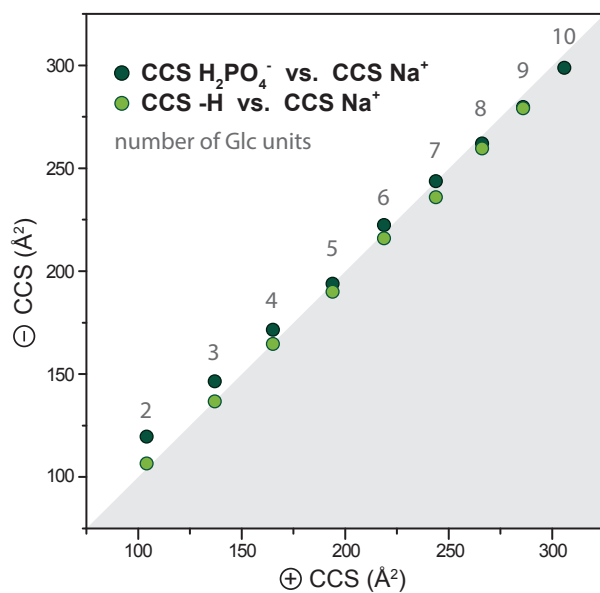
Figure 3.6: Comparison of dextran $^{DT}CCS_{He}$ values in the positive and negative-ion mode. The dots indicate the relation of CCSs of sodiated dextran molecules compared to CCSs of deprotonated species and phosphate adducts. The diagonal line depicts identical CCSs in positive and negative-ion mode.

to the above-mentioned proteins, and different adducts are likely to yield considerably different structures.

To qualitatively assess the impact of ion polarity and adduct formation on the structure, the CCSs of a dextran sample in positive and negative ion polarity are compared in Figure 3.6. Positively charged, sodiated ions, and negatively charged, deprotonated ions, exhibit almost identical CCSs regardless of the number of glucose units. This observation indicates, at least on a coarse scale, that both types of ions adopt comparable gas-phase structures. Phosphate adducts, on the other hand, exhibit considerably increased CCSs for dextran molecules with up to seven glucose units. This is expected to a certain extent, because the large phosphate ions contribute to the overall size of these smaller dextran oligomers. However, these differences seem to disappear with increasing chain length, and almost identical CCSs are obtained for sodiated, deprotonated, and phosphate adducted species consisting of eight and nine glucose units. Therefore, it can be assumed that, regardless of the polarity and type of adduct, comparable structures are adopted by larger dextran molecules in the gas phase. Interestingly, similar trends have also been reported in a systematic study on alkali ion adducts of different oligosaccharide isomers.[170] With increasing radius of the metal ion, a noticeable increase in CCS was observed

for di- and trisaccharides, whereas almost unchanged CCS have been obtained for larger penta- and hexa-saccharides. This influence on metal ion radius on CCSs indicates that the impact of the adduct ion, and polarity becomes negligible at a certain analyte size, but further studies are needed to verify this assumption on a broader basis.

3.4   Conclusion

Over 500 helium and nitrogen CCSs of complex carbohydrates as well as their fragments were measured in the negative-ion mode. The data show that CCSs of glycans and their fragments can be estimated from TW IM-MS data after careful calibration. Furthermore, it was show that partially hydrolyzed dextran, an already widely used carbohydrate reference compound in liquid chromatography, is an additional suitable and convenient calibrant for CCS estimations. Especially for techniques that are based on chromatographic methods coupled to MS and IM-MS, dextran has an outstanding potential to serve as a gold standard in the future. It can be used to simultaneously obtain reference and calibration data for retention times, m/z, and CCSs. This should not only help to simplify the currently time-consuming calibration procedure, but is also the first step towards full automation of IM-MS data acquisition and data analysis. Moreover, the CCS estimation protocol was critically assessed with respect to the utilized drift gases. The data show that a calibration using nitrogen reference CCSs for data measured in nitrogen generally yields smaller errors than those calibrated with helium reference CCSs. These findings clearly show that, besides the obvious mass and polarizability differences of the utilized drift gas, also several other factors play an important role in the separation process of ions in TW IM-MS instruments.

Furthermore, the presented data provide a good starting point for further investigations on the gas-phase structure and behavior of complex carbohydrates. As an example, the differences in CCSs measured for dextran oligomers as different adducts and with different ion polarity were analyzed. These data indicate that these parameters have a significant impact on the gas-phase structure of smaller oligosaccharides, where only minor changes are observed with increasing number of monosaccharide building blocks.

4 Identification of Carbohydrate Anomers*

4.1 Introduction

The inherent structural diversity of glycans poses a major analytical challenge to all aspects of the glycosciences,[9,171] and is one reason why glycomics lags behind the advances that have been made in genomics[1] and proteomics.[172]
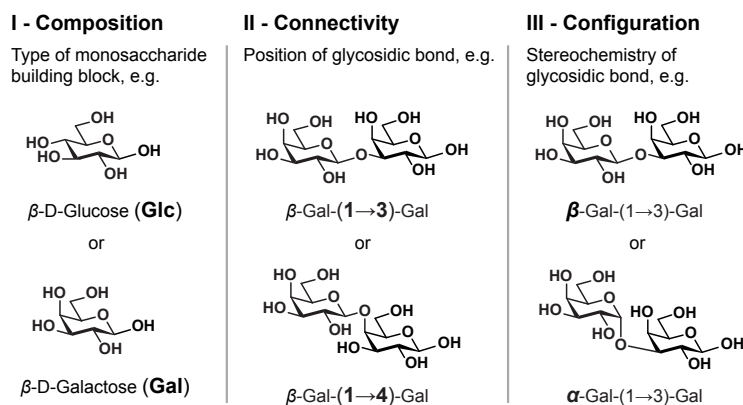
Figure 4.1: Structural features of complex carbohydrates. The composition (I) of a carbohydrate is defined by its monosaccharide building blocks, which are often isomers, as shown for glucose (Glc) and galactose (Gal), which differ only in their C4 stereochemistry. Because of the many possible functional groups, the formation of a new glycosidic bond can occur at several positions, resulting in different connectivities (II), such as those shown here. Each glycosidic linkage is a new stereocenter that can have either α- or β-configuration (III).

The structure of a glycan is described by its composition, connectivity, and configuration (Figure 4.1). The composition (Figure 4.1 I) is defined by its monosaccharides, which are often stereoisomers that differ only in their stereochemistry at one particular carbon atom. Each monosaccharide contains multiple hydroxyl groups that can be a point of attachment for the next building block. Thus, unlike oligonucleotides and proteins, carbohydrates are not necessarily linear, but can rather be branched structures with diverse regiochemistry (Figure 4.1 II). In addition, a new stereocenter emerges when a glycosidic bond is formed, because two monosaccharides

can be connected in two different configurations (Figure 4.1 III). These α- and β-anomers are stereoisomers, even though the connectivity is identical. Anomers are diastereomers, not enantiomers, meaning that they differ in at least one, but not all, of their stereocenters; consequently, anomers may differ in their size and properties.

When synthesizing oligosaccharides, managing different compositions is straightforward, because specific building blocks are added stepwise to generate the desired structure.[173] Protective groups are used to define the connectivity by allowing the selective unveiling of specific hydroxyl groups,[174] thus providing regiocontrol. In contrast, configurational control during glycosidic bond formation is the central challenge for chemical synthesis.[173] *Trans*-glycoside formation is aided by the use of participating protecting groups. *Cis*-glycoside formation, however, cannot rely on participation, and anomeric mixtures are frequently obtained.[175]

The analysis of complex synthetic glycans is key to quality control but remains a major challenge. Glycan structure is typically ascertained by a combination of nuclear magnetic resonance spectroscopy (NMR) and mass spectrometry. Measuring a mass-to-charge ratio (m/z) with mass spectrometry is fast, requires very little amounts of sample and provides precise, high-resolution data about the sample composition. Detailed information regarding connectivity can be obtained following derivatization (chemical modification) and/or elaborate tandem mass spectrometry analysis.[90,176–178] Nevertheless, mass spectrometry is not able to analyze stereoisomers, since they generally cannot be distinguished from each other because of their identical atomic composition and mass. Conversely, NMR is able to determine the configurational information of carbohydrates, but require large sample amounts and are time-consuming; moreover, the resulting spectra are cumbersome to interpret when different stereoisomers need to be distinguished. In addition, the relative detection limit of 3 % to 5 % for larger oligosaccharides in NMR experiments is rather poor. Liquid chromatography can help to differentiate configurational isomers, but an unambiguous identification of one isomer in the presence of another is often not possible either.[9]

A promising approach to overcoming these limitations is the combination of ion mobility spectrometry and mass spectrometry (IM-MS),[22,103] which allows for the separation of species with identical mass but different structure. The sample and

time requirements of IM-MS are similar to those of a conventional mass spectrometry experiment, so the additional information is obtained at no extra cost. Moreover, the measured drift time can be converted into an instrument-independent, rotationally averaged collision cross section (CCS).

IM-MS has already been proven to be of value in the structural analysis of proteins and their assemblies,[179,180] and also showed promise for the separation of carbohydrate and glycopeptide isomers.[23,24,145,146,148,181] Previous IM-MS studies of carbohydrates, however, were almost exclusively focused on pairs of regioisomers; data regarding the equally important compositional and configurational isomers is still lacking. In this chapter, the utility of IM-MS for the in-depth structural analysis of carbohydrates will be illustrated by systematically investigating all types of isomerism simultaneously within one consistent and comparable set of compounds.

4.2 Experimental Details

All oligosaccharides were synthesized by Heung Sik Hahm (Max Planck Institute of Colloids and Interfaces, Potsdam) using automated glycan assembly and purified using preparative HPLC. All compounds were characterized by NMR, and high-resolution mass spectrometry. The structures of the investigated oligosaccharides **1-9** are shown in Figure 4.2. For experimental details of the synthesis see Hofmann et al.[182]
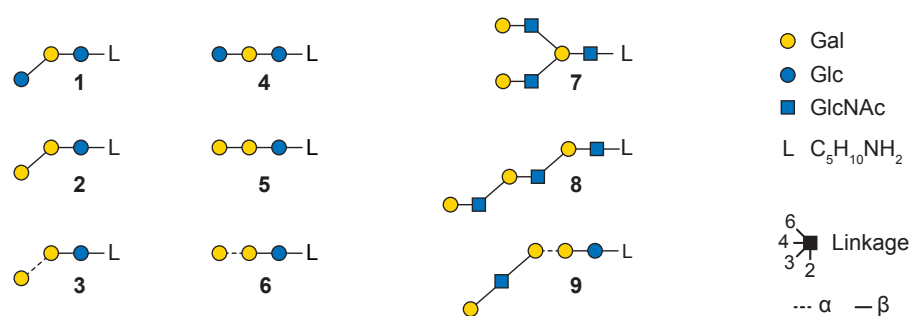
Figure 4.2: Schematic representations of the investigated molecules **1-9** using the SNFG.
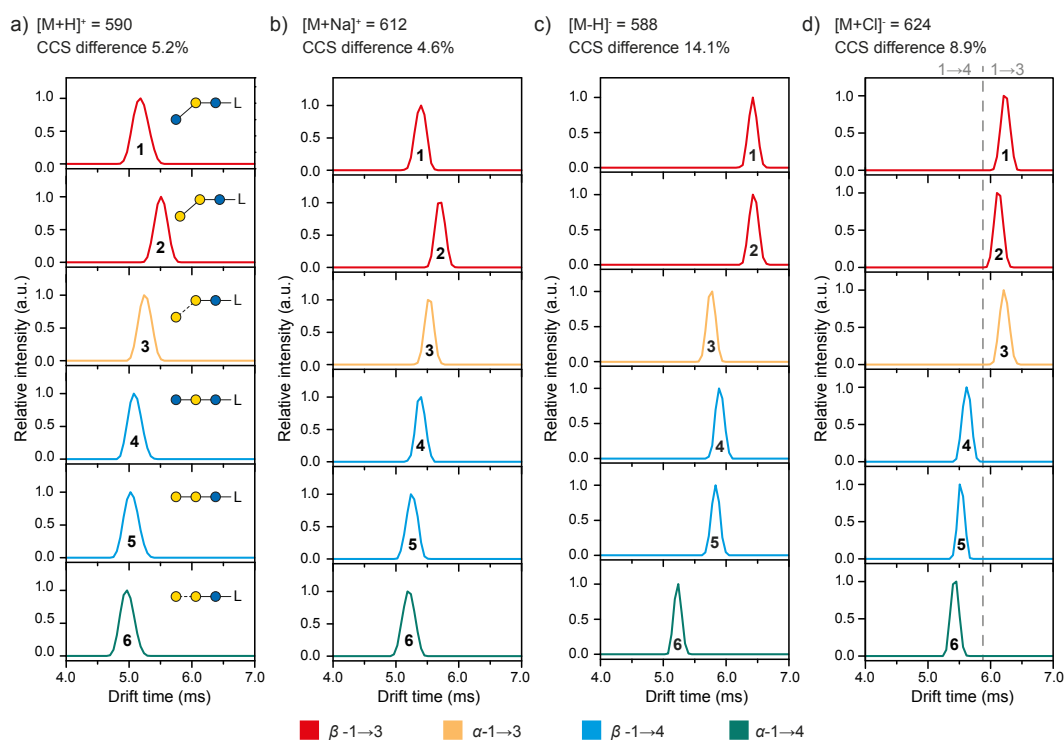
Figure 4.3: Arrival-time distributions of trisaccharides **1-6** as different species in positive and negative-ion mode. The CCS difference between the most compact and the most extended isomer of each set is given as a percentage. Small CCS differences are observed in positive-ion mode (a, b), which makes an unambiguous identification of the trisaccharides difficult. The largest CCS differences are observed using deprotonated ions (c), allowing the identification of linkage isomers (for example, **3 + 6**) and stereoisomers (for example, **2 + 3**). A clear identification of regioisomers with a terminal 1→3 or 1→4 glycosidic bond can be obtained for chloride adducts (d).

IM-MS experiments were performed on a traveling wave quadrupole/ion mobility/orthogonal acceleration time-of-flight mass spectrometer, Synapt G2-S HDMS (Waters Corporation),[131] which was mass-calibrated before measurements using a solution of caesium iodide (100 mg/mL). IM-MS data analysis was performed using MassLynx 4.1, DriftScope 2.4 (Waters Corporation), and OriginPro 8.5 (OriginLab Corporation) software. For IM-MS analysis, compounds **1**-**9** and the crude mixture **5/17** were each dissolved in water/methanol (1:1 by volume) to yield a concentration of 1-10 µmol/L. A nano-electrospray ionization source was used to ionize 3-5 µL of sample from platinum-palladium-coated borosilicate capillaries prepared in-house. Typical settings were: source temperature, 20 °C; needle voltage, 0.8 kV; sample
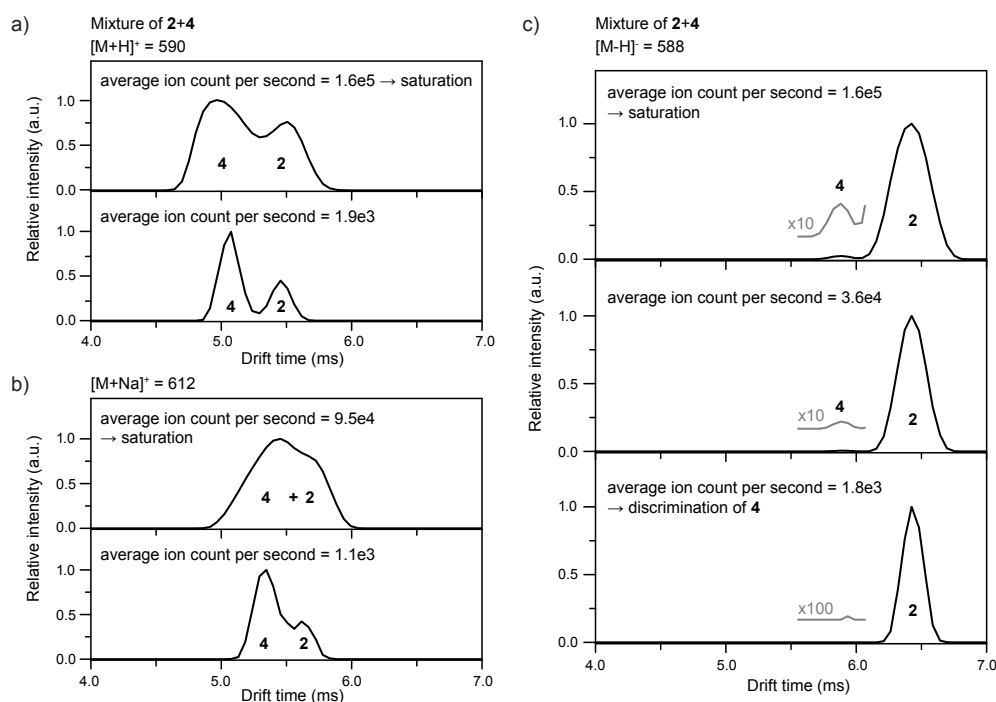
Figure 4.4: Correlation between signal intensity and ion mobility peak width in mixtures of **2** and **4**. Arrival-time distributions of a) $[M + H]^+$ and b) $[M + Na]^+$ ions at high (upper panels) and low (lower panels) signal intensity. The given average ion count per second corresponds to the signal detected for the major isotope peak. High signal intensities result in peak broadening and reduced ion mobility resolution, whereas a considerably improved separation is achieved at lower intensity. c) Arrival-time distributions of $[M \text{-} H]^-$ ions from a mixture of <1 % **4** and >99 % **2**. Measurements at high signal intensity can be used to qualitatively detect **4**. At low intensity, however, **4** is discriminated and no signal can be detected.

cone voltage, 25 V; cone gas, off. The ion mobility parameters were optimized to achieve maximum resolution without excessive heating of the ions upon injection into the ion mobility cell. Values were: trap gas flow, 2 mL/min; helium cell gas flow, 180 mL/min; ion mobility gas flow, 90 mL/min; trap direct-current bias, 35 V; ion mobility wave velocity, 800 m/s; ion mobility wave height, 40 V. For MS/MS experiments the trap collision energy was increased to 30-60 V.

IM-MS spectra of each individual carbohydrate and three trisaccharide mixtures (**6** + **3**, **3** + **2** and **5** + **6**) were recorded separately in positive and negative-ion mode. Arrival-time distributions of **1**-**6** as different adduct ions are shown in Figure 4.3. For the measurement of the individual carbohydrates, the *m/z* signal intensity was

Table 4.1: Estimated nitrogen CCSs ($^{TW}CCS_{N2}$) for trisaccharides **1-6** and by-product **17**. CCSs were estimated from traveling wave measurements in nitrogen. Each $^{TW}CCS_{N2}$ is an average of three independent measurements with the corresponding standard deviation (STD).

substance	ion	CCS in Å^2	STD in Å^2	ion	CCS in Å^2	STD in Å^2
1	[M+H]$^+$	231.9	0.4	[M+Na]$^+$	236.2	0.6
2	[M+H]$^+$	238.7	0.8	[M+Na]$^+$	242.9	0.9
3	[M+H]$^+$	233.6	0.7	[M+Na]$^+$	239.6	0.6
4	[M+H]$^+$	229.8	0.8	[M+Na]$^+$	236.4	0.6
5	[M+H]$^+$	228.9	0.6	[M+Na]$^+$	233.6	0.7
6	[M+H]$^+$	227.0	0.8	[M+Na]$^+$	232.2	0.5
1	[M-H]$^-$	249.4	1.1	[M+Cl]$^-$	244.4	1.1
2	[M-H]$^-$	249.8	1.5	[M+Cl]$^-$	242.2	1.5
3	[M-H]$^-$	233.2	1.3	[M+Cl]$^-$	244.5	1.2
4	[M-H]$^-$	237.4	0.9	[M+Cl]$^-$	229.7	0.8
5	[M-H]$^-$	235.6	1.0	[M+Cl]$^-$	227.3	0.8
6	[M-H]$^-$	219.9	1.6	[M+Cl]$^-$	224.6	1.4
17	[M-H]$^-$	248.4	0.3	[M+Cl]$^-$	256.7	0.2

kept at approximately 10^3 counts per second to avoid saturation and subsequent broadening of the corresponding drift time peak (for an example see Figure 4.4). To avoid discrimination of a minor component, an average signal intensity of 10^4 counts per second was used for the semi-quantitative assessment of mixtures (Figure 4.4c). Under these conditions, minor components with relative concentrations below $1\,\%$ can still be detected qualitatively, but a semi-quantitative assessment is no longer possible. For unknown mixtures, it is therefore best to acquire data at both high- and low-intensity settings. At high intensity, minor components with relative concentrations below $1\,\%$ can be qualitatively detected, whereas the low-intensity case typically yields a better ion mobility resolution and enables a semi-quantitative assessment (Figure 4.4). In addition, an acquisition at different intensity settings can help to evaluate mixtures in which the isomers cannot be fully resolved. For broad and inconclusive drift time distributions, a comparison with neighbouring peaks of similar mass and charge can furthermore be used to distinguish between overlapping and saturated peaks.[139]

CCS estimations were performed using an established protocol and dextran as calibrant (dextran1000, number average molecular weight 1,000; and dextran5000, number average molecular weight 5,000; Sigma Aldrich).[139,183] The calibration solution consisted of 0.1 mg/mL dextran1000, 0.5 mg/mL dextran5000, and 1 mM NaH_2PO_4 in water/methanol (1:1 by volume). The calibrant and each sample were measured on a traveling wave Synapt instrument at five wave velocities in both positive and negative-ion mode. Arrival-time distributions of the ions of interest were extracted from raw data using MassLynx. Drift times were determined manually via Gaussian fitting of the ATDs using Origin 8.5 and corrected for their m/z-dependent flight time. CCS reference values[183] for dextran were corrected for charge and mass, and a logarithmic plot of corrected CCSs against corrected drift times was used as a calibration curve to estimate CCSs. One calibration curve was generated for every wave velocity and each ion polarity. The resulting five estimated CCSs for each sample ion were averaged. These measurements were repeated three times and the averaged values for different ions are presented in Table 4.1. The reported error corresponds to the standard deviation obtained for three independent replicates.

Semiquantitative analysis of trisaccharide mixtures.

For the semi-quantitative analysis of anomeric trisaccharide mixtures, a quantification experiment was performed using isomers **2** and **3**. Stock solutions of **2** and **3** with identical concentration were prepared in water/methanol (1:1 by volume). Each stock solution was diluted individually to yield relative concentrations of 80 %, 56 %, 43 %, 25 %, 11 %, 5 %, 1 %, 0.1 %, and 0.01 %. The serial dilutions were used to obtain isomer mixtures with concentration ratios x(**3**)=[**3**]/[**3** + **2**] between 0 and 1 (see Table 4.2). A value of 0.5 represents equal amounts of **2** and **3**, whereas 0 and 1 indicate the presence of only **2** or only **3**, respectively.

To achieve constant experimental conditions, the semi-quantitative analysis was performed on a Synapt instrument equipped with an online nano-electrospray ionization source that was coupled to an ACQUITY ultraperformance liquid chromatography system (Waters). Settings were: eluents 0.1 % formic acid in methanol/0.1 % formic acid in water at a constant rate of 50 %, flowrate 8 µL/min, sample injection 10 µL. Data were acquired in negative-ion mode with following settings: source

Table 4.2: Relative concentrations of **2** and **3** in the investigated mixtures and their corresponding relative concentration ratio x(**3**)=[**3**]/[**3** + **2**]. Measured relative intensities $\text{Int}_{\text{rel}}(\mathbf{3})=A(\mathbf{3})/(A(\mathbf{2})+A(\mathbf{3}))$ were calculated from the drift time peak areas (A) of the deprotonated species $[\text{M-H}]^- = 588.4$. The standard deviation (STD) was obtained from three independent replicates.

rel. conc. 3	rel. conc. 2	theoretical x(3)	measured $\text{Int}_{\text{rel}}(\mathbf{3})$	STD
1	100	0.01	0.04	0.011
5	100	0.05	0.07	0.004
11	100	0.10	0.10	0.007
25	100	0.20	0.18	0.005
43	100	0.30	0.27	0.005
56	100	0.36	0.35	0.005
80	100	0.44	0.42	0.010
100	100	0.50	0.49	0.007
100	80	0.56	0.55	0.016
100	56	0.64	0.60	0.005
100	43	0.70	0.69	0.008
100	25	0.80	0.78	0.005
100	11	0.90	0.89	0.010
100	5	0.95	0.93	0.012
100	1	0.99	0.97	0.007

temperature 80 °C, needle voltage, 2.7 kV; sample cone voltage, 25 V; desolvation temperature 150 °C; cone gas, off; nanoflow gas, 1.3 bar; purge gas flow, 500.0 mL/h. Ion mobility parameters were: trap gas flow, 0.4 mL/min, helium cell gas flow, 180 mL/min; ion mobility gas flow 90 mL/min; trap direct current bias, 45 V; ion mobility wave velocity, 800 m/s; ion mobility wave height, 40 V.

Extraction of the ATD of the *m/z* 588.4 ion showed two separated features, each of which corresponds to one of the two isomers. The areas under each feature is related to the concentration of the sample. Therefore, the theoretical concentration ratio was compared to the ratio of the drift time peak areas (*A*) such that the relative intensity is $\text{Int}_{\text{rel}}(\mathbf{3})=A(\mathbf{3})/(A(\mathbf{2})+A(\mathbf{3}))$ (Figure 4.7c). A linear correlation was observed, demonstrating the semi-quantification of one isomer in the presence of

another, down to contents of 1 % of the minor component. Relative concentrations between 1 % and 0.1 % were still qualitatively detectable, but a determination of the relative content was no longer possible owing to detector saturation caused by the major component.

4.3 Results and Discussion

Six trisaccharide isomers (Figure 4.5a) that, owing to their similarity in structure, are difficult to distinguish using established techniques were prepared using automated glycan assembly.[173,182,184] The six glycans share the reducing-end lactose motif β-Gal-(1→4)-Glc, and an aminoalkyl linker placed during automated synthesis for conjugation to carrier proteins or array surfaces. The non-reducing-end moiety was varied, to generate isomers that differ in composition, connectivity, or configuration (Figure 4.5a). Each of the glycan pairs **1** + **2** and **4** + **5** share the same regiochemistry and stereochemistry of their glycosidic linkages, but differ in their composition. On the other hand, the trisaccharide pairs **1** + **4**, **2** + **5**, and **3** + **6** are connectivity isomers, where the terminal building block is connected through either a 1→3 or 1→4 glycosidic linkage. Finally, the glycan pairs **2** + **3** and **5** + **6** are configurational isomers that differ in the stereochemistry of the terminal glycosidic linkage. All six carbohydrates were analyzed separately as both positively and negatively charged ions, using a commercially available TW Synapt instrument.[131] Although most previous studies focused on positive-ion adducts,[23,24,145,146,148,181] the most notable drift time differences were here observed for deprotonated [M‐H]⁻ ions (Figure 4.3 and Figure 4.5b). As a result, a higher separation capability was achieved, and therefore these results will be used for the analysis below. The drift times of the individual sugars were further converted into CCSs (Table 4.1) using the previously described calibration protocol (Chapter 3, page 29 *ff.*).[139,183]

A comparison of the drift times and CCSs of the six trisaccharides reveals both similarities and differences (Figure 4.5b). The compositional isomers **1** and **2** exhibit drift times and CCSs that are almost identical to each other; the same is true for compositional isomers **4** and **5**. This observation is not surprising, given that the respective trisaccharide pairs differ only in the orientation of one hydroxyl group, at the C4 carbon atom. Such a minimal structural difference is not expected to result

51
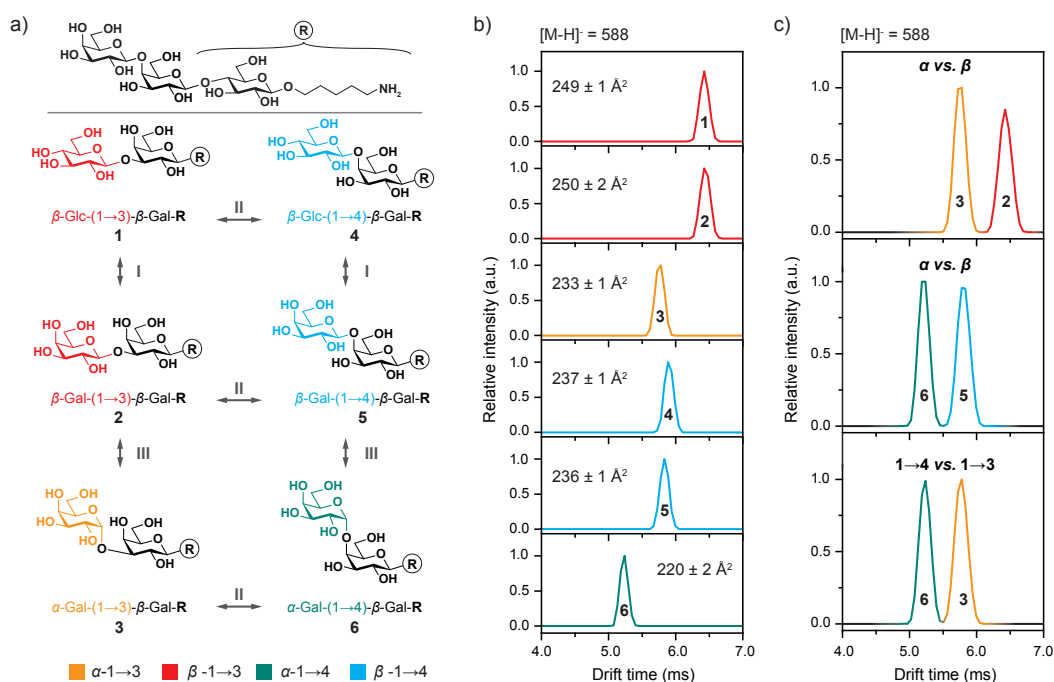
Figure 4.5: Structure and IM-MS data of trisaccharides **1-6**. a) The synthetic trisaccharides **1-6** share the same disaccharide core, and differ merely in the composition, connectivity, or configuration of the last monosaccharide building block. b) IM-MS arrival-time distributions for trisaccharides **1-6** as [M‑H]⁻ ions. The values in Å^2 correspond to the estimated CCSs in the drift gas nitrogen and represent averages of three independent measurements. Although compositional isomers cannot be distinguished, connectivity and configurational isomers are clearly identified on basis of their CCSs. c) Arrival-time distributions of isomeric mixtures show baseline separation between linkage- and stereoisomers.

in a notable difference in CCS. However, the composition of carbohydrates is easily controlled during automated synthesis, because either glucose or galactose building blocks are being used. Thus, compositional differentiation is not essential for the quality control of glycan synthesis.

In contrast to compositional isomers, regioisomers (**1** + **4**, **2** + **5**, and **3** + **6**) can be distinguished readily from each other on the basis of their drift times and CCSs. Here, the trisaccharides containing 1→3 glycosidic linkages exhibit larger CCSs than their 1→4-linked counterparts. Analytically, however, the most striking observations resulted from comparison of the **2** + **3** and **5** + **6** configurational isomers. α-Linked trisaccharides **3** and **6** adopt a more compact structure than do the corresponding β-linked molecules, and both sets of anomers can be clearly
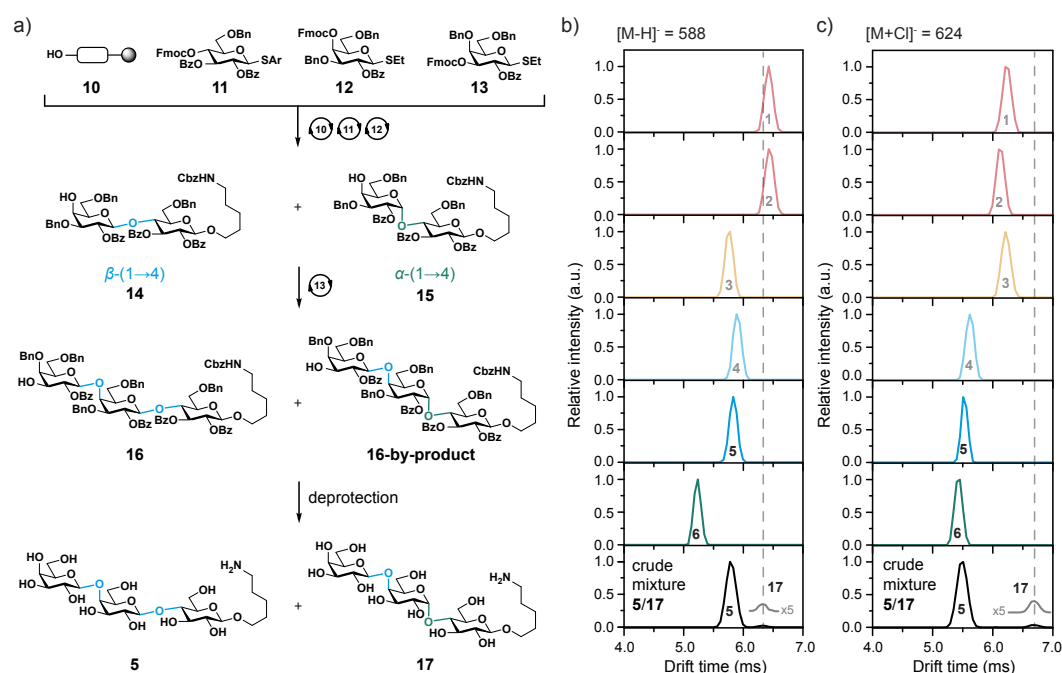
Figure 4.6: Alternative synthesis of oligosaccharide **5** and corresponding IM-MS analysis. a) An alternative route for synthesizing **5** using building block **11**, which containes a benzoyl (Bz) protecting group at the C3 hydroxyl group instead of a benzyl group (Bn). This resulted in a mixture of the disaccharides **14** and **15**, and subsequently in a mixture of trisaccharides 5 and 17. b) [M‐H]⁻ = 588 and c) [M+Cl]⁻ = 624 ATDs of trisaccharides **1-6** compared to the ATD of the crude mixture consisting of **5** and **17** clearly reveals a content of about 5 % by-product **17**.

differentiated. Trisaccharides that differ in both regiochemistry and stereochemistry (for example, **3** and **5**) exhibit similar CCSs in their respective deprotonated states, whereas they can be distinguished in IM-MS as chloride adducts (Figure 4.3).

Although regiocontrol is well established during chemical oligosaccharide assembly, the formation of mixtures of stereoisomers is common when *cis*-glycosides are installed. The characterization and quality control of synthetic oligosaccharides would therefore benefit greatly from the ability to separate and identify different isoforms. Mixtures of connectivity and configuration isomers were systematically analyzed by IM-MS (Figure 4.5c). Strikingly, the linkage isomers (1→3 versus 1→4), as well as the α- and β-anomers, are fully baseline-separated (their peaks do not overlap). A similar quality of separation was also obtained in the quality control of a crude product mixture, where small amounts of an unintended by-product were clearly

identifiable (Figure 4.6). The crude resulted from an alternative synthesis rout for **5** using building block **11**, which contains a benzoyl (Bz) protecting group at the C3 hydroxyl group instead of a benzyl group (Bn). This resulted in a mixture of the protected disaccharides **14** and **15**, and subsequently in a mixture of trisaccharides 5 and 17. Neither the fully protected trisaccharides **16** and **16-by-product**, nor the deprotected sugars **5** and **17**, can be separated by HPLC. The formation of **16-by-product** was detected using NMR analysis, but a clear structural assignment was not possible owing to the low relative concentration. The IM-MS analysis in the negative-ion mode of the crude mixture, consisting of **5** and **17**, clearly reveals a content of about 5 % by-product **17** (Figure 4.6b and c). In particular, the drift time of the chloride adduct of **17** is very diagnostic, because it differs considerably from the drift times of all other trisaccharides investigated here.

This encouraging result raises the question of whether an isomeric impurity can be not only identified qualitatively, but also determined quantitatively by IM-MS. To address this question an experiment was carried out, where trisaccharide **2** was kept at a constant concentration and the content of the corresponding anomer **3** was gradually reduced to mimic different percentages of a typical synthetic impurity (Figure 4.7a). As expected, the intensity of the IM-MS peak of trisaccharide **3** gradually declines with decreasing concentration. An impurity with a relative concentration as little as 1 % is still clearly visible and exhibits a well resolved and well shaped peak; however, although a relative content of 0.1 % can still be identified qualitatively, it is close to the detection limit (see Experimental Details page 47 *ff.* and Figure 4.4c). To better visualize the large range of intensities, it is common to plot IM-MS data as a drift plot, with the drift time on the x-axis, *m/z* on the y-axis, and a logarithmic intensity scale (Figure 4.7b). Here, a relative concentration of 0.1 % is perfectly visible even without further magnification. Furthermore, the linearity of the IM-MS intensity for a broad range of concentrations was tested with mixtures of anomers **2** and **3** (for details see Experimental Details, page 49 *ff.*). For that purpose, the relative peak area of the IM-MS signal of anomer **3** was plotted against the corresponding relative concentration (Figure 4.7c). A value of 0.5 indicates an equal content of **2** and **3**, whereas values of 0 and 1 are expected for the pure oligosaccharides, respectively. Remarkably, the plot is strictly linear over the entire range of relative concentrations

from 0.01 to 0.99, and very little deviation between different replicates is observed. As a result, IM-MS can be used to estimate the relative content of a minor impurity when the investigated compounds are, like anomers, similar in structure and ionization efficiency.
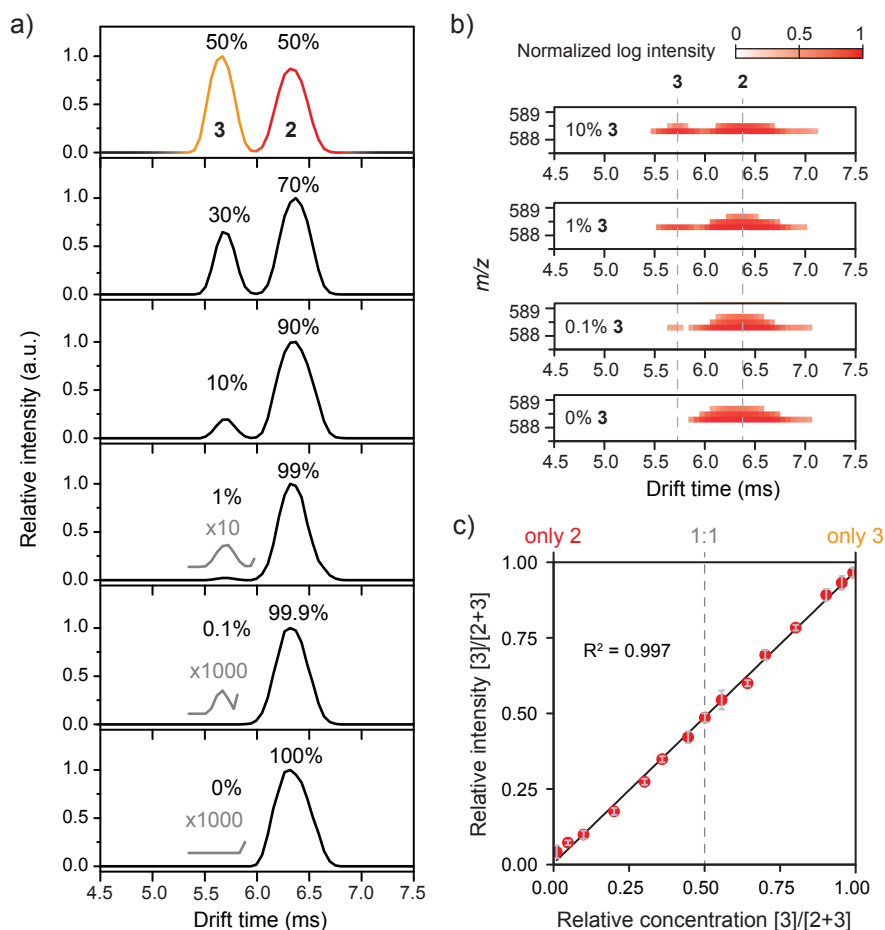
Figure 4.7: Relative quantification of configurational trisaccharide isomers. Mixtures of the configurational isomers **2** and **3** were measured using IM-MS. a) The amount of isomer **2** was kept constant, whereas isomer **3** was diluted to obtain mixtures with contents between 50 % and 0 % **3**. Minor components with relative concentrations as low as 0.1 % can still be qualitatively detected. The gray traces are magnified by the values shown. b) Three-dimensional plot showing the separation of anomers **2** and **3**. The intensity is plotted using a logarithmic scale and impurities of 0.1 % can be clearly identified without magnification. c) Plot of the relative IM-MS intensity of isomer **3** against the corresponding relative concentration, to illustrate the dynamic range of the method. A value of 0.50 represents equal amounts of isomer **2** and **3**, whereas values of 0 and 1 indicate the presence of only isomer **2** or isomer **3**, respectively. The gray error bars correspond to the double standard deviation observed for three independent replicates.
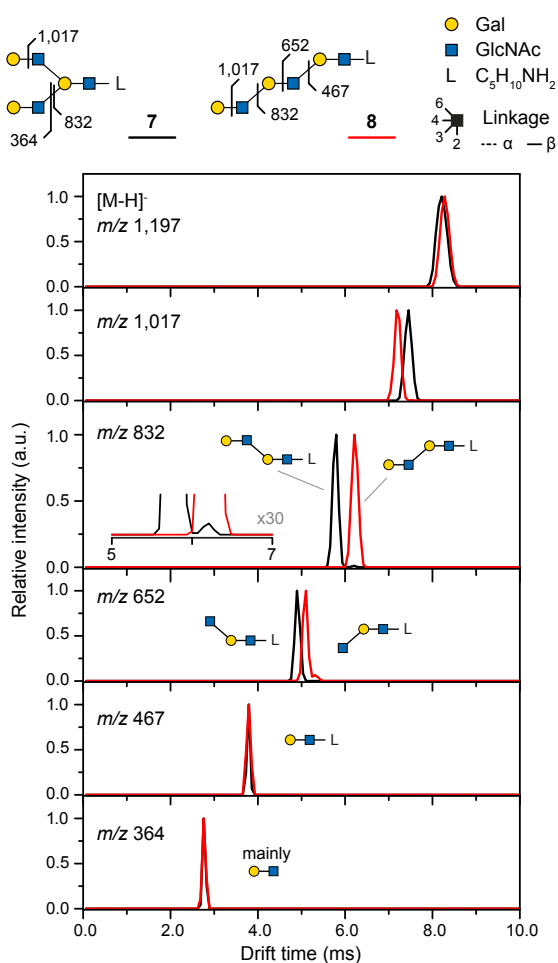
Figure 4.8: IM-MS differentiation and identification of the hexasaccharides **7** (black) and **8** (red). As deprotonated ions, **7** and **8** show almost identical drift times and therefore cannot be distinguished. However, smaller collision-induced dissociation fragments containing five, four, or three monosaccharide building blocks (m/z 1,017, 832, and 652, respectively) exhibit highly diagnostic drift times. At m/z 832, a double peak is observed for the branched oligosaccharide **7** (inset, black trace), because two isomeric fragments are formed. Both fragments can be detected simultaneously using IM-MS, with cleavage at the 3-antenna being clearly preferred. The disaccharide fragments at m/z 467 and 364 are identical for **7** and **8** and consequently exhibit identical drift times.

Larger glycans are known to separate less efficiently in IM-MS as shown for the hexasaccharide isomers **7** and **8** (Figure 4.8). However, their gas-phase fragments, containing three to five monosaccharides, exhibit more diagnostic CCSs than their intact parent ions. In addition, deprotonated trisaccharide fragments generated from larger oligosaccharides exhibit CCSs identical to those of their intact trisaccharide counterparts (Figure 4.9). Seen from a broader perspective, this highlights the exceptional potential of negative ion CCSs to be used as a diagnostic parameter for glycan sequencing.
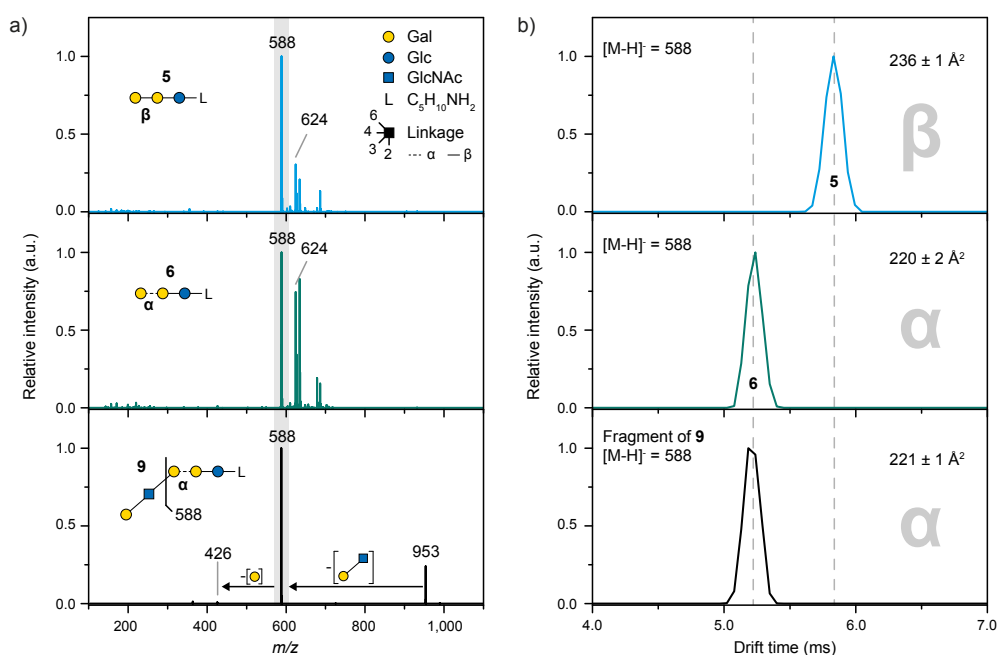
Figure 4.9: Comparison of drift times and CCSs of structurally similar precursor ions and fragments. a) Mass spectra of trisaccharides **5** and **6**, as well as a tandem MS spectrum of **9** in negative-ion mode. The pentasaccharide **9** has the same core structure as the trisaccharide **6**. Consequently, CID of deprotonated **9** produces a fragment with the same m/z as the deprotonated precursor ion of **6**. b) Arrival-time distributions of $[\mathrm{M\text{-}H}]^- = 588$ ions. The CID fragment arising from deprotonated **9** exhibits a drift time and CCS identical to those of the intact deprotonated trisaccharide **6**. This indicates that glycans and glycan fragments with identical structures also exhibit identical CCSs.

4.4 Conclusion

In summary, it was demonstrated that IM-MS is a powerful tool for the structural analysis and quality control of carbohydrates. Connectivity and configurational isomers can be separated efficiently with baseline resolution, especially when deprotonated ions are used. The data show that relative concentrations of coexisting carbohydrate isomers can be determined until 1 % of the minor components and even lower concentrations can be detected qulitatively. Thereby, the relative content of isomeric impurities can be identified easily (Figure 4.6). No other experimental technique can provide the same structural information as quickly and with such minimal sample consumption. Remarkably, a fragment obtained by CID and an intact ion that have the same structures also show identical drift times and CCSs.

Therefore, they have the potential to serve as diagnostic features for quality control and sequencing as well as the analysis of larger glycans.

The full benefit of this method will become apparent once CCS data for carbohydrates and carbohydrate fragments, derived from a variety of synthetic and biological sources, are deposited in databases. These reference data will be essential for the quick and unambiguous identification of unknown compounds. The existence of commercially available mass spectrometers will enable IM-MS to become a routine technique for non-specialists or in automated analyzes. IM-MS has the potential to fundamentally change quality control and analysis in carbohydrate chemistry.

5 Identification of Carbohydrate Epitopes[*]

5.1 Introduction

Analysis of glycoconjugates remains a particular challenge in structural biology because of their vast complexity and intricate biosynthesis. One of the most familiar examples of isomeric glycoconjugates are the ABO and Lewis blood group systems, which were already briefly discussed in Chapter 2.1.3 (page 11 *ff.*). They contain carbohydrate epitopes which consist of a disaccharide core structure of galactose (Gal) and N-acetylglucosamine (GlcNAc) with differently attached fucose (Fuc) residues. These are mediated in individuals by expression of α1,2-fucosyltransferases and/or α1,3/4-fucosyltransferases and result in different defined glycan antigens throughout the body. The altered expression of ABO and Lewis glycosyltransferases and changes in glycan structures are commonly associated with cancer formation and regression. [60–66,69,185–187] The sialylated Lewis a (Sialyl-Le[a]) epitope, also known as carbohydrate antigen CA19.9, is the only biomarker for pancreatic ductal adenocarcinoma screening approved by the US Food and Drug Administration (FDA). However, there are concerns with its use including specificity, levels of detection and its nonexpression in Le[-] patients. [68] The ability to discern subtle changes in fucosylation, which are observed in disease progression and host-pathogen interactions is, therefore, decidedly important but also analytically challenging.

There are several strategies used for characterizing terminal fucose linkages, but each approach has inherent drawbacks and is not always comprehensive. For example, sequential mass spectrometry (MS[n]) following sample permethylation [102,188] is highly informative but requires glycan derivatization and is not high-throughput nor as sensitive as HPLC and LC-MS methods. [189,190] Conversely, HPLC with fluorescence detection requires sequential treatment with numerous exoglycosidase enzymes and the limited availability of linkage-specific fucosidases hinders coverage of these epitopes. Porous graphitized carbon LC-MS^2 of negative glycan ions can effectively separate isomers and diagnostic fragments can support a structural assignment. [191]

---

[*]This chapter is based on the publication "Identification of Lewis and blood group carbohydrate epitopes by ion mobility-tandem-mass spectrometry fingerprinting" J. Hofmann, A. Stuckmann, M. Crispin, D. J. Harvey, K. Pagel, W. B. Struwe, *Anal. Chem.* **2017**, *89*, 2318-2325, http://dx.doi.org/10.1021/acs.analchem.6b03853. Figures and content adapted with permission. Copyright 2017 American Chemical Society.

However, fragmentation data can be ambiguous and not all fucose linkages can be resolved, particularly Le[a/x] and Le[b/y] structural isomers.[192] An additional complication in the analysis of Lewis antigens is migration and rearrangement of fucose residues along the glycan antennae during collision-induced dissociation (CID) of protonated glycan ions.[193,194] It was reported that $\alpha1{\rightarrow}3$-fucose residues migrated to neighboring Le[x] epitopes leading to false identification of Le[y] structures, but this occurrence was not seen with sodiated glycans which are the focus of this study.

Ion mobility-mass spectrometry (IM-MS) has shown promising results in its capacity to separate isomeric carbohydrates that cannot be resolved by orthogonal methods. To date the use of IM-MS for glycomics has been shown for small oligosaccharides, intact N-glycans, and glycosaminoglycans.[24,105,150,170,182,195–198] As shown in the previous Chapter, it can become increasingly difficult to distinguish small structural differences in larger oligosaccharides. However, first experiments showed that smaller glycans or glycan fragments seem to have more characteristic CCSs. Motivated by these results, Lewis and blood group epitope isomers are here investigated by IM-MS. Furthermore, the ability of generating glycan fragments by CID prior to IM is used to obtain additional collision cross section (CCS) values of fragment ions. This method provides a dual set of *m/z* and CCS information, which can be used to identify blood group (BG)/Le epitopes by fragmentation of larger glycoconjugates. To investigate whether glycans can effectively be identified by their diagnostic fragment CCS fingerprints, this integrated approach is then applied to rapidly distinguish BG/Le motifs in milk oligosaccharides and parotid N-glycans, without sample derivatization.

5.2 Experimental Details

Synthetically derived Lewis and blood group oligosaccharides were purchased from Dextra Laboratories (Reading, UK), with the exception of BG-H[1], which was purchased from Elicityl SA (Crolles, France), and used as received. For the stock solutions the samples were diluted with HPLC grade water to a final concentration of 150 µM. Prior to use, one µL of stock solution was added to 8 µL 1:1 methanol/water (HPLC grade) and 1 µL 0.1 % formic acid to promote proton adduct formation. Fucosyllacto-*N*-hexaose (FLNH), difucosyllacto-*N*-hexaose (DFLNH),

and trifucosyllacto-*N*-hexaose (TFLNH) milk oligosaccharides were purchased from Sigma Chemical Co. Ltd. (Poole, Dorset, UK). Milk oligosaccharide stock solutions were prepared with a concentration of 100 ng/µL in water. Prior to analysis, 1 µL stock solution was added to 19 µL water/methanol (50:50, *v/v*). Parotid N-glycans were isolated from tissue as described previously.[199] N-glycans were released chemically by hydrazinolysis and subsequently re-*N*-acetylated. Sample solutions were stored at -20 °C until analysis.

IM-MS measurements were performed on a Synapt G2-Si instrument (Waters, Manchester, UK). For each analysis 2 µL of sample were ionized by nano-electrospray ionization (nano-ESI) from gold-coated borosilicate glass capillaries prepared in-house.[143] Instrument settings were as follows: capillary voltage, 0.8-1.0 kV; sample cone, 100 V; extraction cone, 25 V; cone gas, 40 L/h; source temperature, 150 °C; trap collision voltage, 4-160 V; transfer collision voltage, 4 V; trap DC bias, 35-65 V; IMS wave velocity, 450 m/s; IMS wave height, 40 V; trap gas flow, 2 mL/min; IMS gas flow, 80 mL/min. Data was acquired and processed with MassLynx v4.1 and Driftscope version 2.8 software (Waters, Manchester, UK), and OriginPro 8.5 (OriginLab Corporation, Northampton).

Arrival-time distributions (ATDs) were fitted with a single or double Gaussian distribution prior to estimating experimental ^{TW}CCSs. A dextran calibration ladder with known absolute drift tube ^{DT}CCS$_{N2}$ was used for estimating N-glycan ^{TW}CCS values as previously described (see Chapter 3, page 29).[136,139,183] All CCS data were deposited in the GlycoMob database.[200] Sample preparation and MS reporting are in accordance with MIRAGE guidelines.[201,202]

5.3 Results and Discussion

5.3.1 IM-MS of Intact Le and BG Epitope Precursors

The separation potential of individual Lewis and blood group oligosaccharides (Le^a, Le^x, BG-A, BG-H^1, BG-H^2, Le^b, and Le^y) was first tested for intact ions by traveling wave ion mobility-mass spectrometry (TW IM-MS) (Figure 5.1). Le^a, Le^x, BG-H^1, and BG-H^2 are isomeric trisaccharides consisting of fucose (Fuc), galactose (Gal) and *N*-acetylglucosamine (GlcNAc) residues. BG-A is an isomeric structure which
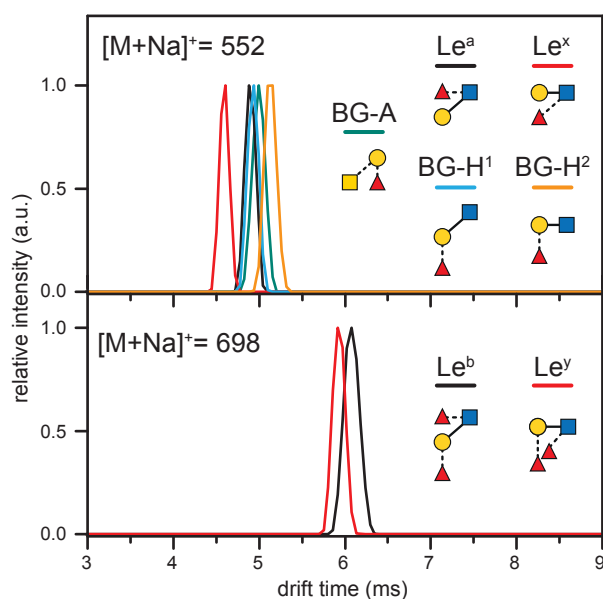
Figure 5.1: Arrival-time distributions (ATDs) of Lewis and blood group oligosaccharides measured as sodium adducts. Trisaccharide isomers Le^a, Le^x, BG-A, BG-H^1, BG-H^2 (upper panel) and tetrasaccharide isomers Le^b and Le^y are shown (lower panel). Glycan structures are represented using the SNFG.

differs in regio- and stereochemistry. Aside from fucose and galactose it additionally contains *N*-acetylgalactosamine (GalNAc) instead of GlcNAc.

Le and BG epitopes are structurally similar and contain a disaccharide core in which Gal and GlcNAc are either connected via a $\beta1{\rightarrow}3$ or a $\beta1{\rightarrow}4$ linkage resulting in so-called type 1 and 2 structures, respectively. The attachment of fucose leads to BG-H structures via $\alpha1{\rightarrow}2$ linkages, Le^x via $\alpha1{\rightarrow}3$ linkages, and Le^a via $\alpha1{\rightarrow}4$ linkages. The exception is the BG-A structure where the fucose is attached as penultimate residue to a GalNAc-Gal core motif. Le^b and Le^y are tetrasaccharide isomers similar to Le^a and Le^x structures, respectively, but containing two fucose residues.

When analyzing these structures using IM-MS, different arrival-time distributions (ATDs) were observed among sodium adduct ions: for trisaccharides (*m/z* 552) Le^a (4.90 ms), Le^x (4.59 ms), BG-A (5.00 ms), BG-H^1 (4.93 ms), BG-H^2 (5.13 ms) and for tetrasaccharides (*m/z* 698) Le^b (6.08 ms) and Le^y (5.93 ms) (Figure 5.1). Notable is the difference between Le^x and Le^a, which were nearly baseline separated despite minor structural differences (Fuc and Gal linkages are switched). Le^x had a much shorter drift time compared to other trisaccharides and the BG-H^1/BG-H^2 isomers also differed, but not as much as Le^x/Le^a. Intact tetrasaccharide $[M + Na]^+$ adducts

could also be differentiated, where the drift time of Le^y (5.93 ms) was shorter than of Le^b (6.08 ms). The observation that both Le^x and Le^y had the lowest drift times implies they adopt more compact gas-phase structures and may correlate with $\alpha1\rightarrow3$ fucose linkages that are present on both ions. Overall the results show that IM can distinguish Le and BG isomers as sodium adduct ions by TW IM-MS.

5.3.2 IM-MS of Le and BG Epitope Fragment Ions

In the next step IM separation of fragment ions is explored using a Synapt HDMS instrument that permits CID of m/z selected ions before IM separation and thus a CCS determination of fragments. MS/MS of Le and BG $[M+Na]^+$ ions resulted primarily in the neutral loss of fucose residues (Le^b/Le^y: m/z 698 $\rightarrow$ 552 $\rightarrow$ 406 and Le^a/Le^x/BG-A/BG-H^1/BG-H^2: m/z 552 $\rightarrow$ 406) (Figure 5.2a). These spectra were identical, yet the drift times of fragment ions are remarkably different (Figure 5.2). Most noticeable was Le^y, which yielded four drift peaks from three fragment ions (m/z 698, 552 and 406), with two peaks arising from the m/z 552 fragment. These m/z 552 fragments arise from a $\alpha1\rightarrow2$ fucose or $\alpha1\rightarrow3$ fucose loss and yield fragment structures that are similar to those of the intact Le^x and BG-H^2 precursors, respectively. As a result, the ATDs of the Le^y m/z 552 fragments (4.61 and 5.12 ms) align very well with the drift times of parent Le^x and BG-H^2 epitopes. In addition, the drift time of the m/z 406 ion (β-Gal-(1$\rightarrow$4)-GlcNAc) from Le^y was equal to the m/z 406 fragment from Le^x and BGH^2, which is expected as they all correspond to the same type 1 core structure. In contrast to the good separation of fragments arising from Le^y, the IM spectrum of Le^b fragment ions showed only three peaks, one for each MS/MS ion. A single drift peak at 4.96 ms is observed for the m/z 552 fragment, which can be assigned to a loss of $\alpha1\rightarrow2$ fucose or $\alpha1\rightarrow4$ fucose with fragment structures similar to intact Le^a and BG-H^1 precursors, respectively. This behavior, however, was expected since the intact Le^a and BG-H^1 trisaccharides had very similar drift times, which did not allow separation. The 552 ATD from Le^b is, therefore, likely to arise from a mixture of both fragment structures (α-Fuc-(1$\rightarrow$2)-β-Gal-(1$\rightarrow$3)-GlcNAc and α-Fuc-(1$\rightarrow$4)-[β-Gal-(1$\rightarrow$3)-]GlcNAc). The m/z 406 ions (α-Gal-(1$\rightarrow$3)-GalNAc) that are formed from Le^b, BG-H^1, and Le^a structures on the other hand, all correspond to the same type 2 epitopes and, as a result, exhibit a similar drift time, which is slightly
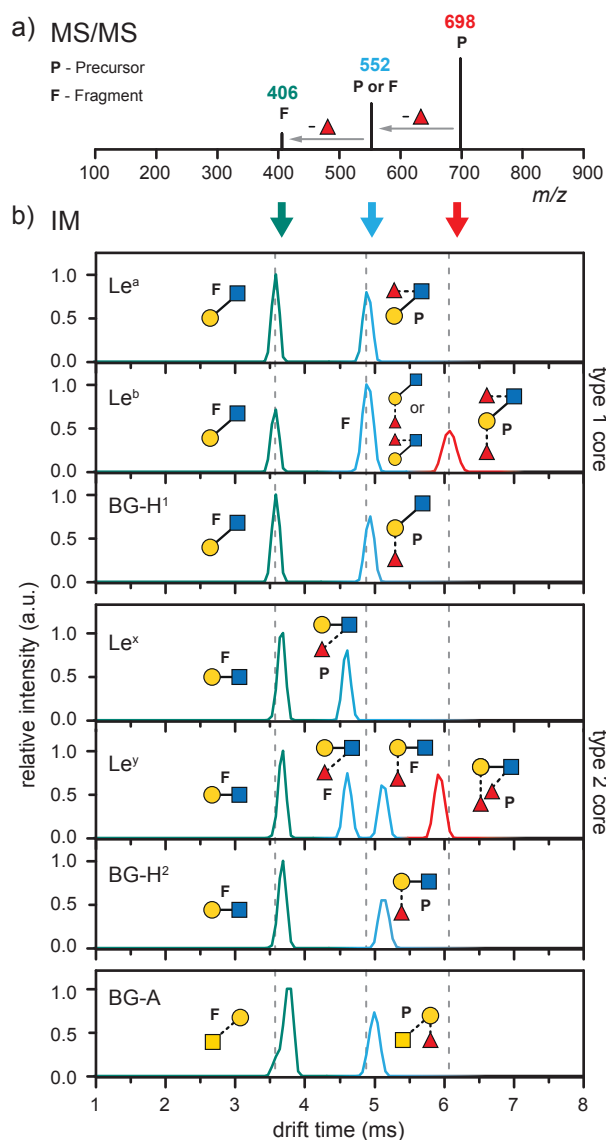
Figure 5.2: Tandem MS spectra a) and IM arrival-time distributions b) of Lewis and blood group precursor (P) and fragment (F) ions as $[M + Na]^+$ species. The major fragments (406, green; 552, blue) resulted from the neutral loss of fucose from the parent ions at m/z 698 (red) and 552.

smaller than that observed for type 1 fragments. MS/MS of BG-A also yields a m/z 406 fragment ion, which structurally, however, neither corresponds to those observed for a type 1 nor a type 2 core structure. As a result, the α-Gal-(1→3)-GalNAc fragment from BG-A differed in drift time from both Gal-GlcNAc structures, which underlines that this disaccharide is also diagnostic in IM.

5.3.3 CCSs of Epitope Fragment Ions

The different ATDs of Le and BG parent and fragment ions support IM as a robust method to identify these epitopes. However, analogous to HPLC retention times, ion mobility drift times can vary considerably between instruments/laboratories. To ensure consistent and accurate glycan assignement using this method it is more practical to compare CCSs, which are absolute values for each glycan ion and can be used as standard values for their identification. CCS measurements of sodiated ions were carried out on a TW IM-MS instrument with nitrogen drift gas ($^{TW}CCS_{N2}$) using a dextran homopolymer ladder as a calibrant.[139,183] Le and BG epitopes were measured in triplicate and $^{TW}CCS_{N2}$ values from all parent/fragment ions are presented in Table 5.1. The CCS deviation between individual replicates was below 1 % and, therefore, well within the error of CCS estimation for oligosaccharides as previously described.[139,203]

In addition to neutral fucose loss fragments, the CID product ions Fuc-Gal (m/z 349, C-type), Gal-GlcNAc or GalNAc-Gal (m/z 406), and the loss of water from parent ions (-18 Da) were observed. Expectedly the m/z 349 ion was not detected in Le^a and Le^x samples, since they do not have Fuc-Gal linkages. The measured $^{TW}CCS_{N2}$ values reflected the ATD data shown in Figure 5.2 and were consistent between experiments, demonstrating the robustness of the method. CCSs for Le^b and Le^y (m/z 698) were 252 Å^2 (252 Å^2 for water loss) and 248 Å^2 (247 Å^2 for water loss), respectively. As discussed above, Le^y exhibits two drift peaks at m/z 552 with CCSs of 229 Å^2 and 216 Å^2. The Le^y m/z 552 fragments would produce both Le^x and BG-H^2 structures and correspondingly the CCSs were consistent with those measured for intact Le^x (215 Å^2) and BG-H^2 (229 Å^2). Similarly, the Le^b m/z 552 fragment CCS (224 Å^2) was identical to the two possible Le^a (223 Å^2) and BG-H^1 (224 Å^2) precursor CCSs. The CCS values of the m/z 534 ions (water loss from m/z 552) were uniform for all structures (Le^y: 218 Å^2, Le^b: 219 Å^2, Le^a: 219 Å^2, Le^x: 217 Å^2, BG-H^1: 218 Å^2, BG-H^2: 219 Å^2) except for BG-A, which with 222 Å^2 was considerably larger. Therefore, the m/z 534 B-type fragments are only diagnostic for the BG-A epitope. The Gal-GlcNAc disaccharide (m/z 406) CCSs on the other hand differed and were consistent between $\beta1{\rightarrow}3$ (189 Å^2) or $\beta1{\rightarrow}4$ linkages (191 Å^2), whereas the isomer α-GalNAc-(1$\rightarrow$3)-Gal (m/z 406) from BG-A had an even larger

Table 5.1: Estimated collision cross sections for the drift gas nitrogen ($^{TW}CCS_{N2}$) of Lewis and blood group precursor and fragment ions as $[M + Na]^+$ Ions. $^{TW}CCS_{N2}$ values represent the average of three independent measurements and the error results from their standard deviation. Fuc-Gal fragments (m/z 349) are not available for Le^a and Le^x structures. Glycan structures are represented using the SNFG.

	parent and fragment ion $^{TW}CCS_{N2}$ (Å^2)					
m/z	349	406	534	552	680	698
type	C / *Y	Y	Z / -H$_2$O	Y / intact	- H$_2$O	intact
Le^a	-	189 ± 1	219 ± 2	223 ± 2		
Le^b	179 ± 2	190 ± 2	219 ± 1	224 ± 1	252 ± 1	252 ±1
BG-H^1	180 ± 1	188 ± 1	218 ± 2	224 ± 1		
Le^x	-	191 ± 1	217 ± 2	215 ± 2		
Le^y	179 ± 2	190 ± 2	218 ± 1	216 ± 1 229 ± 1	247 ± 1	248 ±1
BG-H^2	179 ± 1	191 ± 1	219 ± 2	229 ± 2		
BG-A	177 ± 2	193 ± 2	222 ± 2	225 ± 1		

CCS of 193 Å^2. Lastly, α-Fuc-(1→2)-Gal fragment ions, which were present on all epitopes, except Le^x/Le^a, were constant with a CCS of 179 Å^2, but was unexpectedly dissimilar for BG-A (177 Å^2). It is unclear why the BG-A α-Fuc-(1→2)-Gal CCS deviates, but it could result from the type of cleavage (i.e., Y-type opposed to C-type) or orientation of hydroxyl groups post-fragmentation. However, these postulations are difficult to test experimentally. Together the combination of CCSs and MS/MS data are conclusively diagnostic of each epitope and should be considered benchmark values for the sequencing of larger glycan structures by IM-MS/MS.

5.3.4 Epitope Fragments from Milk Oligosaccharides

To test if the previously discussed epitope fragment ions are similarly diagnostic for larger structures, the fucosylated milk oligosaccharides FLNH (fucosyllacto-
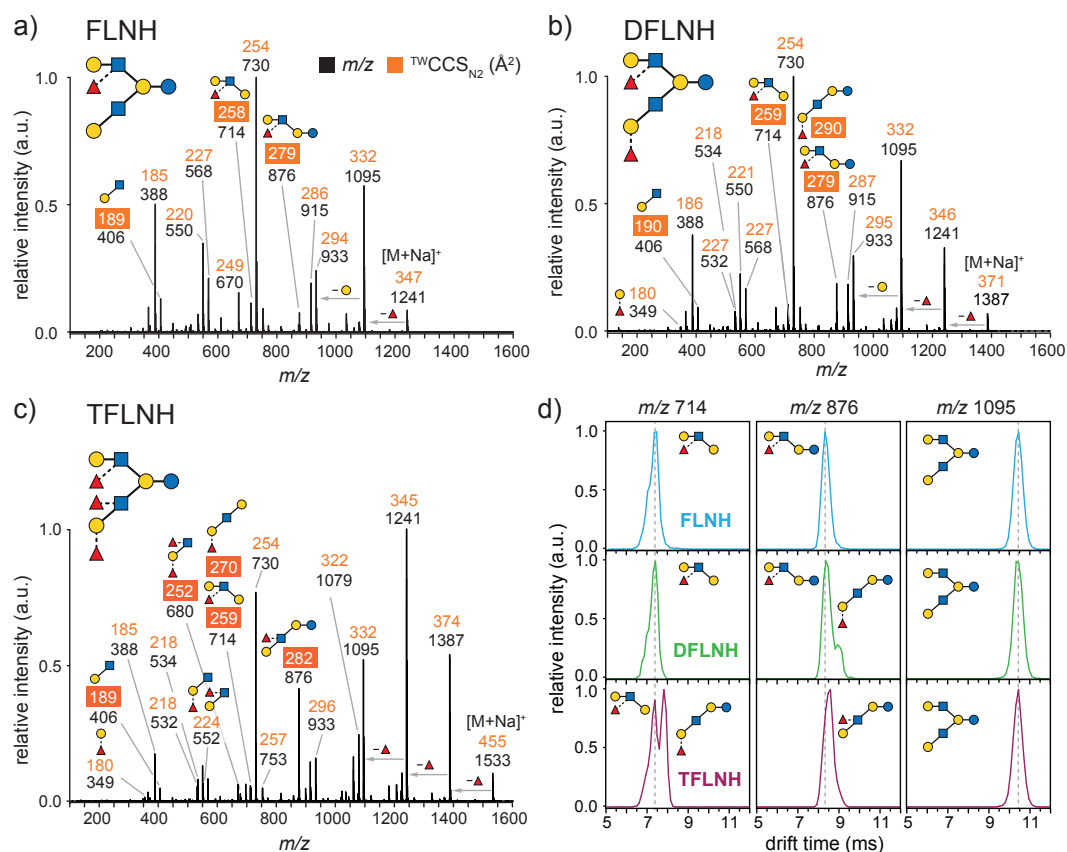
Figure 5.3: IM-MS/MS data of a) FLNH, b) DFLNH, and c) TFLNH milk oligosaccharides as $[M + Na]^+$ ions. The m/z values (black) with the corresponding $^{TW}CCS_{N2}$ (orange) are shown. Diagnostic CCSs are highlighted by orange squares. d) ATDs of diagnostic ions m/z 714, 876, and 1095 from FLNH (blue), DFLNH (green), and TFLNH (purple).

N-hexaose), DFLNH (difucosyllacto-N-hexaose), and TFLNH (trifucosyllacto-N-hexaose) were analyzed. All oligosaccharides share the same lacto-N-hexaose (LNH) backbone structure (β-Gal-(1→3)-β-GlcNAc-(1→3)-[β-Gal-(1→4)-β-GlcNAc-(1→6)-]β-Gal-(1→4)-Glc), which is fucosylated to give a Le^x epitope on FLNH, Le^x and BG-H^1 on DFLNH, and Le^x and Le^b on TFLNH.

Importantly, it is known for DFLNH that the primary CID product is the neutral loss of fucose,[204] which is also the case here for CID of FLNH (Figure 5.3). However, some fragments of FLNH, DFLNH, and TFLNH retain fucose and CCSs could be used to identify individual epitope structures. Le^x is the only fucosylated structure on FLNH and CID produced fucosylated fragments m/z 876 (β-Gal-

(1→4)-[αFuc-(1→3)-]β-GlcNAc-(1→6)-β-Gal-(1→4)-Glc) and m/z 714 (β-Gal-(1→4)-[α-Fuc-(1→3)-]β-GlcNAc-(1→6)-Gal). The extracted ATDs of each ion gave single peaks (Figure 5.3d). The CCSs of the ions m/z 714 and m/z 876 were 279 Å^2 and 258 Å^2, respectively. Although the m/z 534 B-type Le^x fragment is present in the MS/MS spectra (Figure 5.3a), the CCS of this fragment is not diagnostic as discussed above. The m/z 876 ion from DFLNH yielded two ATDs (Figure 5.3d) with CCSs of 279 Å^2 and 290 Å^2 (Figure 5.3b) and can be assigned as β-Gal-(1→4)-[α-Fuc-(1→3)-]β-GlcNAc-(1→6)-β-Gal-(1→4)-Glc (similar to FLNH) and α-Fuc-(1→2)-β-Gal-(1→3)-β-GlcNAc-(1→3)-β-Gal-(1→4)-Glc, which contains the BG-H^1 epitope. There was a single ATD peak for m/z 714 suggesting the presence of the β-Gal-(1→4)-[α-Fuc-(1→3)]-β-GlcNAc-(1→6)-Gal fragment, similar to FLNH, but the presence of α-Fuc-(1→2)-β-Gal-(1→3)-β-GlcNAc-(1→3)-Gal with the same CCS (259 Å^2) could not be excluded. However, based on the observation that BG-H^1 and BG-H^1-containing fragments (such as m/z 876 from DFLNH) have greater CCSs than Le^x equivalents, would suggest that the m/z 714 from DFLNH is the β-Gal-(1→4)-[α-Fuc-(1→3)-]β-GlcNAc-(1→6)-Gal structure. Notable for both FLNH and DFLNH was the CCS of the m/z 406 fragment (Gal-GlcNAc, 190 Å^2), which indicates that this fragment primarily arises from cleavage at the lower antenna leading to a β1→3 linked structure.

IM-MS/MS of TFLNH (Figure 5.3c) supported this hypothesis as demonstrated by the ATD and CCS (282 Å^2) of the m/z 876 ion which is smaller than the BG-H^1 equivalent (290 Å^2) yet larger than the Le^x containing ion (279 Å^2). The CCS of this structure (β-Gal-(1→3)-[α-Fuc-(1→4)-]β-GlcNAc-(1→3)-β-Gal-(1→4)-Glc) is diagnostic of the Le^a epitope. There was no evidence of the Le^x structure from the m/z 552 fragment, but is detected from the m/z 714 fragment CCS (259 Å^2), which is similar to that obtained for FLNH. A second peak (270 Å^2) from m/z 714 was identified (Figure 5.3d) and is the (α-Fuc-(1→2)-β-Gal-(1→3)-β-GlcNAc-(1→3)-Gal) fragment and again has a larger CCS owing to the presence of BG-H^1. Importantly the m/z 680 ion (252 Å^2) accurately identifies the Le^b epitope, matching the CCS fragment from the Le^b standard in Table 5.1. Furthermore, the absence of an m/z 552 doublet ATD refutes a Le^y epitope and the measured CCS of 224 Å^2 indicates the presence of a BG-H^1 or Le^a epitope. Expectedly, the CCS of the α-Fuc-(1→2)-Gal

m/z 349 fragment from DFLNH and TFLNH was 180 Å^2 and, therefore, consistent with fragments generated from BG-H^1. Finally, the m/z 1095 fragment ATDs from FLNH, DFLNH, and TFLNH are equivalent as each oligosaccharide has the same LNH backbone structure. These data provide the first example of CCS fragment assignments of milk oligosaccharides, which demonstrate that fucose linkages can be identified by characteristic CCS values of fragment ions.

5.3.5 Epitope Fragments from N-Linked Glycans

Lastly, N-glycans purified from human parotid gland were investigated, which are extensively fucosylated and differ among individuals depending on individual secretor status.[192,199,205] N-Glycan samples used in this study have previously been characterized primarily as biantennary structures with up to five fucose residues on the core GlcNAc and the antennae.[199] Salivary protein glycosylation is an important factor in pathogen interactions,[205] but direct links between glycan structure and susceptibility are debated.[206,207] Mass spectrometry methods have failed to successfully discriminate Le$^{a/x}$ or Le$^{b/y}$ epitopes on parotid N-glycans,[192,205] which highlights the need for new approaches to characterize these terminal epitopes.

Tandem MS of the biantennary precursor Fuc$_5$Hex$_5$HexNAc$_4$ at m/z 2394 predominantly led to neutral loss fragments at m/z 2248, 2101, 1956, and 1810 (Figure 5.4). However, also smaller fucosylated fragments were detected and their CCSs could be used to characterize the Le or BG epitope. These include the C-type ions at m/z 349 (Fuc-Hex), m/z 406 (Hex-HexNAc), m/z 552 (Fuc-Hex-HexNAc), and B-type ion m/z 680 (2Fuc-Hex-HexNAc). The overall composition of the N-glycan suggests four antennae fucose residues and one on the core GlcNAc. Therefore, the m/z 680 fragment is either a Le^b or Le^y fragment, whereas the m/z 552 ion is a secondary fragment produced from m/z 680 (additional fucose loss), equivalent to those in Figure 5.2 and Table 5.1. An ATD with a single feature for m/z 680 and the corresponding CCS (248 Å^2) are consistent with a Le^y (247 Å^2) but not a Le^b (252 Å^2) epitope. More importantly an ATD exhibiting two features was observed for the m/z 552 fragment, which is characteristic for the CID products of Le^y (Figure 5.2), with CCS values of 219 Å^2 and 230 Å^2, representing the Le^x and BG-H^2 structures, respectively. The CCS of the Le^x fragment from the parotid N-glycan was slightly larger than that
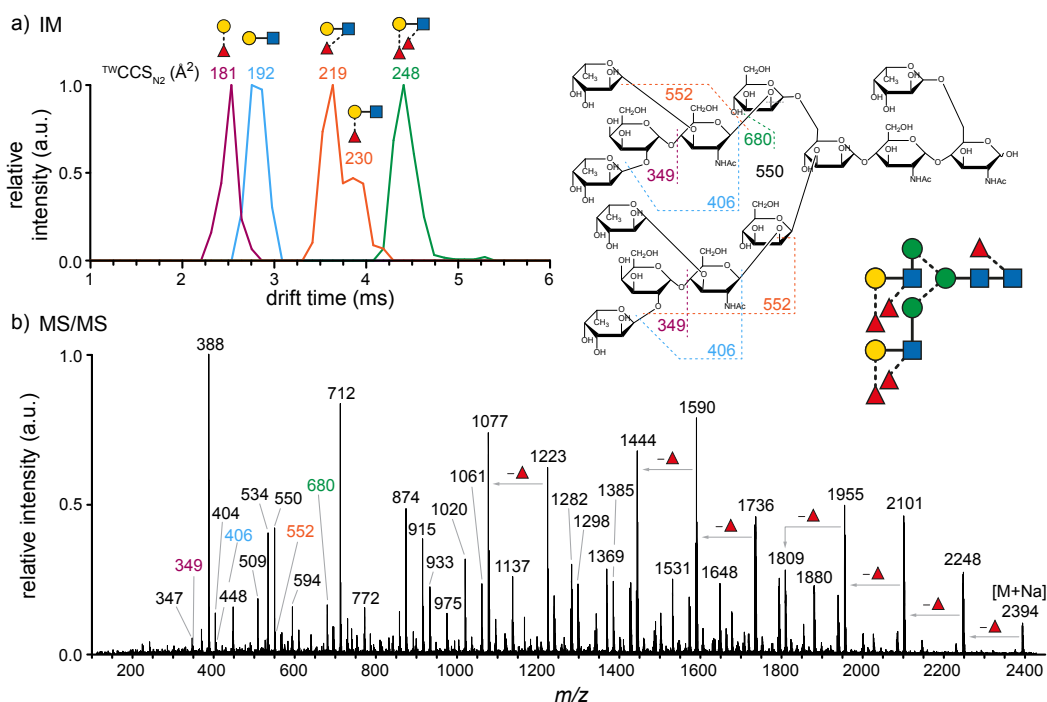
Figure 5.4: IM-MS/MS data of the $[M + Na]^+ = 2394$ N-glycan from human parotid gland. a) ATDs and $^{TW}CCS_{N2}$ of diagnostic fragments allow a clear epitope assignment. b) MS/MS spectrum of m/z 2394 with representation of the known precursor structure. Fragment assignments of the diagnostic ions are illustrated on the right.

of the individual trisaccharide ($215 \, \text{Å}^2$) shown above, which is likely a result of an overlap with a doubly charged species at m/z 550 (Hex$_2$-HexNAc fragment, $220 \, \text{Å}^2$) in the extracted ATD of the m/z 552 fragment. Nonetheless, this observation does not impact the identification of the Le^y structure due to the presence of multiple diagnostic ATD features. Overall, the CCS of m/z 349 identifies α-Fuc-(1→2)-Gal ($181 \, \text{Å}^2$), the m/z 406 fragment is a β-Gal-(1→4)-GlcNAc species ($192 \, \text{Å}^2$), and taken together with the m/z 680 fragment (Le^y, $248 \, \text{Å}^2$) and the doublet ATD at m/z 552 (Le^x, $219 \, \text{Å}^2$ and BGH^2, $230 \, \text{Å}^2$), the presence of Le^y epitopes on both antennae is demonstrated convincingly.

Tandem MS of the Fuc$_2$Hex$_5$HexNAc$_4$ ion at m/z 1956 resulted in neutral loss of fucose residues from the parent ion and consequently the m/z 552 C-type fragment was not abundant (Figure 5.5). Although the m/z 534 B-type fragment is present, again the CCS of this ion is not diagnostic. However, the absence of the m/z 349 Fuc-Hex
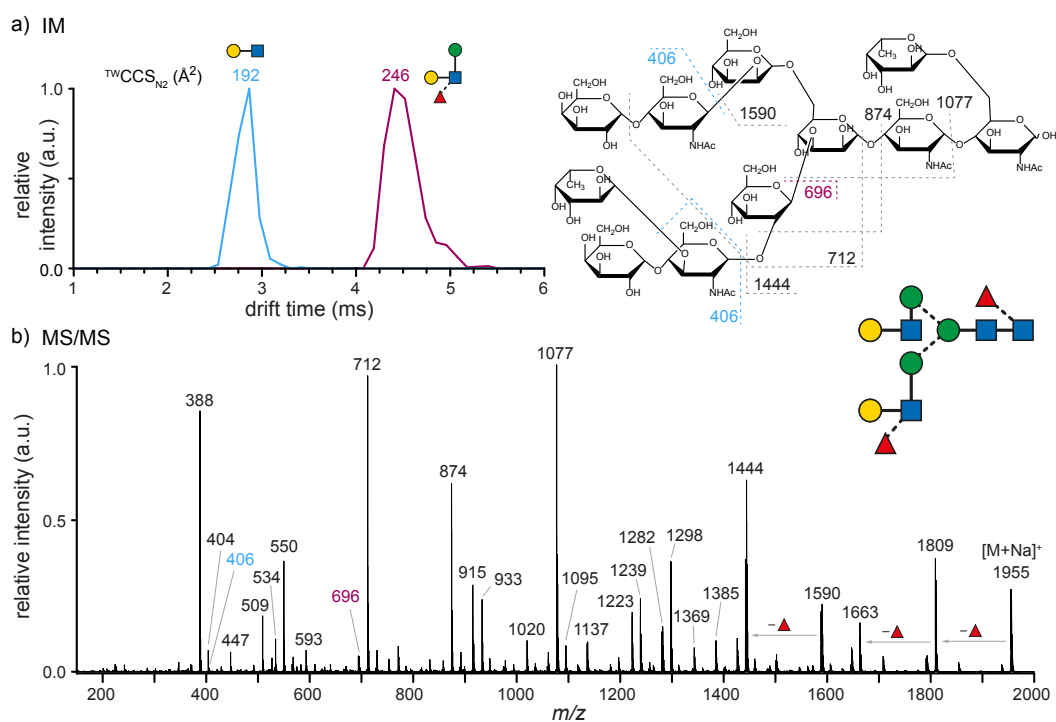
Figure 5.5: IM-MS/MS of the $[M + Na]^+ = 1955$ N-glycan from human parotid gland with a) ATDs and CCSs of diagnostic fragments shown. b) MS/MS spectrum of m/z 2394 with the known precursor structure represented using the SNFG. Fragment assignments of the diagnostic ions are illustrated.

ion and the presence of an m/z 406 CCS of 192 Å^2 suggests a β-Gal-(1→4)-GlcNAc linkage and a Le^x structure. This result was expected as the β-Gal-(1→4)-[α-Fuc-(1→3)-]GlcNAc structure (Le^x) has been confirmed for this parotid biantennary N-glycan.[199] Accordingly, the CCS of the β-Gal-(1→4)-[α-Fuc-(1→3)-]β-GlcNAc-(1→4)-Man fragment (m/z 696, 246 Å^2) is potentially diagnostic for this epitope. As a final point, IM of complex N-glycans relies on generating sample diagnostic fucosylated CID products and owing to the propensity of fucose loss upon activation, the presence of these ions can be relatively low. Therefore, monitoring CID activation energies is critically important for Le and BG identification by IM-MS/MS.

5.4 Conclusion

This study demonstrates that IM-MS/MS offers a new dimension for glycan analysis by combining glycan CID fragmentation with gas-phase separation. It was shown that the CCSs of individual Le and BG precursor and fragment ions are decidedly unique and allow to differentiate between isomers. Furthermore, the investigated epitopes were identified in multiply fucosylated parotid gland N-glycans and milk oligosaccharides by analyzing characteristic fragments and their CCSs.

There is sufficient and growing evidence that glycan isomers adopt distinct gas-phase structures allowing for separation and identification of previously indistinguishable structures. [146,182,197,208] To date the majority of IM studies for glycomics have focused on intact molecular ions, particularly for N-glycans. Here it is demonstrated that highly informative structural information lies beneath MS/MS fragmentation spectra when IM is explored. With the combined m/z and CCS information of intact ions and their fragments, unique glycan fingerprints are generated that can differentiate complex terminal fucose epitopes that have persistently challenged glycomics analyses. MS/MS analysis of sodiated N-glycans is typically less popular owing to the scarcity of informative cross-ring fragments compared to negative ion analysis. Conversely, analysis of negative ions for sequencing of glycoconjugates is less favorable compared to positive ions, because glycans ionize more efficiently as cation metal complexes. [95] However, it is currently not possible to predict which ion polarity and/or adduct leads to the best separation of a given set of isomers. This makes the here presented approach even more valuable, because the search for characteristic markers (e.g., the here presented sodiated BG and Le epitopes) that can be derived by fragmentation does not require prior or in-depth knowledge about the investigated molecules and make it thus more versatile. It might therefore also be suitable to be applied for cancer screening and the finding of new, diagnostic biomarker.

Lastly, the here described approach is fully compatible with already existing LC-MS/MS workflows. Such a combination has tremendous potential for glycomics and also resolve potential complications arising from complex samples. Specifically, the presence of isomeric molecular ions would be difficult to resolve through a direct infusion ESI approach as the MS/MS spectrum would include data from multiple

glycan structures. The data presented here establishes that IM information from fragment ions are exceedingly informative and provide the means for automated, high throughput glycan analysis.

6   Glycopeptide Analysis[*]

6.1   Introduction

In nature glycans are regularly found in the form of glycoconjugates. Protein glycosylation as post-translational modification for example tremendously influences cellular events such as cell-cell interactions and receptor recognition.[209,210] Glycosylation is highly dynamic, cell-type specific and depends on a variety of additional factors such as the developmental status of the cell.[2,6] Understanding the impact of glycosylation on protein function requires detailed knowledge of individual glycan structures and their site-specific distribution, as glycoprotein macro- and microheterogeneity can vary tremendously within a single protein.[211–215] Therefore, knowledge of both individual glycan structure and the location on a given protein is important in revealing these complex structure-function relationships.[212]

Liquid chromatography-mass spectrometry (LC-MS) is a very sensitive technique that is widely used for studying site-specific protein glycosylation.[211,213,215,216] Due to limits in LC separation and the isobaric nature of fragments observed by MS, differentiation of minor changes in glycan structure, such as terminal *N*-acetylneuraminic acid (NeuAc) linkages, directly from glycopeptides is very challenging.[213,216] A promising technique capable of providing additional structural information is ion mobility spectrometry (IM) coupled to mass spectrometry (IM-MS).[22] As previously shown, IM-MS studies on isolated glycan isomers show great potential,[123,145,146,181,182] however, very few reports focus on isomeric glycopeptides.[181,217]

In this chapter, a universally applicable and rapid approach is reported that is capable of differentiating $\alpha2{\rightarrow}3$ and $\alpha2{\rightarrow}6$ NeuAc linkages in N-glycopeptides without any additional sample preparation steps. Using IM-MS a small set of well-defined, synthetic glycopeptides is evaluated carrying N-glycans containing either $\alpha2{\rightarrow}3$ or $\alpha2{\rightarrow}6$ linked NeuAc residues. To illustrate the robustness of the method,

complex mixtures are tested using two forms of α-1 proteinase inhibitor (A1PI) produced in different cell types.

6.2 Experimental Details

Synthetic glycopeptides

All glycopeptides were synthesized by Hannes Hinneburg (Max Planck Institute of Colloids and Interfaces, Potsdam). Briefly, an asparagine (Asn) building block carrying biantennary, mono- or disialylated N-glycans was obtained from egg yolk using a combination of extraction and proteolytic digestion steps.[218,219] This glycan-Asn building block was Fmoc protected, NeuAc residues benzylated and the molecule subsequently used to synthesize N-glycopeptides by solid-phase peptide synthesis (SPPS).

For terminal glycan modification, the NeuAc residues of the synthetic glycopeptide GP3 were removed by chemical desialylation. Subsequently, the desialylated glycopeptide was subjected to enzymatic $\alpha2\rightarrow3$ sialylation with the help of a murine β-galactoside α-2,3-sialyltransferase 3 (ST3Gal3) resulting in glycopeptides GP4. For details see supporting information of Hinneburg et al.[195]

Proteolytic digestion of α1-proteinase inhibitor (A1PI)

The proteolytic digestion of α1-proteinase inhibitor (A1PI) was performed by Hannes Hinneburg. A1PI, either isolated from human plasma (Sigma-Aldrich, St. Louis, MO, USA) or recombinantly produced in Chinese hamster ovary (CHO) cells (ProBioGen AG, Berlin, Germany), was first separated by sodium dodecyl sulfate polyacrylamide gel electrophoresis (SDS-PAGE).[220] Protein bands of interest were excised, cut into cubes, and destained, and trypsin (Roche, Indianapolis, IN, USA) was added to perform a proteolytic digestion. Extracts were enriched for glycopeptides via an offline hydrophilic interaction chromatography (HILIC) step to remove unglycosylated peptides, which can suppress the detection of glycopeptides.[219] Glycopeptides were measured and identified by HPLC-MS. To additionally confirm that different NeuAc linkages were present on A1PI obtained from human plasma and CHO cells, glycans were enzymatically released and analyzed using porous graphitized carbon (PGC) LC coupled to an ion trap mass spectrometer (IT-MS) equipped with CaptiveSpray

nanoBooster (Bruker, Bremen, Germany). For details see supporting information of Hinneburg et al. [195]

Ion Mobility-Mass Spectrometry

Ion mobility experiments were performed on a traveling wave quadrupole/IMS/oa-ToF MS instrument, Synapt G2-S HDMS (Waters Corporation, Manchester, U.K.). [131,140] All samples were dissolved in water/methanol (1:1, *v/v*) and ionized using a nano-electrospray source (nESI) from platinum-palladium-coated borosilicate capillaries prepared in-house. CCS estimations were performed using an established protocol with dextran as calibrant (Dextran M_n = 1000 and Dextran M_n = 5000, Sigma Aldrich). [139,183] The calibration solution consisted of 0.1 mg/mL dextran1000, 0.5 mg/mL dextran5000, and 1 mM NaH_2PO_4 in water/methanol (1:1, *v/v*).

Typical settings in positive-ion mode were: Source temperature, 25 °C; needle voltage, 0.8 kV; sample cone voltage, 25 V; desolvation temperature, 150 °C; cone gas, off; purge gas flow, off. Ion mobility parameters were: trap gas flow, 2 mL/min; helium cell gas flow, 180 mL/min; IM gas flow, 90 mL/min; drift time trimming, 5 bins; mobility delay after trap release, 0 µs; trap DC entrance, 3 V; trap DC bias, 35 V; trap DC exit, 0 V; IM wave velocity, 1000 m/s; IM wave height, 40 V; for MS/MS: trap collision energy, 15-25 V.

Typical settings in negative-ion mode were: Source temperature, 25 °C; needle voltage, 0.8 kV; sample cone voltage, 25 V; desolvation temperature, 150 °C; cone gas, off; purge gas flow, off. Ion mobility parameters were: trap gas flow, 2 mL/min; helium cell gas flow, 180 mL/min; IM gas flow, 90 mL/min; mobility delay after trap release, 1000 µs; trap DC entrance, 3 V; trap DC bias, 45 V; trap DC exit 0 V; IM wave velocity, 800 m/s; IM wave height, 40 V.

All synthetic glycopeptides as well as the above described tryptic glycopeptides of A1PI, obtained from human plasma and recombinantly produced in CHO cells, were analysed using IM-MS. For the A1PI samples, a variety of peptides and glycopeptides were observed as shown in Figure 6.1 and 6.2.

77
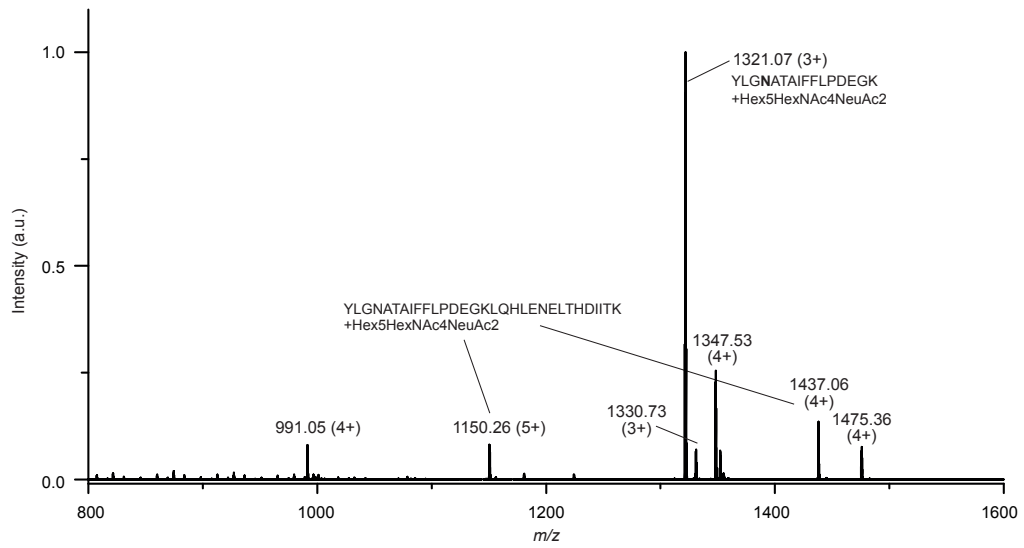
Figure 6.1: MS spectra of glycopeptides derived from human plasma A1PI in positive-ion mode.
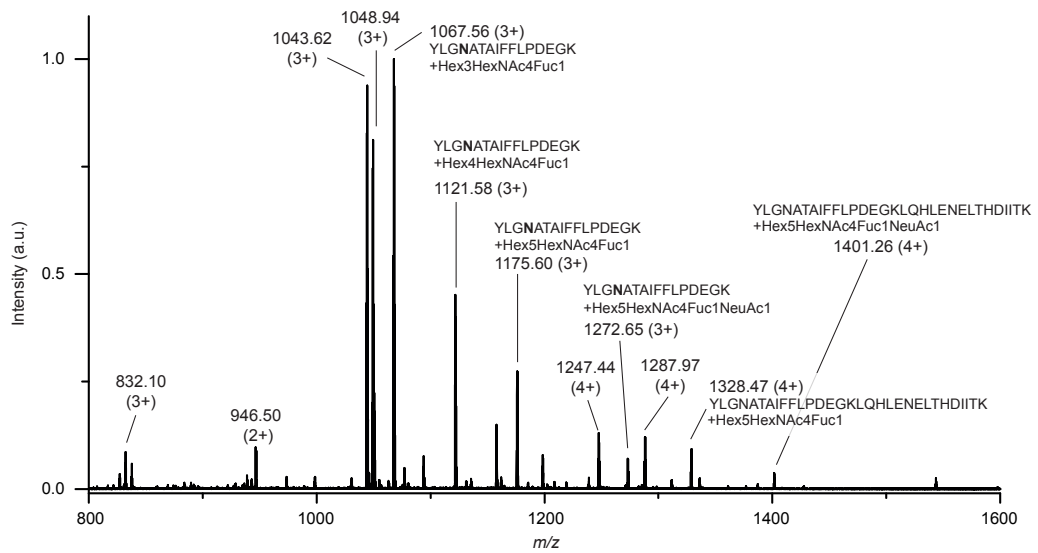
Figure 6.2: MS spectra of glycopeptides derived from recombinant A1PI (CHO) in positive-ion mode.

6.3 Results and Discussion

Homogeneous glycopeptides were generated by chemical and chemo-enzymatic synthesis for systematic IM-MS method development. The first set of glycopeptides was designed based on the naturally occurring tryptic peptide sequence [505]YGNP**N**ETQ**NN**STSWPVFK[522] from human butyrylcholinesterase (UniProt entry P06276).[221] This peptide contains three possible glycosylation sites (boldface) defined by the consensus sequence N-X-S/T (X ≠ P), two of which are glycosylated in serum.[221] To reduce complexity, the sequence was simplified to YGNV**N**ETQ**N**NSFK and an $\alpha2{\rightarrow}6$ disialylated, biantennary glycan was selectively incorporated by SPPS at one glycosylation site, either near the N-(GP1) or near the C-terminus (GP2). IM-MS experiments were performed to determine whether the method can separate the isobaric glycopeptides. As protonated ions, both isomers, regardless of the charge state, could not be separated and showed identical drift times (Figure 6.3a). However, when quadruply deprotonated ions ($[\text{M-4H}]^{4-} = 928$) were measured, GP1 and GP2 had noticeably different drift times of 5.80 and 5.33 ms (Figure 6.3b,c). Both isomers, when examined as mixtures, were nearly baseline separated illustrating that IM-MS can in principle be used to differentiate isobaric glycopeptides that merely differ in their glycosylation site.

Next, two glycopeptides are examined with a single glycosylation site but different glycan structures. Specifically, the attached complex-type glycans differed in the linkage of the terminal NeuAc residue, that is either $\alpha2{\rightarrow}3$- or $\alpha2{\rightarrow}6$-linked to galactose. Subtle differences in NeuAc regiochemistry are of biological and biopharmaceutical importance[214,222] and are challenging to characterise using established glycoproteomics techniques.[223,224] The investigated peptides are designed based on the human protein C fragment [284]EVFVHP**N**YSK[293] (UniProt entry P04070) that contains one glycosylation site (boldface). The peptide was synthesized by SPPS using an Asn building block containing an $\alpha2{\rightarrow}6$ monosialylated, biantennary N-glycan. Subsequently, a fraction of the resulting glycopeptide (GP3) was desialylated using trifluoroacetic acid followed by enzymatic re-sialylation using recombinant β-galactoside α2,3-sialyltransferase 3 (see 6.2 Experimental Details, page 76). Finally, a glycopeptide (GP4) exclusively carrying α3 linked NeuAc residues was obtained.
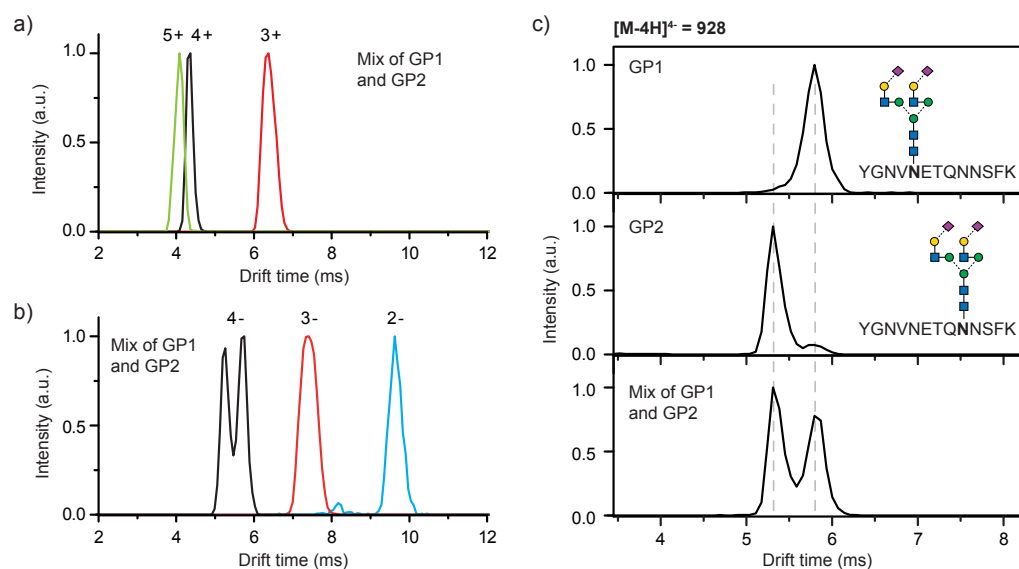
Figure 6.3: IM-MS analysis of isobaric glycopeptides GP1 and GP2. Two glycopeptides that share the same sequence and attached glycan, but differ in the site of glycan attachment were analysed as mixture. a) Arrival-time distributions (ATDs) of differently charged intact ions in positive-ion mode (green, $[\text{M}+5\text{H}]^{5+} = 745$; black, $[\text{M}+4\text{H}]^{4+} = 931$; red, $[\text{M}+3\text{H}]^{3+} = 1240$) did not show separation of the isomers GP1 and GP2. b) For negatively charged ions no separation of the glycopeptides were observed for charge states 2 and 3 (red, $[\text{M}-3\text{H}]^{3-} = 1238$; blue, $[\text{M}-2\text{H}]^{2-} = 1858$). c) The quadruply charged intact ions of GP1 and GP2 (black, $[\text{M}-4\text{H}]^{4-} = 928$), however, can be distinguished based on their drift times (top and middle) and separated in a mixture (bottom).

Only marginal, non-significant drift time differences between GP3 and GP4 were observed for 3+ molecular ions of the intact glycopeptides such that they cannot be separated in mixtures (Figure 6.4b). Given the minor structural differences in the glycan moiety compared to the overall size of the molecule this result was not surprising.

When collision-induced dissociation (CID) is applied to positively charged glycopeptide ions, glycosidic cleavages are the preferred fragmentation pathway resulting in a multitude of oligosaccharide-only fragment ions (B- and Y-type fragments* in Figure 6.4).[81] Tandem MS analysis of GP3 and GP4 yielded almost identical CID fragment spectra and did not provide diagnostic information for any glycan structural features (Figure 6.4a). However, from these oligosaccharide-only fragment

---

*The glycan fragment annotation is based on a nomenclature introduced by Domon and Costello.[88] To differentiate between peptide and oligosaccharide fragments, small and capital letters are used, respectively.
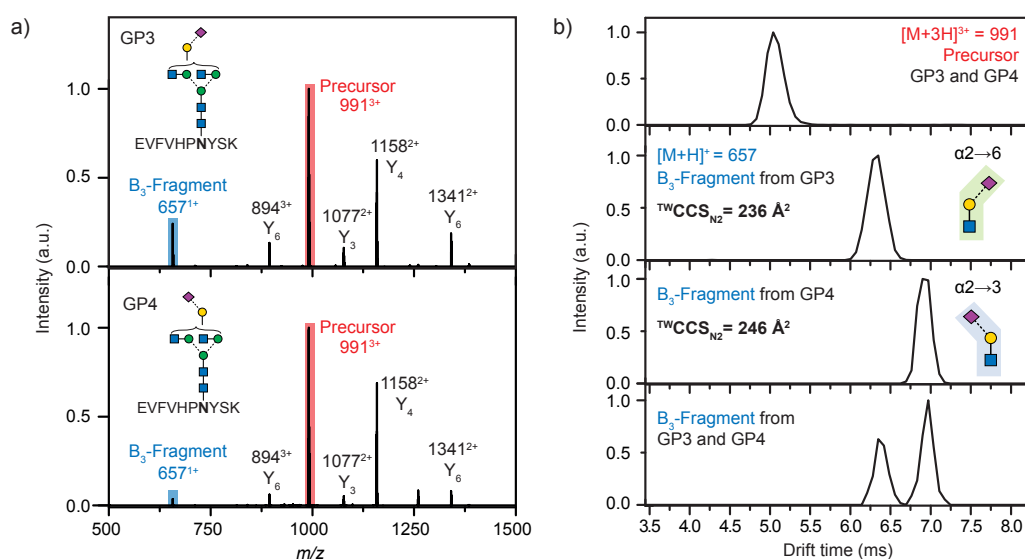
Figure 6.4: Differentiation of *N*-acetylneuraminic acid (NeuAc) linkage isomers using CID fragmentation and subsequent IM-MS analysis. Two isomeric glycopeptides, which either carry $\alpha2{\rightarrow}6$ (GP3) or $\alpha2{\rightarrow}3$ (GP4) linked NeuAc were analysed. a) Both peptides exhibit identical MS/MS spectra, as shown for the triply protonated precursor ion (red). b) When analysed as mixture the intact glycopeptide ions cannot be separated by IM-MS (m/z 991, red). B_3-trisaccharide fragments (m/z 657, blue) directly cleaved from the glycopeptide by CID on the other hand show characteristic drift times depending on the regiochemistry of the NeuAc linkage, which allows unambiguous identification $\alpha2{\rightarrow}3$ and $\alpha2{\rightarrow}6$ linked isoforms.

ions the m/z 657 B_3 type fragment is of particular interest because this oxonium ion corresponds to a trisaccharide consisting of Gal, GlcNAc and NeuAc residues in N-glycopeptides. To elucidate whether regiochemical differences of the NeuAc linkage in GP3 and GP4 leads to drift time differences of the resulting fragments, CID experiments were followed by IM-MS analysis. The extracted arrival-time distributions (ATDs) of these m/z 657 B_3 ions were vastly different for GP3 and GP4 (Figure 6.4b), with the $\alpha2{\rightarrow}6$ fragment exhibiting a considerably shorter drift time when compared to the $\alpha2{\rightarrow}3$ equivalent. When both glycopeptides were mixed, the isomeric NeuAc-containing fragments showed baseline separation. In addition, the collision cross sections in nitrogen drift gas ($^{TW}CCS_{N2}$) of 236 Å^2 for the $\alpha2{\rightarrow}6$ linked NeuAc and 246 Å^2 for the $\alpha2{\rightarrow}3$ linked NeuAc fragments differed about 4 %, well above the 1.5 % error of the method.[183] These values are highly diagnostic to the regiochemistry of the underlying NeuAc linkage and can be used to gain site-
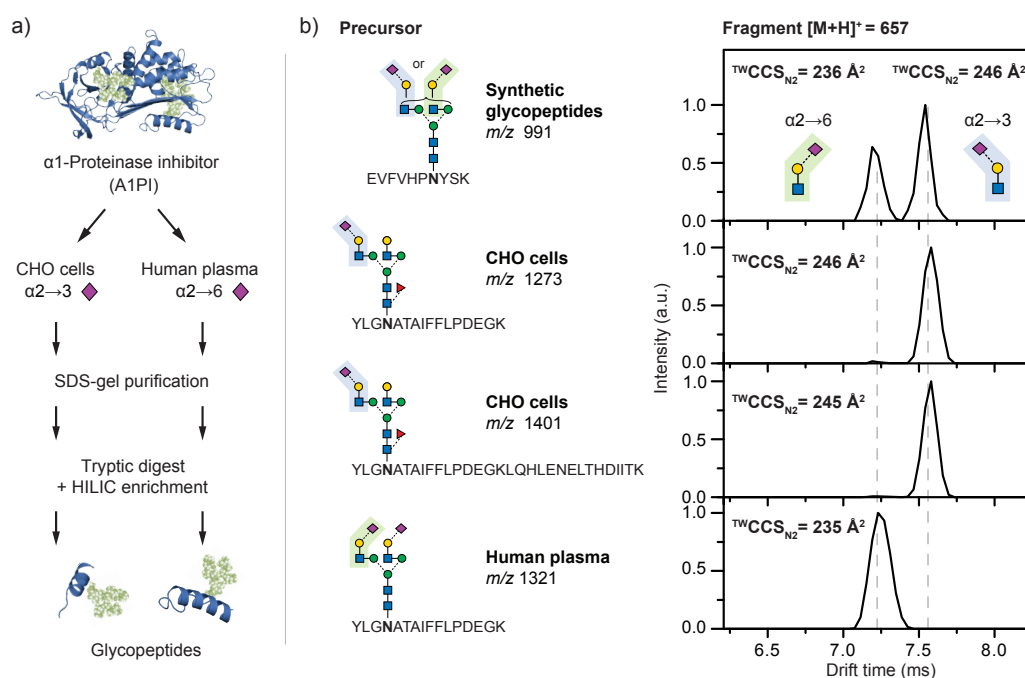
Figure 6.5: Regiochemistry analysis of *N*-acetylneuraminic acid (NeuAc) linkages in a1-proteinase inhibitor (A1PI). a) A1PI isolated from human plasma and recombinantly expressed in Chinese hamster ovary (CHO) cells was purified, digested with trypsin, and the glycopeptides HILIC-enriched. b) Fragmentation of the obtained glycopeptides and subsequent IM-MS analysis of the characteristic B_3-trisaccharide fragments (m/z 657) enabled the differentiation of $\alpha2\rightarrow3$ from $\alpha2\rightarrow6$ linked NeuAc. The observed fragment drift times and $^{TW}CCS_{N2}$ are independent of the underlying precursor sequence.

specific information on important glycan structural features directly from individual glycopeptides in a single experiment.

To evaluate whether similar diagnostic fragments could be obtained from complex mixtures within a glycoproteomics workflow, two forms of the glycoprotein A1PI were investigated (Figure 6.5a). N-Glycan NeuAc linkages on A1PI differ depending on the biological source of the protein. Human plasma A1PI contains mostly $\alpha2\rightarrow6$ linked NeuAc residues[223] whereas the same protein recombinantly expressed in Chinese hamster ovary (CHO) cells only contains $\alpha2\rightarrow3$ sialylated glycans.[225] A1PI samples from both sources were purified using SDS-gel electrophoresis followed by in-gel tryptic digestion and glycopeptide enrichment using hydrophilic interaction chromatography (HILIC) to remove unglycosylated peptides as these can suppress efficient glycopeptide detection.[219] Subsequently, the purified glycopeptides were analysed offline by

IM-MS (Figure 6.1 and 6.2, page 78). Known glycopeptide precursor ions[223] were m/z-selected for tandem IM-MS experiments and characteristic B_3 fragments were observed after CID (Figure 6.5b). Importantly, the drift times of the obtained B_3 fragments of 7.03 ms (from CHO precursor m/z 1273 and 1401) and 6.44 ms (from human plasma precursor m/z 1321) were essentially identical to those observed for the synthetic glycopeptides GP4 (6.96 ms) and GP3 (6.38 ms), respectively. In addition, the $^{TW}CCS_{N2}$ of the oxonium fragment ions (Figure 6.5b) were consistent with the synthetic reference glycopeptide data and can be used to differentiate $\alpha2\rightarrow3$ from $\alpha2\rightarrow6$ sialylated N-glycans from all sialylated glycopeptides obtained from CHO-derived and human A1PI (Figure 6.5b). The universal applicability of this approach is demonstrated, as size and sequence of the glycopeptide precursors did not affect the drift time of the resulting B_3 fragment. This finding underscores the diagnostic nature of the $\alpha2\rightarrow3$ or $\alpha2\rightarrow6$ fragments and justifies this approach as a reliable fragment-based method to obtain N-glycan structure information directly from glycopeptides.

6.4 Conclusion

In conclusion, this study shows that IM-MS can significantly improve the analysis of isomeric glycopeptides. Peptides carrying the same glycan at two different glycosylation sites were separated as intact, quadruply negatively charged molecular ions. Furthermore, the previously described IM-MS/MS approach was applied to glycopeptide isomers that only differed in their attached glycan. More specific, the regiochemistry of terminal attached NeuAc that are prevalent in N-glycosylated peptides were identified. B_3-type fragments with diagnostic CCSs, which are cleaved directly from glycopeptide precursors using CID, allow for the unambiguous identification of $\alpha2\rightarrow3$ and $\alpha2\rightarrow6$ linked NeuAc even when present in mixtures. The approach is fast, does not require derivatization and fits seamlessly to existing glycoproteomics workflows. Overall, the data highlight again the strength of marker fragments with characteristic CCSs for the identification of glycan motifs. IM-MS/MS has the immense potential to be universally applied regardless of the nature of the investigated glycopeptides or glycoproteins.

7 Summary and Future Perspectives

In this thesis, fundamental aspects of glycan analysis by ion mobility-mass spectrometry were discussed and a universal approach to investigate glycans and glycoconjugates was developed. N-glycans released from several glycoproteins were studied using IM-MS and over 450 absolute CCSs of native glycans and their fragments were measured in helium and nitrogen drift gas. These CCSs are vital reference values that can be used to calibrate TW IM-MS instruments for carbohydrate analysis. In addition, an improved calibration approach was presented based on dextran, a commercial available reference substance, which is widely used in HPLC analyses. Dextran has the advantage that a large number of reference signals of different charge states can be easily generated in the positive and negative-ion mode in a m/z range from 300 to 2000. Estimated CCSs obtained from a calibration with either N-glycans or dextran were in good agreement with previously reported absolute CCS values. Furthermore, it was shown that measurements using nitrogen as buffer gas can be calibrated using helium reference values to estimate pseudo-helium CCSs, even though, a slightly increased error is associated with these values. The most crucial point, however, is that for ions of different charge states individual calibrations need to be employed to obtain the most accurate $^{\text{TW}}$CCSs.

It was shown in a systematic study of six synthetic oligosaccharide isomers that IM-MS can distinguish glycans, which only differ in their regio- and stereochemistry. Especially when negatively charged ions were investigated, large differences in the CCSs were observed. Even for isomeric mixtures baseline separations were achieved. Furthermore, a semi-quantification of a minor component in a mixture was possible down to a content of 1 % and even lower concentration were detected qualitatively. The presented data indicate that deprotonated ions are more prone to form unique conformations compared to metal ion adducts. This is supported by theoretical calculations performed by several groups, which showed that the presence of a metal ion often dictates the arrangement of the glycan to ensure its optimal coordination. [97,111,146] Conversely, for deprotonated ions intrinsic structural differences are more pronounced in the resulting glycan conformations. This in turn affects the CCS and isomers are more likely be discerned using deprotonated ions.

In the last years, several studies were carried out on this topic and similar results as well as exceptions were found, depending on the investigated system.[97,226,227] It therefore remains very difficult to predict which ion polarity and/or adduct lead to the best separation of a given set of isomers, and a clear trend does not seem to exist. Unknown systems should therefore ideally be tested for both ion polarities and if possible for various adducts in order to achieve the best possible separation.

With increasing size of glycans the identification of small structural changes becomes increasingly difficult. However, fragments of m/z selected ions can be produced and subsequently separated in an ion mobility cell to obtain additional structural information. The unique feature of the Synapt instrument was thus employed, to obtain CCSs of intact ions and their fragments. As a result, a dual data set of m/z and CCS values can be generated, which forms unique glycan fingerprints. It was demonstrated that fragments containing between two and five monosaccharides often exhibit more diagnostic CCSs than their precursors. Of particular interest are fragments arising from cleavages of the glycosidic bonds. These were shown to exhibit the same CCSs as intact ions of the same structure. This provides the fundamental basis for the identification of unique carbohydrate motifs and the sequencing of oligosaccharides.

Several Lewis and blood group tri- and tetrasaccharides, which are common glycan motifs, were shown to have characteristic CCS fingerprints. Thus, they are ideally suited to function as glycan markers. Furthermore, a trisaccharide fragment was found that can be used to identify $\alpha 2{\rightarrow}3$ and $\alpha 2{\rightarrow}6$ linked N-acetylneuraminic acids within larger glycans. The power of the described IM-MS/MS approach was demonstrated by identifying the mentioned glycan motifs in N-glycans, milk oligosaccharides, synthetic glycopeptides as well as tryptic digests of a glycoprotein.

IM-MS/MS is thus an extremely versatile technique, because structural assignments are purely based on diagnostic fragment CCSs and independent of the investigated glycan or glycoconjugate. The analysis is furthermore fast, requires small sample amount, and no derivatization is needed. In addition, it can be automated and coupled to other techniques such as HPLC, which also enables high-throughput analyses.

Within the last decade, IM-MS quickly developed from an exotic technique utilized only by specialists into a ready-to-use and commercially available technique. IM-MS can be applied for synthesis control of glycans as well as the investigation of biological samples. There are, however, several challenges remaining that need to be addressed in the near future.[228]

One of the most important tasks is the creation of a curated database where IM-MS data can be stored and shared. Currently, most CCSs of carbohydrates are only reported in individual publications, and it is thus difficult to access all available information and continuously keep track of new data. Furthermore, the comparison of data can be very complex as the same molecule is often investigated by different groups utilizing distinct chemical modifications or adduct ions. This emphasizes the necessity of a structured database that also provides search tools to enable straightforward access to connected data of similar structures. These features will furthermore enable the implementation of fragment data, which are necessary for a marker-based structural identification. One of the few platforms that is suitable for the integration and connection of MS, HPLC, and IM-MS data is the database network unicarbKB.[200,229] However, even in this case there is no universally accepted format to store and share acquired data, and further development is clearly needed. This includes the establishing of common standards for data reporting, to enable a clear identification of the experimental conditions under which for example a CCS is obtained.

Another challenge is the increasing volume of data that can be obtained within a relatively short amount of time, particularly when LC methods and IM-MS are coupled. New and optimized tools are necessary to analyze the data and automate the glycan identification, especially for high-throughput screenings. The connection of software solutions for automated data processing with CCS databases would thereby allow to access the full potential of IM-MS/MS.

IM-MS cannot only be applied to differentiate between specific isomers, but can also serve as a separation technique to elegantly reduce the complexity of acquired data. For example, the charge-state dependence of the drift time can be exploited during data analysis. Singly-charged ions generally exhibit a considerably lower mobility than multiply charged ions, which results in the formation of signal groups
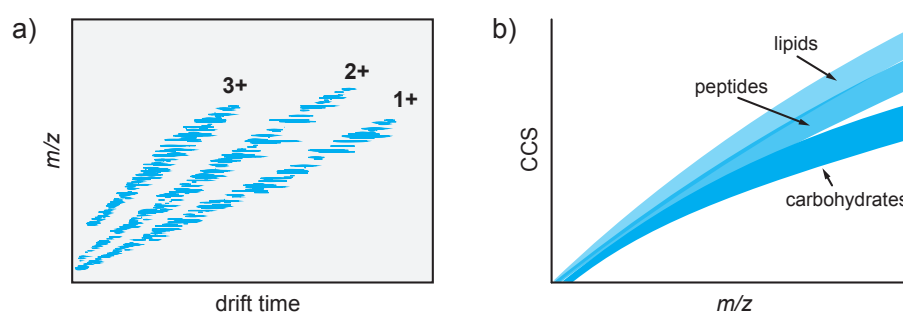
Figure 7.1: Aspects of IM-MS separations that allow to reduce spectral complexity. a) In IM-MS ions are separated depending on their charge, which is visible in a plot of m/z against drift time in the form of charge series. b) With increasing m/z the increase of the CCS is dependent on the class of the investigated ions, as shown by May et al. [26]

(Figure 7.1a). During data analysis these areas can be selectively extracted from a spectrum and analyzed separately, which for example enables an easier identification of signals that overlap with detergent signals. [51,230,231] In addition, different molecular classes exhibit distinct ion mobility behavior, because their interaction potential with the IM drift gas depends on their different chemical nature. [26] May et al. showed that carbohydrates on average exhibit smaller CCSs than peptides or lipids of the same m/z (Figure 7.1b). [26] This in turn enables a rapid classification based on trendlines in a plot of CCSs against m/z. Using this approach, it was for example demonstrated that peptides and glycopeptides can be distinguished within one measurement and analyzed separately. [232]

In the future, also technological developments of ion mobility instruments will be needed to provide higher ion mobility resolution and more precise CCS values. At the moment, the typical error of a CCS is around 1 % and probably even higher for TW IM-MS instruments. A more accurate and precise CCS determination combined with higher resolution will in the future enable the differentiation of isomers that can currently not be distinguished. This will therefore pave the way for the analysis of more complex samples.

A technique that could be of interest for carbohydrate analysis in the future is gas-phase infrared spectroscopy. [233,234] Recent experiments using cold ions showed that glycans exhibit a variety of well-resolved absorption features that are remarkably diagnostic even in the case of isomers. [234]

Another important aspect for future research is the theoretical prediction of ion mobility separations and CCSs. This would be beneficial for virtually all of the above-mentioned applications. The calculation of CCSs itself is relatively straightforward and can be performed using various established methods.[109,114,115] Generating meaningful and relevant structural candidates, however, is considerably more challenging, especially in the case of glycans. The most straightforward approach would be to use force fields to generate a series of structural candidates. Unfortunately, there are currently no force fields available that provide satisfactory results for gas-phase ions of carbohydrates.[235] Most of the existing glycan force fields are designed and optimized for the condensed phase and were developed on basis of experimental NMR data.[236] Thus, they will be biased towards condensed-phase conformers and in most of the cases an idealized chair conformation is assumed. This, however, does not necessary reflect reality and additionally hinders the flexibility and structural space of the glycan.[235] As a consequence, density functional theory (DFT) methods are often the only suitable option to obtain meaningful theoretical gas-phase structures for oligosaccharides. Unfortunately, this leads to high computational costs, especially for larger glycans, where exploring the full structural space requires the investigation of a large number of conformers.

The location of the charge is another aspect that further complicates theoretical calculations. Metal ion adducts are relatively straightforward because the glycan structure is largely dictated by the solvation of the cation. For deprotonated ions, on the other hand, multiple potential deprotonation sites exist, all of which are chemically more or less identical. A clear prediction of where the negative charge is located is therefore rather difficult. To make matters worse, it was recently shown that the position of the charge in deprotonated glycan ions is by no means static. Instead the charge migrates rapidly between different hydroxyl groups that are temporarily brought in close spatial proximity by a dynamic structural reorganization.[97]

Although many challenges and open questions in the field of glycomics remain, there has never been a time that provided more analytical tools for the structural characterization of glycans. The combined analysis of intact glycan ions and their fragments to obtain characteristic CCS fingerprints is essential for the structural identification of glycans and glycoconjugates. Especially the investigation of diagnos-

tic fragments arising from larger macromolecules is of exceptional use for the rapid analysis of structural features of more complex samples. The future implementation of connected m/z and CCS information in publicly available databases is key to exploit the full potential of IM-MS and to simplify routine analyses. Certainly IM-MS will not answer all open questions in the glycosciences, however, it will be crucial in developing a better understanding of the biological role of complex oligosaccharides.

References

[1] J. C. Venter, M. D. Adams, E. W. Myers, P. W. Li, R. J. Mural, G. G. Sutton, H. O. Smith, M. Yandell, C. A. Evans, R. A. Holt, *et al.*, *Science* **2001**, *291*, 1304–1351.

[2] A. Varki, R. D. Cummings, J. D. Esko, H. H. Freeze, P. Stanley, C. R. Bertozzi, G. W. Hart, M. E. Etzler, *Essentials of Glycobiology 2nd Edition*, Cold Spring Harbor Laboratory Press, Cold Spring Harbor (NY), USA, 2nd ed., **2009**.

[3] A. Varki, *Glycobiology* **1993**, *3*, 97–130.

[4] R. A. Dwek, *Chem. Rev.* **1996**, *96*, 683–720.

[5] A. Varki, *Glycobiology* **2017**, *27*, 3–49.

[6] K. W. Moremen, M. Tiemeyer, A. V. Nairn, *Nat. Rev. Mol. Cell Biol.* **2012**, *13*, 448–462.

[7] M. Molinari, *Nat. Chem. Biol.* **2007**, *3*, 313–320.

[8] A. Varki, *Trends Mol. Med.* **2008**, *14*, 351–360.

[9] K. Mariño, J. Bones, J. J. Kattla, P. M. Rudd, *Nat. Chem. Biol.* **2010**, *6*, 713–723.

[10] J. Ø. Duus, C. H. Gotfredsen, K. Bock, *Chem. Rev.* **2000**, *100*, 4589–4614.

[11] D. M. Sheeley, V. N. Reinhold, *Anal. Chem.* **1998**, *70*, 3053–3059.

[12] D. J. Harvey, *Proteomics* **2001**, *1*, 311–328.

[13] D. Ashline, S. Singh, A. Hanneman, V. Reinhold, *Anal. Chem.* **2005**, *77*, 6250–6262.

[14] J. Zaia, *OMICS: J. Integrative Biol.* **2010**, *14*, 401–418.

[15] N. Leymarie, J. Zaia, *Anal. Chem.* **2012**, *84*, 3040–3048.

[16] Z. Zhuang, J. A. Starkey, Y. Mechref, M. V. Novotny, S. C. Jacobson, *Anal. Chem.* **2007**, *79*, 7170–7175.

[17] J. Schwarzer, E. Rapp, U. Reichl, *Electrophoresis* **2008**, *29*, 4203–4214.

[18] A. Guttman, *Trends Anal. Chem.* **2013**, *48*, 132–143.

[19] S.-C. Bunz, E. Rapp, C. Neusüss, *Anal. Chem.* **2013**, *85*, 10218–10224.

[20] G. R. Guile, P. M. Rudd, D. R. Wing, S. B. Prime, R. A. Dwek, *Anal. Biochem.* **1996**, *240*, 210–226.

[21] A. B. Kanu, P. Dwivedi, M. Tam, L. Matz, H. H. Hill, *J. Mass Spectrom.* **2008**, *43*, 1–22.

[22] B. C. Bohrer, S. I. Merenbloom, S. L. Koeniger, A. E. Hilderbrand, D. E. Clemmer, *Annu. Rev. Anal. Chem.* **2008**, *1*, 293–327.

[23] M. Zhu, B. Bendiak, B. Clowers, H. H. Hill Jr., *Anal. Bioanal. Chem.* **2009**, *394*, 1853–1867.

[24] J. P. Williams, M. Grabenauer, R. J. Holland, C. J. Carpenter, M. R. Wormald, K. Giles, D. J. Harvey, R. H. Bateman, J. H. Scrivens, M. T. Bowers, *Int. J. Mass Spectrom.* **2010**, *298*, 119–127.

[25] F. Lanucara, S. W. Holman, C. J. Gray, C. E. Eyers, *Nat. Chem.* **2014**, *6*, 281–294.

[26] J. C. May, C. R. Goodwin, N. M. Lareau, K. L. Leaptrot, C. B. Morris, R. T. Kurulugama, A. Mordehai, C. Klein, W. Barry, *et al.*, *Anal. Chem.* **2014**, *86*, 2107–2116.

[27] C. A. Hayes, N. G. Karlsson, W. B. Struwe, F. Lisacek, P. M. Rudd, N. H. Packer, M. P. Campbell, *Bioinformatics* **2011**, *27*, 1343–1344.

[28] T. Lütteke, *Beilstein J. Org. Chem.* **2012**, *8*, 915–929.

[29] A. D. McNaught, *Pure Appl. Chem.* **1996**, *68*, 1919–2008.

[30] S. Kornfeld, E. Li, I. Tabas, *J. Biol. Chem.* **1978**, *253*, 7771–7778.

[31] IUPAC-IUB Joint Commission on Biochemical Nomenclature (JCBN), *Eur. J. Biochem.* **1984**, *138*, 9–37.

[32] A. Varki, R. D. Cummings, J. D. Esko, H. H. Freeze, P. Stanley, J. D. Marth, C. R. Bertozzi, G. W. Hart, M. E. Etzler, *Proteomics* **2009**, *9*, 5398–5399.

[33] A. Varki, R. D. Cummings, M. Aebi, N. H. Packer, P. H. Seeberger, J. D. Esko, P. Stanley, G. Hart, A. Darvill, T. Kinoshita, *et al.*, *Glycobiology* **2015**, *25*, 1323–1324.

[34] D. J. Harvey, A. H. Merry, L. Royle, M. P. Campbell, R. A. Dwek, P. M. Rudd, *Proteomics* **2009**, *9*, 3796–3801.

[35] S. Wu, N. Tao, J. B. German, R. Grimm, C. B. Lebrilla, *J. Proteome Res.* **2010**, *9*, 4138–4151.

[36] S. Albrecht, J. A. Lane, K. Mariño, K. A. Al Busadah, S. D. Carrington, R. M. Hickey, P. M. Rudd, *Br. J. Nutr.* **2014**, *111*, 1313–1328.

[37] B. L. Ridley, M. A. O'Neill, D. Mohnen, *Phytochemistry* **2001**, *57*, 929–967.

[38] H. V. Scheller, P. Ulvskov, *Annu. Rev. Plant Biol.* **2010**, *61*, 263–89.

[39] L. Kjellén, U. Lindahl, *Annu. Rev. Biochem* **1991**, *60*, 443–475.

[40] K. Sugahara, H. Kitagawa, *Curr. Opin. Struct. Biol.* **2000**, *10*, 518–527.

[41] J. R. E. Fraser, T. C. Laurent, U. B. G. Laurent, *J. Intern. Med.* **1997**, *242*, 27–33.

[42] E. Papakonstantinou, M. Roth, G. Karakiulakis, *Dermato-Endocrinology* **2012**, *4*, 253–258.

[43] M. A. J. Ferguson, T. Kinoshita, G. W. Hart in *Essentials of Glycobiology* (Eds.: A. Varki, R. D. Cummings, J. D. Esko, H. H. Freeze, P. Stanley, C. R. Bertozzi, G. W. Hart, M. E. Etzler), Cold Spring Harbor Laboratory Press, Cold Spring Harbor, New York, 2nd ed., **2009**, Chapter 11.

[44] M. G. Paulick, C. R. Bertozzi, *Biochemistry* **2008**, *47*, 6991–7000.

[45] T. Kinoshita, *J. Lipid Res.* **2016**, *57*, 4–5.

[46] E. Barboni, B. Rivero, A. George, S. Martin, D. Renoup, E. Hounsell, P. Barber, R. Morris, *J. Cell Sci.* **1995**, *108*, 487–497.

[47] C. R. Bertozzi, D. Rabuka in *Essentials of Glycobiology* (Eds.: A. Varki, R. D. Cummings, J. D. Esko, H. H. Freeze, P. Stanley, C. R. Bertozzi, G. W. Hart, M. E. Etzler), Cold Spring Harbor Laboratory Press, Cold Spring Harbor, New York, 2nd ed., **2009**, Chapter 2.

[48] R. Kleene, M. Schachner, *Nat. Rev. Neurosci.* **2004**, *5*, 195–208.

[49] A. Varki, *Nature* **2007**, *446*, 1023–1029.

[50] D. Kolarich, B. Lepenies, P. H. Seeberger, *Curr. Opin. Chem. Biol.* **2012**, *16*, 214–220.

[51] L. K. Pritchard, D. J. Harvey, C. Bonomelli, M. Crispin, K. J. Doores, *J. Virol.* **2015**, *89*, 8932–8944.

[52] W. B. Struwe, A. Stuckmann, A.-J. Behrens, K. Pagel, M. Crispin, *ACS Chem. Biol.* **2017**, *12*, 357–361.

[53] K. J. Doores, *FEBS J.* **2015**, *282*, 4679–4691.

[54] A. Helenius, M. Aebi, *Annu. Rev. Biochem.* **2004**, *73*, 1019–1049.

[55] A. Helenius, M. Aebi, *Science* **2001**, *291*, 2364–2369.

[56] M. R. Pratt, C. R. Bertozzi, *Chem. Soc. Rev.* **2005**, *34*, 58–68.

[57] S. Marionneau, A. Cailleau-Thomas, J. Rocher, B. Le Moullac-Vaidye, N. Ruvoën, M. Clément, J. Le Pendu, *Biochimie* **2001**, *83*, 565–573.

[58] W. M. Watkins, *Transfus. Med.* **2001**, *11*, 243–265.

[59] W. M. Watkins, W. T. J. Morgan, *Nature* **1957**, *180*, 1038–1040.

[60] S. H. Itzkowitz, M. Yuan, L. D. Ferrell, R. M. Ratcliffe, Y. S. Chung, K. Satake, K. Umeyama, R. T. Jones, Y. S. Kim, *J. Natl. Cancer Inst.* **1987**, *79*, 425–434.

[61] Y. S. Kim, S. H. Itzkowitz, M. Yuan, Y. Chung, K. Satake, K. Umeyama, S. Hakomori, *Cancer Res.* **1988**, *48*, 475–482.

[62] M. H. Schuessler, S. Pintado, S. Welt, F. X. Real, M. Xu, M. R. Melamed, K. O. Lloyd, H. F. Oettgen, *Int. J. Cancer* **1991**, *47*, 180–187.

[63] A. Takada, K. Ohmori, T. Yoneda, K. Tsuyuoka, A. Hasegawa, M. Kiso, R. Kannagi, *Cancer Res.* **1993**, *53*, 354–361.

[64] B. W. Yin, C. L. Finstad, K. Kitamura, M. G. Federici, M. Welshinger, V. Kudryashov, W. J. Hoskins, S. Welt, K. O. Lloyd, *Int. J. Cancer* **1996**, *65*, 406–412.

[65] X. Xie, M. Boysen, O. P. Clausen, M. A. Bryne, *Laryngoscope* **1999**, *109*, 1474–1480.

[66] J. Le Pendu, S. Marionneau, A. Cailleau-Thomas, J. Rocher, B. Le Moullac-Vaidye, M. Clement, *APMIS* **2001**, *109*, 9–31.

[67] E. Yuriev, W. Farrugia, A. M. Scott, P. A. Ramsland, *Immunol. Cell Biol.* **2005**, *83*, 709–717.

[68] D. E. Misek, T. H. Patwa, D. M. Lubman, D. M. Simeone, *J. Natl. Compr. Canc. Netw.* **2007**, *5*, 1034–1041.

[69] P. Sozzani, R. Arisio, M. Porpiglia, C. Benedetto, *Int. J. Surg. Pathol.* **2008**, *16*, 365–374.

[70] R. G. Spiro, *Glycobiology* **2002**, *12*, 43R–56R.

[71] K. G. Ten Hagen, T. A. Fritz, L. A. Tabak, *Glycobiology* **2003**, *13*, 1R–16R.

[72] L. A. Tabak, *Annu. Rev. Physiol.* **1995**, *57*, 547–564.

[73] M. N. Christiansen, J. Chik, L. Lee, M. Anugraham, J. L. Abrahams, N. H. Packer, *Proteomics* **2014**, *14*, 525–546.

[74] H. Hinneburg, P. Korać, F. Schirmeister, S. Gasparov, P. H. Seeberger, V. Zoldoš, D. Kolarich, *Mol. Cell. Proteomics* **2017**, *16*, 524–536.

[75] D. H. Dube, C. R. Bertozzi, *Nat. Rev. Drug Discov.* **2005**, *4*, 477–488.

[76] B. Küster, S. F. Wheeler, A. P. Hunter, R. A. Dwek, D. J. Harvey, *Anal. Biochem.* **1997**, *250*, 82–101.

[77] J. F. Rakus, L. K. Mahal, *Annu. Rev. Anal. Chem.* **2011**, *4*, 367–392.

[78] L. R. Ruhaak, G. Zauner, C. Huhn, C. Bruggink, A. M. Deelder, M. Wuhrer, *Anal. Bioanal. Chem.* **2010**, *397*, 3457–3481.

[79] R. P. Kozak, L. Royle, R. A. Gardner, D. L. Fernandes, M. Wuhrer, *Anal. Biochem.* **2012**, *423*, 119–128.

[80] K. Mariño, J. A. Lane, J. L. Abrahams, W. B. Struwe, D. J. Harvey, M. Marotta, R. M. Hickey, P. M. Rudd, *Glycobiology* **2011**, *21*, 1317–1330.

[81] J. Nilsson, *Glycoconj. J.* **2016**, *33*, 261–272.

[82] M. Pabst, F. Altmann, *Proteomics* **2011**, *11*, 631–643.

[83] L. Veillon, Y. Huang, W. Peng, X. Dong, B. G. Cho, Y. Mechref, *Electrophoresis* **2017**, *38*, 2100–2114.

[84] H. Yan, R. Yalagala, F. Yan, *Glycoconj. J.* **2015**, *32*, 559–574.

[85] D. J. Harvey, *Int. J. Mass Spectrom.* **2003**, *226*, 1–35.

[86] M. J. Kailemia, L. R. Ruhaak, C. B. Lebrilla, I. J. Amster, *Anal. Chem.* **2013**, *86*, 196–212.

[87] J. Zaia, *Chem. Biol.* **2008**, *15*, 881–892.

[88] B. Domon, C. E. Costello, *Glycoconj. J.* **1988**, *5*, 397–409.

[89] W. R. Alley, Y. Mechref, M. V. Novotny, *Rapid Commun. Mass Spectrom.* **2009**, *23*, 161–170.

[90] D. J. Harvey, *J. Am. Soc. Mass Spectrom.* **2005**, *16*, 622–630.

[91] D. J. Harvey, *J. Am. Soc. Mass Spectrom.* **2005**, *16*, 631–646.

[92] D. J. Harvey, *J. Am. Soc. Mass Spectrom.* **2005**, *16*, 647–659.

[93] D. J. Harvey, L. Royle, C. M. Radcliffe, P. M. Rudd, R. A. Dwek, *Anal. Biochem.* **2008**, *376*, 44–60.

[94] J. Zaia, *Mass Spectrom. Rev.* **2004**, *23*, 161–227.

[95] D. J. Harvey, *J. Mass Spectrom.* **2000**, *35*, 1178–1190.

[96] D. J. Harvey, R. H. Bateman, M. R. Green, *J. Mass Spectrom.* **1997**, *32*, 167–187.

[97] W. B. Struwe, C. Baldauf, J. Hofmann, P. M. Rudd, K. Pagel, *Chem. Commun.* **2016**, *52*, 12353–12356.

[98] Y. Mechref, M. V. Novotny, C. Krishnan, *Anal. Chem.* **2003**, *75*, 4895–4903.

[99] A. Kurimoto, O. Kanie, *Rapid Commun. Mass Spectrom.* **2007**, *21*, 2770–2778.

[100] N. Viseux, E. de Hoffmann, B. Domon, *Anal. Chem.* **1998**, *70*, 4951–4959.

[101] L. Han, C. E. Costello, *J. Am. Soc. Mass Spectrom.* **2011**, *22*, 997–1013.

[102] V. Reinhold, H. Zhang, A. Hanneman, D. Ashline, *Mol. Cell. Proteomics* **2013**, *12*, 866–873.

[103] C. Uetrecht, R. J. Rose, E. van Duijn, K. Lorenzen, A. J. R. Heck, *Chem. Soc. Rev.* **2010**, *39*, 1633–1655.

[104] Y. Huang, A. Gelb, E. Dodds, *Curr. Metabolomics* **2014**, *1*, 291–305.

[105] C. J. Gray, B. Thomas, R. Upton, L. G. Migas, C. E. Eyers, P. E. Barran, S. L. Flitsch, *Biochim. Biophys. Acta* **2016**, *1860*, 1688–1709.

[106] J. C. May, J. A. McLean, *Anal. Chem.* **2015**, *87*, 1422–1436.

[107] R. Cumeras, E. Figueras, C. E. Davis, J. I. Baumbach, I. Gracia, *Analyst* **2015**, *140*, 1376–1390.

[108] R. Cumeras, E. Figueras, C. E. Davis, J. I. Baumbach, I. Gracia, *Analyst* **2015**, *140*, 1391–1410.

[109] G. von Helden, M. T. Hsu, N. Gotts, M. T. Bowers, *J. Phys. Chem.* **1993**, *97*, 8182–8192.

[110] T. Wyttenbach, G. von Helden, M. T. Bowers, *J. Am. Chem. Soc.* **1996**, *118*, 8355–8364.

[111] S. Lee, T. Wyttenbach, M. T. Bowers, *Int. J. Mass Spectrom. Ion Process.* **1997**, *167*, 605–614.

[112] Y. Liu, D. E. Clemmer, *Anal. Chem.* **1997**, *69*, 2504–2509.

[113] C. S. Hoaglund, Y. Liu, A. D. Ellington, M. Pagel, D. E. Clemmer, *J. Am. Chem. Soc.* **1997**, *119*, 9051–9052.

[114] A. A. Shvartsburg, M. F. Jarrold, *Chem. Phys. Lett.* **1996**, *261*, 86–91.

[115] M. F. Mesleh, J. M. Hunter, A. A. Shvartsburg, G. C. Schatz, M. F. Jarrold, *J. Phys. Chem.* **1996**, *100*, 16082–16086.

[116] H. E. Revercomb, E. A. Mason, *Anal. Chem.* **1975**, *47*, 970–983.

[117] E. A. Mason, E. W. McDaniel, *Transport Properties of Ions in Gases*, Wiley-VCH Verlag GmbH & Co. KGaA, **1988**.

[118] J. C. May, J. A. McLean, *Int. J. Ion Mobil. Spectrom.* **2013**, *16*, 85–94.

[119] T. Wyttenbach, C. Bleiholder, M. T. Bowers, *Anal. Chem.* **2013**, *85*, 2191–2199.

[120] C. Bleiholder, N. R. Johnson, S. Contreras, T. Wyttenbach, M. T. Bowers, *Anal. Chem.* **2015**, *87*, 7196–7203.

[121] P. Dwivedi, B. Bendiak, B. H. Clowers, H. H. Hill, *J. Am. Soc. Mass Spectrom.* **2007**, *18*, 1163–1175.

[122] S. Warnke, J. Seo, J. Boschmans, F. Sobott, J. H. Scrivens, C. Bleiholder, M. T. Bowers, S. Gewinner, W. Schöllkopf, K. Pagel, G. von Helden, *J. Am. Chem. Soc.* **2015**, *137*, 4236–4242.

[123] B. H. Clowers, P. Dwivedi, W. E. Steiner, J. Hill, H. H., B. Bendiak, *J. Am. Soc. Mass Spectrom.* **2005**, *16*, 660–669.

[124] J. Ujma, K. Giles, M. Morris, P. E. Barran, *Anal. Chem.* **2016**, *88*, 9469–9478.

[125] S. I. Merenbloom, R. S. Glaskin, Z. B. Henson, D. E. Clemmer, *Anal. Chem.* **2009**, *81*, 1482–1487.

[126] J. F. de la Mora, S. Ude, B. A. Thomson, *Biotechnol. J.* **2006**, *1*, 988–997.

[127] M. Kliman, J. C. May, J. A. McLean, *Biochim. Biophys. Acta - Mol. Cell Biol. L.* **2011**, *1811*, 935–945.

[128] I. A. Buryakov, E. V. Krylov, E. G. Nazarov, U. K. Rasulev, *Int. J. Mass Spectrom. Ion Process.* **1993**, *128*, 143–148.

[129] R. Guevremont, *J. Chromatogr. A* **2004**, *1058*, 3–19.

[130] K. Giles, S. D. Pringle, K. R. Worthington, D. Little, J. L. Wildgoose, R. H. Bateman, *Rapid Commun. Mass Spectrom.* **2004**, *18*, 2401–2414.

[131] S. D. Pringle, K. Giles, J. L. Wildgoose, J. P. Williams, S. E. Slade, K. Thalassinos, R. H. Bateman, M. T. Bowers, J. H. Scrivens, *Int. J. Mass Spectrom.* **2007**, *261*, 1–12.

[132] A. A. Shvartsburg, R. D. Smith, *Anal. Chem.* **2008**, *80*, 9689–9699.

[133] F. Fernandez-Lima, D. A. Kaplan, J. Suetering, M. A. Park, *Int. J. Ion Mobil. Spectrom.* **2011**, *14*, 93–98.

[134] K. Michelmann, J. A. Silveira, M. E. Ridgeway, M. A. Park, *J. Am. Soc. Mass Spectrom.* **2015**, *26*, 14–24.

[135] J. A. Silveira, K. Michelmann, M. E. Ridgeway, M. A. Park, *J. Am. Soc. Mass Spectrom.* **2016**, *27*, 585–595.

[136] K. Thalassinos, M. Grabenauer, S. E. Slade, G. R. Hilton, M. T. Bowers, J. H. Scrivens, *Anal. Chem.* **2009**, *81*, 248–254.

[137] M. F. Bush, Z. Hall, K. Giles, J. Hoyes, C. V. Robinson, B. T. Ruotolo, *Anal. Chem.* **2010**, *82*, 9557–9565.

[138] M. F. Bush, I. D. Campuzano, C. V. Robinson, *Anal. Chem.* **2012**, *84*, 7124–7130.

[139] K. Pagel, D. J. Harvey, *Anal. Chem.* **2013**, *85*, 5138–5145.

[140] K. Giles, J. P. Williams, I. Campuzano, *Rapid Commun. Mass Spectrom.* **2011**, *25*, 1559–1566.

[141] X. Zhang, R. Knochenmuss, W. F. Siems, W. Liu, S. Graf, H. H. Hill, *Anal. Chem.* **2014**, *86*, 1661–1670.

[142] L. Konermann, E. Ahadi, A. D. Rodriguez, S. Vahidi, *Anal. Chem.* **2013**, *85*, 2–9.

[143] H. Hernandez, C. V. Robinson, *Nat. Protoc.* **2007**, *2*, 715–726.

[144] M. Wilm, M. Mann, *Anal. Chem.* **1996**, *68*, 1–8.

[145] W. Gabryelski, K. L. Froese, *J. Am. Soc. Mass Spectrom.* **2003**, *14*, 265–277.

[146] M. D. Plasencia, D. Isailovic, S. I. Merenbloom, Y. Mechref, D. E. Clemmer, *J. Am. Soc. Mass Spectrom.* **2008**, *19*, 1706–1715.

[147] C. W. N. Damen, W. B. Chen, A. B. Chakraborty, M. van Oosterhout, J. R. Mazzeo, J. C. Gebler, J. H. M. Schellens, H. Rosing, J. H. Beijnen, *J. Am. Soc. Mass Spectrom.* **2009**, *20*, 2021–2033.

[148] L. S. Fenn, J. A. McLean, *Phys. Chem. Chem. Phys.* **2011**, *13*, 2196–2205.

[149] S. M. Zucker, S. Lee, N. Webber, S. J. Valentine, J. P. Reilly, D. E. Clemmer, *J. Am. Soc. Mass Spectrom.* **2011**, *22*, 1477–1485.

[150] H. Li, K. Giles, B. Bendiak, K. Kaplan, W. F. Siems, H. H. Hill, *Anal. Chem.* **2012**, *84*, 3231–3239.

[151] F. Zhu, S. Lee, S. J. Valentine, J. P. Reilly, D. E. Clemmer, *J. Am. Soc. Mass Spectrom.* **2012**, *23*, 2158–2166.

[152] D. J. Harvey, C. A. Scarff, M. Crispin, C. N. Scanlan, C. Bonomelli, J. H. Scrivens, *J. Am. Soc. Mass Spectrom.* **2012**, *23*, 1955–1966.

[153] C. Lapthorn, F. Pullen, B. Z. Chowdhry, *Mass Spectrom. Rev.* **2013**, *32*, 43–71.

[154] S. Y. Vakhrushev, J. Langridge, I. Campuzano, C. Hughes, J. Peter-Katalinić, *Anal. Chem.* **2008**, *80*, 2506–2513.

[155] B. T. Ruotolo, J. L. Benesch, A. M. Sandercock, S. J. Hyung, C. V. Robinson, *Nat. Protoc.* **2008**, *3*, 1139–1152.

[156] A. Arcella, G. Portella, M. L. Ruiz, R. Eritja, M. Vilaseca, V. Gabelica, M. Orozco, *J. Am. Chem. Soc.* **2012**, *134*, 6596–6606.

[157] T. Patel, J. Bruce, A. Merry, C. Bigge, M. Wormald, R. Parekh, A. Jaques, *Biochemistry* **1993**, *32*, 679–693.

[158] D. R. Wing, T. W. Rademacher, M. C. Field, R. A. Dwek, B. Schmitz, G. Thor, M. Schachner, *Glycoconj. J.* **1992**, *9*, 293–301.

[159] D. Fu, L. Chen, R. A. O'Neill, *Carbohydr. Res.* **1994**, *261*, 173–186.

[160] E. D. Green, G. Adelt, J. U. Baenziger, S. Wilson, H. Van Halbeek, *J. Biol. Chem.* **1988**, *263*, 18253–18268.

[161] J. P. Kamerling, I. Rijkse, A. A. M. Maas, J. A. van Kuik, J. F. G. Vliegenthart, *FEBS Lett.* **1988**, *241*, 246–250.

[162] P. de Waard, A. Koorevaar, J. P. Kamerling, J. F. Vliegenthart, *J. Biol. Chem.* **1991**, *266*, 4237–4243.

[163] M. L. C. Da Silva, H. J. Stubbs, T. Tamura, K. G. Rice, *Arch. Biochem. Biophys.* **1995**, *318*, 465–475.

[164] D. J. Harvey, D. R. Wing, B. Küster, I. B. H. Wilson, *J. Am. Soc. Mass Spectrom.* **2000**, *11*, 564–571.

[165] A. M. Rashid, G. Saalbach, S. Bornemann, *Rapid Commun. Mass Spectrom.* **2014**, *28*, 191–199.

[166] R. Čmelík, M. Štikarovská, J. Chmelík, *J. Mass Spectrom.* **2004**, *39*, 1467–1473.

[167] D. Morsa, V. Gabelica, E. De Pauw, *Anal. Chem.* **2011**, *83*, 5775–5782.

[168] S. I. Merenbloom, T. G. Flick, E. R. Williams, *J. Am. Soc. Mass Spectrom.* **2012**, *23*, 553–562.

[169] S. J. Allen, A. M. Schwartz, M. F. Bush, *Anal. Chem.* **2013**, *85*, 12055–12061.

[170] Y. Huang, E. D. Dodds, *Anal. Chem.* **2013**, *85*, 9728–9735.

[171] R. F. Service, *Science* **2012**, *338*, 321–323.

[172] B. Domon, R. Aebersold, *Science* **2006**, *312*, 212–217.

[173] O. J. Plante, E. R. Palmacci, P. H. Seeberger, *Science* **2001**, *291*, 1523–1527.

[174] Z. Wang, Z. S. Chinoy, S. G. Ambre, W. Peng, R. McBride, R. P. de Vries, J. Glushka, J. C. Paulson, G.-J. Boons, *Science* **2013**, *341*, 379–383.

[175] T. J. Boltje, T. Buskas, G.-J. Boons, *Nat. Chem.* **2009**, *1*, 611–622.

[176] A. Dell, H. R. Morris, *Science* **2001**, *291*, 2351–2356.

[177] J. M. Prien, D. J. Ashline, A. J. Lapadula, H. Zhang, V. N. Reinhold, *J. Am. Soc. Mass Spectrom.* **2009**, *20*, 539–556.

[178] S. Daikoku, G. Widmalm, O. Kanie, *Rapid Commun. Mass Spectrom.* **2009**, *23*, 3713–3719.

[179] B. T. Ruotolo, K. Giles, I. Campuzano, A. M. Sandercock, R. H. Bateman, C. V. Robinson, *Science* **2005**, *310*, 1658–1661.

[180] C. Bleiholder, N. F. Dupuis, T. Wyttenbach, M. T. Bowers, *Nat. Chem.* **2011**, *3*, 172–177.

[181] P. Both, A. P. Green, C. J. Gray, R. Sardzik, J. Voglmeir, C. Fontana, M. Austeri, M. Rejzek, D. Richardson, R. A. Field, G. Widmalm, S. L. Flitsch, C. E. Eyers, *Nat. Chem.* **2014**, *6*, 65–74.

[182] J. Hofmann, H. S. Hahm, P. H. Seeberger, K. Pagel, *Nature* **2015**, *526*, 241–244.

[183] J. Hofmann, W. B. Struwe, C. A. Scarff, J. H. Scrivens, D. J. Harvey, K. Pagel, *Anal. Chem.* **2014**, *86*, 10789–10795.

102

[184] L. Kröck, D. Esposito, B. Castagner, C.-C. Wang, P. Bindschädler, P. H. Seeberger, *Chem. Sci.* **2012**, *3*, 1617–1622.

[185] P. Engel, E. Dabelsteen, D. Francis, N. Graem, *APMIS* **1996**, *104*, 741–749.

[186] R. B. Myers, S. Srivastava, W. E. Grizzle, *J. Urol.* **1995**, *153*, 1572–1574.

[187] J. Ogawa, A. Sano, H. Inoue, S. Koide, *Ann. Thorac. Surg.* **1995**, *59*, 412–415.

[188] D. J. Ashline, A. J. Hanneman, H. Zhang, V. N. Reinhold, *J. Am. Soc. Mass Spectrom.* **2014**, *25*, 444–453.

[189] P. H. Jensen, N. G. Karlsson, D. Kolarich, N. H. Packer, *Nat. Protoc.* **2012**, *7*, 1299–1310.

[190] H. Stockmann, R. O'Flaherty, B. Adamczyk, R. Saldova, P. M. Rudd, *Integr. Biol.* **2015**, *7*, 1026–1032.

[191] N. G. Karlsson, B. L. Schulz, N. H. Packer, *J. Am. Soc. Mass Spectrom.* **2004**, *15*, 659–672.

[192] A. V. Everest-Dass, D. Jin, M. Thaysen-Andersen, H. Nevalainen, D. Kolarich, N. H. Packer, *Glycobiology* **2012**, *22*, 1465–1479.

[193] M. Wuhrer, C. A. Koeleman, C. H. Hokke, A. M. Deelder, *Rapid Commun. Mass Spectrom.* **2006**, *20*, 1747–1754.

[194] D. J. Harvey, T. S. Mattu, M. R. Wormald, L. Royle, R. A. Dwek, P. M. Rudd, *Anal. Chem.* **2002**, *74*, 734–740.

[195] H. Hinneburg, J. Hofmann, W. B. Struwe, A. Thader, F. Altmann, D. Varón Silva, P. H. Seeberger, K. Pagel, D. Kolarich, *Chem. Commun.* **2016**, *52*, 4381–4384.

[196] H. L. Li, B. Bendiak, W. F. Siems, D. R. Gang, H. H. Hill, *Rapid Commun. Mass Spectrom.* **2013**, *27*, 2699–2709.

[197] M. M. Gaye, R. Kurulugama, D. E. Clemmer, *Analyst* **2015**, *140*, 6922–6932.

[198] Y. Huang, E. D. Dodds, *Anal. Chem.* **2015**, *87*, 5664–5668.

[199] G. R. Guile, D. J. Harvey, N. O'Donnell, A. K. Powell, A. P. Hunter, S. Zamze, D. L. Fernandes, R. A. Dwek, D. R. Wing, *Eur. J. Biochem.* **1998**, *258*, 623–656.

[200] W. B. Struwe, K. Pagel, J. L. P. Benesch, D. J. Harvey, M. P. Campbell, *Glycoconj. J.* **2016**, *33*, 399–404.

[201] W. B. Struwe, S. Agravat, K. F. Aoki-Kinoshita, M. P. Campbell, C. E. Costello, A. Dell, F. Ten, S. M. Haslam, N. G. Karlsson, K. H. Khoo, *et al.*, *Glycobiology* **2016**, *26*, 907–910.

[202] D. Kolarich, E. Rapp, W. B. Struwe, S. M. Haslam, J. Zaia, R. McBride, S. Agravat, M. P. Campbell, M. Kato, R. Ranzinger, C. Kettner, W. S. York, *Mol. Cell. Proteomics* **2013**, *12*, 991–995.

[203] A. S. Gelb, R. E. Jarratt, Y. Huang, E. D. Dodds, *Anal. Chem.* **2014**, *86*, 11396–11402.

[204] S. G. Penn, M. T. Cancilla, C. B. Lebrilla, *Anal. Chem.* **1996**, *68*, 2331–2339.

[205] M. E. Albertolle, M. E. Hassis, C. J. Ng, S. Cuison, K. Williams, A. Prakobphol, A. B. Dykstra, S. C. Hall, R. K. Niles, H. Ewa Witkowska, S. J. Fisher, *Clin. Proteomics* **2015**, *12*, 29.

[206] A. P. Burford-Mason, J. C. Weber, J. M. Willoughby, *J. Med. Vet. Mycol.* **1988**, *26*, 49–56.

[207] E. S. Shin, S. C. Chung, Y. K. Kim, S. W. Lee, H. S. Kho, *Oral. Surg. Oral. Med. O.* **2003**, *96*, 48–53.

[208] W. B. Struwe, J. L. Benesch, D. J. Harvey, K. Pagel, *Analyst* **2015**, *140*, 6799–6803.

[209] P. R. Crocker, J. C. Paulson, A. Varki, *Nat. Rev. Immunol.* **2007**, *7*, 255–266.

[210] A. Grigorian, S. Torossian, M. Demetriou, *Immunol. Rev.* **2009**, *230*, 232–246.

[211] R. Plomp, P. J. Hensbergen, Y. Rombouts, G. Zauner, I. Dragan, C. A. M. Koeleman, A. M. Deelder, M. Wuhrer, *J. Proteome Res.* **2014**, *13*, 536–546.

[212] K.-T. C. Shade, B. Platzer, N. Washburn, V. Mani, Y. C. Bartsch, M. Conroy, J. D. Pagan, C. Bosques, T. R. Mempel, E. Fiebiger, R. M. Anthony, *J. Exp. Med.* **2015**, *212*, 457–467.

[213] H. Hinneburg, K. Stavenhagen, U. Schweiger-Hufnagel, S. Pengelley, W. Jabs, P. H. Seeberger, D. V. Silva, M. Wuhrer, D. Kolarich, *J. Am. Soc. Mass Spectrom.* **2016**, *27*, 507–519.

[214] J. Stadlmann, M. Pabst, F. Altmann, *J. Clin. Immunol.* **2010**, *30*, 15–19.

[215] I. Loke, N. H. Packer, M. Thaysen-Andersen, *Biomolecules* **2015**, *5*, 1832–1854.

[216] K. Stavenhagen, R. Plomp, M. Wuhrer, *Anal. Chem.* **2015**, *87*, 11691–11699.

[217] A. J. Creese, H. J. Cooper, *Anal. Chem.* **2012**, *84*, 2597–2601.

[218] C. Piontek, D. Varón Silva, C. Heinlein, C. Pöhner, S. Mezzato, P. Ring, A. Martin, F. Schmid, C. Unverzagt, *Angew. Chem. Int. Ed.* **2009**, *48*, 1941–1945.

[219] K. Stavenhagen, H. Hinneburg, M. Thaysen-Andersen, L. Hartmann, D. V. Silva, J. Fuchser, S. Kaspar, E. Rapp, P. H. Seeberger, D. Kolarich, *J. Mass Spectrom.* **2013**, *48*, 627–639.

[220] D. Kolarich, P. H. Jensen, F. Altmann, N. H. Packer, *Nat. Protoc.* **2012**, *7*, 1285–1298.

[221] D. Kolarich, A. Weber, M. Pabst, J. Stadlmann, W. Teschner, H. Ehrlich, H.-P. Schwarz, F. Altmann, *Proteomics* **2008**, *8*, 254–263.

[222] R. M. Anthony, F. Nimmerjahn, D. J. Ashline, V. N. Reinhold, J. C. Paulson, J. V. Ravetch, *Science* **2008**, *320*, 373–376.

[223] D. Kolarich, A. Weber, P. L. Turecek, H.-P. Schwarz, F. Altmann, *Proteomics* **2006**, *6*, 3369–3380.

[224] M. Thaysen-Andersen, M. R. Larsen, N. H. Packer, G. Palmisano, *RSC Advances* **2013**, *3*, 22683–22705.

[225] H. Sasaki, N. Ochi, A. Dell, M. Fukuda, *Biochemistry* **1988**, *27*, 8618–8626.

[226] T. Yamagaki, A. Sato, *Anal. Sci.* **2009**, *25*, 985–988.

[227] X. Zheng, X. Zhang, N. S. Schocker, R. S. Renslow, D. J. Orton, J. Khamsi, R. A. Ashmus, I. C. Almeida, K. Tang, C. E. Costello, R. D. Smith, K. Michael, E. S. Baker, *Anal. Bioanal. Chem.* **2017**, *409*, 467–476.

[228] J. Hofmann, K. Pagel, *Angew. Chem. Int. Ed.* **2017**, *56*, 8342–8349.

[229] M. P. Campbell, R. Peterson, J. Mariethoz, E. Gasteiger, Y. Akune, K. F. Aoki-Kinoshita, F. Lisacek, N. H. Packer, *Nucleic Acids Res.* **2014**, *42*, D215–D221.

[230] D. J. Harvey, F. Sobott, M. Crispin, A. Wrobel, C. Bonomelli, S. Vasiljevic, C. N. Scanlan, C. A. Scarff, K. Thalassinos, J. H. Scrivens, *J. Am. Soc. Mass Spectrom.* **2011**, *22*, 568–581.

[231] M. Sarbu, F. F. Zhu, J. Peter-Katalinic, D. E. Clemmer, A. D. Zamfir, *Rapid Commun. Mass Spectrom.* **2015**, *29*, 1929–1937.

[232] H. Li, B. Bendiak, W. F. Siems, D. R. Gang, J. Hill, H. H., *Int. J. Ion Mobil. Spectrom.* **2013**, *16*, 105–115.

[233] J. P. Simons, R. A. Jockusch, P. ÇarÇabal, I. Hünig, R. T. Kroemer, N. A. Macleod, L. C. Snoek, *Int. Rev. Phys. Chem.* **2005**, *24*, 489–531.

[234] E. Mucha, A. I. González Flórez, M. Marianski, D. A. Thomas, W. Hoffmann, W. B. Struwe, H. S. Hahm, S. Gewinner, W. Schöllkopf, P. H. Seeberger, G. von Helden, K. Pagel, *Angew. Chem. Int. Ed.* **2017**, *65*, 11248–11251.

[235] M. Marianski, A. Supady, T. Ingram, M. Schneider, C. Baldauf, *J. Chem. Theory Comput.* **2016**, *12*, 6157–6168.

[236] K. N. Kirschner, A. B. Yongye, S. M. Tschampel, J. González-Outeiriño, C. R. Daniels, B. L. Foley, R. J. Woods, *J. Comput. Chem.* **2008**, *29*, 622–655.

Appendix

Table 7.1: Absolute ^{DT}CCSs of desialylated fetuin glycans and their fragments. The composition of the ions is given by the number of hexoses (H), N-acetylated hexose (N), and sialic acids (S). Native glycan structures (intact ions) are indicated in bold.

type	H	N	S	m/z	z	MW in Da	CCS$_{He}$ in Å^2	CCS$_{N2}$ in Å^2
[M‑H]$^-$	2	1	0	406.14	1	406.14	111.64	174.37
[M‑H]$^-$	2	1	0	526.18	1	526.18	124.57	188.18
[M‑H]$^-$	3	1	0	602.19	1	602.19	137.78	201.29
[M‑H]$^-$	2	1	1	673.23	1	673.23	173.76	247.58
[M‑H]$^-$	2	1	1	715.24	1	715.24	167.86	238.53
[M‑H]$^-$	3	2	0	845.30	1	845.30	183.60	262.44
[M‑H]$^-$	2	2	1	1038.36	1	1038.36	226.62	310.09
[M + H$_2$PO$_4$]$^-$	**5**	**4**	**0**	**1737.56**	**1**	**1737.56**	**302.62**	**396.59**
[M‑H]$^-$	**6**	**5**	**1**	**1930.68**	**1**	**1930.68**	**337.78**	**429.95**
[M + H$_2$PO$_4$]$^-$	**6**	**5**	**0**	**2102.69**	**1**	**2102.69**	**343.21**	**434.21**
[M‑H]$^-$	**6**	**5**	**1**	**2295.81**	**1**	**2295.81**	**371.84**	**466.54**
[M + 2H$_2$PO$_4$]$^{2-}$	**5**	**4**	**0**	**917.27**	**2**	**1834.53**	**298.28**	**401.55**
[M‑H + H$_2$PO$_4$]$^{2-}$	**5**	**4**	**1**	**1013.82**	**2**	**2027.65**	**330.24**	**435.87**
[M + 2H$_2$PO$_4$]$^{2-}$	**6**	**5**	**0**	**1099.83**	**2**	**2199.66**	**336.65**	**444.31**
[M‑2H]$^{2-}$	**5**	**4**	**2**	**1110.38**	**2**	**2220.77**	**361.75**	**473.29**
[M‑H + H$_2$PO$_4$]$^{2-}$	**6**	**5**	**1**	**1196.39**	**2**	**2392.78**	**367.99**	**479.90**
[M‑2H]$^{2-}$	**6**	**5**	**2**	**1292.95**	**2**	**2585.90**	**401.28**	**519.36**
[M‑2H]$^{2-}$	**6**	**5**	**3**	**1438.50**	**2**	**2877.00**	**437.89**	**556.48**
[M‑3H]$^{3-}$	**6**	**5**	**3**	**958.66**	**3**	**2875.99**	**430.42**	**558.53**

Table 7.2: Absolute ^{DT}CCSs of desialylated thyrogloblin glycans and their fragments. Native glycan structures (intact ions) are indicated in bold. frag - glycan fragment, Fuc - fucose, GlcNAc - N-acetylglucosamine, H - hexose, Man - mannose, N - N-acetylated hexose, S - sialic acid.

type	structure	m/z	z	MW (Da)	CCS$_{He}$ (Å^2)	CCS$_{N2}$ (Å^2)
[M‑H]$^-$	frag	332.10	1	332.10	105.60	170.63
[M‑H]$^-$	frag	350.11	1	350.11	107.65	172.22
[M‑H]$^-$	frag	388.12	1	388.12	107.73	169.62
[M‑H]$^-$	frag	406.14	1	406.14	110.64	172.52
[M‑H]$^-$	frag	448.15	1	448.15	121.80	183.45
[M‑H]$^-$	frag	462.16	1	462.16	126.09	192.56
[M‑H]$^-$	frag	470.15	1	470.15	130.52	195.49
[M‑H]$^-$	frag	480.17	1	480.17	124.93	186.43
[M‑H]$^-$	frag	624.21	1	624.21	149.26	220.13
[M‑H]$^-$	frag	639.23	1	639.23	146.77	213.27
[M‑H]$^-$	frag	642.23	1	642.23	151.88	222.06
[M‑H]$^-$	frag	673.23	1	673.23	172.09	245.11
[M‑H]$^-$	frag	835.28	1	835.28	194.14	271.63
[M‑H]$^-$	frag	845.30	1	845.30	184.58	262.20

type	structure	m/z	z	MW (Da)	CCS_{He} (Å^2)	CCS_{N2} (Å^2)
[M - H]$^-$	frag	929.33	1	929.33	211.15	295.81
[M - H]$^-$	frag	1091.38	1	1091.38	232.83	320.52
[M - H]$^-$	frag	1153.38	1	1153.38	234.59	319.83
[M + H$_2$PO$_4$]$^-$	**Man$_4$GlcNAc$_2$**	**1169.35**	**1**	**1169.35**	**234.20**	**321.18**
[M - H]$^-$	frag	1269.43	1	1269.43	261.47	337.41
[M + H$_2$PO$_4$]$^-$	**Man$_5$GlcNAc$_2$**	**1331.40**	**1**	**1331.40**	**265.95**	**350.63**
[M - H]$^-$	frag	1396.46	1	1396.46	285.76	366.83
[M - H]$^-$	frag	1431.49	1	1431.49	286.37	369.68
[M + H$_2$PO$_4$]$^-$	**Man$_6$GlcNAc$_2$**	**1493.46**	**1**	**1493.46**	**291.85**	**374.88**
[M - H]$^-$	frag	1500.50	1	1500.50	293.18	378.03
[M - H]$^-$	frag	1516.51	1	1516.51	295.66	380.40
[M + H$_2$PO$_4$]$^-$	**H$_4$N$_3$Fuc**	**1518.47**	**1**	**1518.47**	**293.80**	**377.26**
[M - H]$^-$	frag	1524.52	1	1524.52	301.97	387.10
[M - H]$^-$	frag	1593.54	1	1593.54	307.80	392.24
[M + H$_2$PO$_4$]$^-$	**Man$_7$GlcNAc$_2$**	**1655.51**	**1**	**1655.51**	**312.34**	**396.23**
[M - H]$^-$	frag	1703.58	1	1703.58	323.74	409.46
[M - H]$^-$	**S$_1$H$_4$N$_3$Fuc**	**1711.61**	**1**	**1711.61**	**320.49**	**408.35**
[M + H$_2$PO$_4$]$^-$	**H$_4$N$_4$Fuc**	**1721.57**	**1**	**1721.57**	**321.78**	**405.75**
[M + H$_2$PO$_4$]$^-$	**Man$_8$GlcNAc$_2$**	**1817.56**	**1**	**1817.56**	**332.71**	**421.46**
[M + H$_2$PO$_4$]$^-$	**H$_5$N$_4$Fuc**	**1883.62**	**1**	**1883.62**	**338.31**	**426.18**
[M - H]$^-$	**SH$_4$N$_4$Fuc**	**1914.69**	**1**	**1914.69**	**352.59**	**441.11**
[M + H$_2$PO$_4$]$^-$	**Man$_9$GlcNAc$_2$**	**1979.61**	**1**	**1979.61**	**352.40**	**441.72**
[M + H$_2$PO$_4$]$^-$	**H$_6$N$_4$Fuc**	**2045.67**	**1**	**2045.67**	**356.90**	**446.61**
[M - H]$^-$	**S$_1$H$_5$N$_4$Fuc**	**2076.74**	**1**	**2076.74**	**372.37**	**462.23**
[M - 2H]$^{2-}$	frag	778.77	2	1557.55	269.05	372.54
[M - 2H]$^{2-}$	frag	787.77	2	1575.55	274.39	372.89
[M - 2H]$^{2-}$	frag	827.79	2	1655.58	279.92	379.88
[M - 2H]$^{2-}$	frag	837.29	2	1674.58	286.51	388.32
[M - 2H]$^{2-}$	frag	848.78	2	1697.57	282.27	383.72
[M - 2H]$^{2-}$	frag	857.80	2	1715.60	283.00	387.36
[M - 2H]$^{2-}$	frag	860.31	2	1720.62	285.38	388.70
[M - 2H]$^{2-}$	frag	890.82	2	1781.64	292.05	394.88
[M - 2H]$^{2-}$	frag	938.83	2	1877.66	307.40	408.09
[M - 2H]$^{2-}$	frag	941.32	2	1882.64	304.82	406.26
[M - 2H]$^{2-}$	frag	972.34	2	1944.67	315.48	416.62
[M - 2H]$^{2-}$	frag	978.34	2	1956.67	323.65	427.01
[M - 2H]$^{2-}$	frag	981.34	2	1962.67	311.78	414.97
[M - 2H]$^{2-}$	frag	990.34	2	1980.68	311.77	414.15
[M - 2H]$^{2-}$	frag	1001.36	2	2002.71	313.80	416.09
[M - 2H]$^{2-}$	frag	1005.86	2	2011.72	324.56	429.32
[M - 2H]$^{2-}$	frag	1011.35	2	2022.69	320.48	423.13
[M - 2H]$^{2-}$	frag	1013.85	2	2027.71	326.60	430.58
[M - 2H]$^{2-}$	frag	1071.37	2	2142.74	332.07	435.98
[M - 2H]$^{2-}$	frag	1183.41	2	2366.83	374.28	482.71

Table 7.3: Absolute ^{DT}CCSs of ribonuclease B glycans and their fragments. Native glycan structures (intact ions) are indicated in bold. frag - glycan fragment, GlcNAc - N-acetylglucosamine, Man - mannose.

type	structure	m/z	z	MW (Da)	CCS$_{He}$ (Å^2)	CCS$_{N2}$ (Å^2)
[M - H]$^-$	frag	425.13	1	425.13	132.07	194.10
[M - H]$^-$	frag	526.18	1	526.18	148.15	213.87
[M - H]$^-$	frag	575.18	1	575.18	144.19	211.43
[M - H]$^-$	frag	586.20	1	586.20	146.28	213.37
[M - H]$^-$	frag	601.20	1	601.20	139.53	207.65
[M - H]$^-$	frag	624.21	1	624.21	148.74	215.91
[M - H]$^-$	frag	629.19	1	629.19	144.97	215.96
[M - H]$^-$	frag	647.20	1	647.20	148.35	219.41
[M - H]$^-$	frag	748.25	1	748.25	168.40	247.42
[M - H]$^-$	frag	763.25	1	763.25	164.42	237.49
[M - H]$^-$	frag	775.26	1	775.26	197.08	283.63
[M + H$_2$PO$_4$]$^-$	**Man$_2$GlcNAc$_2$**	**845.24**	**1**	845.24	**178.75**	**253.89**
[M - H]$^-$	frag	869.28	1	869.28	190.85	271.45
[M - H]$^-$	frag	929.30	1	929.30	210.12	290.76
[M + H$_2$PO$_4$]$^-$	**Man$_3$GlcNAc$_2$**	**1007.30**	**1**	1007.30	**201.92**	**281.11**
[M - H]$^-$	frag	1072.36	1	1072.36	218.89	302.20
[M - H]$^-$	frag	1091.35	1	1091.35	231.09	313.29
[M - H]$^-$	frag	1114.37	1	1114.37	228.62	311.36
[M - H]$^-$	frag	1128.38	1	1128.38	225.50	306.31
[M - H]$^-$	frag	1132.38	1	1132.38	233.21	315.33
[M + H$_2$PO$_4$]$^-$	**Man$_4$GlcNAc$_2$**	**1169.35**	**1**	1169.35	**233.57**	**313.81**
[M - H]$^-$	frag	1269.43	1	1269.43	260.59	338.59
[M - H]$^-$	frag	1276.42	1	1276.42	260.05	338.64
[M - H]$^-$	frag	1294.43	1	1294.43	261.58	341.13
[M - H]$^-$	frag	1313.43	1	1313.43	263.43	341.64
[M + H$_2$PO$_4$]$^-$	**Man$_5$GlcNAc$_2$**	**1331.40**	**1**	1331.40	**263.19**	**343.86**
[M - H]$^-$	frag	1431.48	1	1431.48	290.10	365.65
[M - H]$^-$	frag	1438.47	1	1438.47	295.76	371.19
[M - H]$^-$	frag	1475.51	1	1475.51	291.12	368.99
[M + H$_2$PO$_4$]$^-$	**Man$_6$GlcNAc$_2$**	**1493.46**	**1**	1493.46	**291.94**	**369.99**
[M - H]$^-$	frag	1558.52	1	1558.52	310.10	388.77
[M + H$_2$PO$_4$]$^-$	**Man$_7$GlcNAc$_2$**	**1655.51**	**1**	1655.51	**313.28**	**396.13**
[M - H]$^-$	frag	1678.56	1	1678.56	317.20	396.25
[M - H]$^-$	frag	1720.57	1	1720.57	332.73	411.89
[M + H$_2$PO$_4$]$^-$	**Man$_8$GlcNAc$_2$**	**1817.56**	**1**	1817.56	**338.74**	**423.22**
[M + H$_2$PO$_4$]$^-$	**Man$_9$GlcNAc$_2$**	**1979.61**	**1**	1979.61	**356.13**	**443.14**
[M - 2H]$^{2-}$	frag	598.69	2	1197.38	234.71	333.37
[M - 2H]$^{2-}$	frag	700.23	2	1400.46	254.25	356.06
[M - 2H]$^{2-}$	frag	714.23	2	1428.47	244.53	349.02
[M - 2H]$^{2-}$	frag	758.24	2	1516.48	262.41	365.58

type	structure	m/z	z	MW (Da)	CCS$_{He}$ (Å^2)	CCS$_{N2}$ (Å^2)
[M‑2H]$^{2-}$	frag	782.76	2	1565.51	268.33	374.87
[M‑2H]$^{2-}$	frag	795.26	2	1590.52	268.16	370.76
[M‑2H]$^{2-}$	frag	827.28	2	1654.56	279.12	378.99

Table 7.4: Absolute ^{DT}CCSs of ovalbumin glycans and their fragments. Native glycan structures (intact ions) are indicated in bold. frag - glycan fragment, GlcNAc - N-acetylglucosamine, H - hexose, Man - mannose, N - N-acetylated hexose, S - sialic acid.

type	structure	m/z	z	MW (Da)	CCS$_{He}$ (Å^2)	CCS$_{N2}$ (Å^2)
[M‑H]$^{-}$	frag	424.15	1	424.15	123.61	188.74
[M‑H]$^{-}$	frag	470.15	1	470.15	130.76	196.67
[M‑H]$^{-}$	frag	493.17	1	493.17	142.51	207.85
[M‑H]$^{-}$	frag	507.18	1	507.18	142.29	206.46
[M‑H]$^{-}$	frag	508.17	1	508.17	138.13	204.82
[M‑H]$^{-}$	frag	602.19	1	602.19	145.40	213.47
[M‑H]$^{-}$	frag	605.22	1	605.22	147.11	216.09
[M‑H]$^{-}$	frag	629.19	1	629.19	149.19	219.24
[M‑H]$^{-}$	frag	647.20	1	647.20	155.76	226.69
[M‑H]$^{-}$	frag	665.21	1	665.21	158.23	230.36
[M‑H]$^{-}$	frag	669.24	1	669.24	165.67	237.69
[M‑H]$^{-}$	frag	673.23	1	673.23	170.35	243.59
[M‑H]$^{-}$	frag	683.25	1	683.25	160.59	232.73
[M‑H]$^{-}$	frag	703.23	1	703.23	168.52	239.08
[M‑H]$^{-}$	frag	711.25	1	711.25	177.90	251.69
[M‑H]$^{-}$	frag	748.25	1	748.25	168.65	241.95
[M‑H]$^{-}$	frag	751.25	1	751.25	181.81	254.25
[M‑H]$^{-}$	frag	770.28	1	770.28	174.31	252.08
[M‑H]$^{-}$	frag	790.26	1	790.26	175.26	252.90
[M‑H]$^{-}$	frag	808.27	1	808.27	182.64	261.62
[M‑H]$^{-}$	frag	827.29	1	827.29	188.38	267.09
[M‑H]$^{-}$	frag	835.28	1	835.28	189.75	268.93
[M‑H]$^{-}$	frag	845.30	1	845.30	182.55	257.34
[M‑H]$^{-}$	frag	850.28	1	850.28	188.07	269.53
[M‑H]$^{-}$	frag	869.28	1	869.28	196.58	276.24
[M‑H]$^{-}$	frag	876.31	1	876.31	197.40	275.85
[M‑H]$^{-}$	frag	891.31	1	891.31	191.78	273.47
[M‑H]$^{-}$	frag	914.33	1	914.33	214.18	292.70
[M‑H]$^{-}$	frag	929.33	1	929.33	213.69	294.42
[M‑H]$^{-}$	frag	951.33	1	951.33	203.65	284.09
[M‑H]$^{-}$	frag	964.33	1	964.33	215.19	285.64
[M‑H]$^{-}$	frag	970.35	1	970.35	212.77	292.79
[M‑H]$^{-}$	frag	993.34	1	993.34	211.57	292.38
[M+H$_2$PO$_4$]$^{-}$	**Man$_3$GlcNAc$_2$**	**1007.30**	**1**	**1007.30**	**200.89**	**283.67**

type	structure	m/z	z	MW (Da)	CCS_{He} (Å^2)	CCS_{N2} (Å^2)
[M - H]$^-$	frag	1011.35	1	1011.35	215.33	294.85
[M - H]$^-$	frag	1038.36	1	1038.36	222.49	306.37
[M - H]$^-$	frag	1049.38	1	1049.38	212.39	295.42
[M - H]$^-$	frag	1053.36	1	1053.36	231.82	299.46
[M - H]$^-$	frag	1072.36	1	1072.36	224.61	308.57
[M - H]$^-$	frag	1091.38	1	1091.38	234.55	316.88
[M + H$_2$PO$_4$]$^-$	**Man$_4$GlcNAc$_2$**	**1169.35**	**1**	**1169.35**	**231.67**	**317.18**
[M - H]$^-$	frag	1192.43	1	1192.43	240.93	324.47
[M - H]$^-$	frag	1196.42	1	1196.42	245.82	329.02
[M + H$_2$PO$_4$]$^-$	**Man$_3$GlcNAc$_3$**	**1210.38**	**1**	**1210.38**	**236.60**	**324.09**
[M - H]$^-$	frag	1234.45	1	1234.45	252.89	335.74
[M - H]$^-$	frag	1256.44	1	1256.44	259.24	340.30
[M - H]$^-$	frag	1294.46	1	1294.46	264.82	345.30
[M - H]$^-$	frag	1316.46	1	1316.46	270.54	351.94
[M + H$_2$PO$_4$]$^-$	**Man$_5$GlcNAc$_2$**	**1331.40**	**1**	**1331.40**	**265.34**	**348.74**
[M - H]$^-$	frag	1354.48	1	1354.48	269.12	349.83
[M - H]$^-$	frag	1357.49	1	1357.49	279.61	359.92
[M + H$_2$PO$_4$]$^-$	**Man$_4$GlcNAc$_3$**	**1372.43**	**1**	**1372.43**	**259.19**	**347.54**
[M - H]$^-$	frag	1395.51	1	1395.51	279.44	362.43
[M - H]$^-$	frag	1399.50	1	1399.50	283.38	364.28
[M + H$_2$PO$_4$]$^-$	**Man$_3$GlcNAc$_4$**	**1413.46**	**1**	**1413.46**	**273.95**	**357.93**
[M - H]$^-$	frag	1455.54	1	1455.54	285.99	367.84
[M - H]$^-$	frag	1478.52	1	1478.52	289.47	373.07
[M + H$_2$PO$_4$]$^-$	**Man$_6$GlcNAc$_2$**	**1493.46**	**1**	**1493.46**	**299.54**	**380.46**
[M - H]$^-$	frag	1516.53	1	1516.53	294.74	375.22
[M - H]$^-$	frag	1519.54	1	1519.54	304.01	385.74
[M + H$_2$PO$_4$]$^-$	**Man$_5$GlcNAc$_3$**	**1534.48**	**1**	**1534.48**	**297.38**	**380.72**
[M - H]$^-$	frag	1557.56	1	1557.56	300.41	385.42
[M - H]$^-$	frag	1560.57	1	1560.57	311.08	393.42
[M - H]$^-$	frag	1565.57	1	1565.57	304.52	387.19
[M + H$_2$PO$_4$]$^-$	**Man$_4$GlcNAc$_4$**	**1575.51**	**1**	**1575.51**	**293.67**	**378.23**
[M - H]$^-$	frag	1598.58	1	1598.58	310.22	391.28
[M + H$_2$PO$_4$]$^-$	**Man$_3$GlcNAc$_5$**	**1616.54**	**1**	**1616.54**	**309.25**	**392.05**
[M - H]$^-$	frag	1636.57	1	1636.57	314.78	397.73
[M - H]$^-$	frag	1640.57	1	1640.57	320.43	404.15
[M + H$_2$PO$_4$]$^-$	**Man$_7$GlcNAc$_2$**	**1655.51**	**1**	**1655.51**	**316.61**	**402.30**
[M - H]$^-$	frag	1678.60	1	1678.60	315.10	400.86
[M - H]$^-$	frag	1681.60	1	1681.60	323.90	408.21
[M + H$_2$PO$_4$]$^-$	**Man$_6$GlcNAc$_3$**	**1737.56**	**1**	**1737.56**	**320.13**	**405.62**
[M - H]$^-$	frag	1757.64	1	1757.64	330.77	416.51
[M - H]$^-$	frag	1763.65	1	1763.65	339.98	425.79
[M - H]$^-$	frag	1768.65	1	1768.65	330.98	418.68
[M + H$_2$PO$_4$]$^-$	**Man$_4$GlcNAc$_5$**	**1778.59**	**1**	**1778.59**	**327.93**	**414.03**
[M + H$_2$PO$_4$]$^-$	**Man$_3$GlcNAc$_6$**	**1819.61**	**1**	**1819.61**	**337.04**	**422.96**
[M - H]$^-$	frag	1861.65	1	1861.65	344.54	429.35

type	structure	m/z	z	MW (Da)	CCS_{He} (Å²)	CCS_{N2} (Å²)
[M - H]⁻	frag	1919.69	1	1919.69	350.28	436.53
[M - H]⁻	frag	1925.70	1	1925.70	356.48	443.07
[M + H₂PO₄]⁻	**Man₅GlcNAc₅**	**1940.64**	**1**	**1940.64**	**344.03**	**432.02**
[M + H₂PO₄]⁻	**Hex₄GlcNAc₆**	**1981.67**	**1**	**1981.67**	**353.59**	**441.39**
[M + H₂PO₄]⁻	**Man₃GlcNAc₇**	**2022.69**	**1**	**2022.69**	**359.98**	**447.68**
[M + H₂PO₄]⁻	**Hex₆GlcNAc₅**	**2102.69**	**1**	**2102.69**	**365.23**	**455.20**
[M - H]⁻	**SH₄N₆**	**2174.79**	**1**	**2174.79**	**380.63**	**471.23**
[M + H₂PO₄]⁻	**Hex₄GlcNAc₇**	**2184.75**	**1**	**2184.75**	**376.73**	**467.74**
[M + H₂PO₄]⁻	**Man₃GlcNAc₈**	**2225.77**	**1**	**2225.77**	**385.38**	**472.16**
[M + H₂PO₄]⁻	**Hex₅GlcNAc₇**	**2387.83**	**1**	**2387.83**	**400.20**	**486.24**
[M - 2H]²⁻	frag	446.14	2	892.27	201.85	302.32
[M - 2H]²⁻	frag	468.65	2	937.29	213.21	314.00
[M - 2H]²⁻	frag	489.16	2	978.32	198.76	291.94
[M - 2H]²⁻	frag	496.66	2	993.32	215.05	315.12
[M - 2H]²⁻	frag	523.20	2	1046.39	202.32	299.38
[M - 2H]²⁻	frag	558.69	2	1117.38	215.80	315.49
[M - 2H]²⁻	frag	573.70	2	1147.39	223.59	323.20
[M - 2H]²⁻	frag	651.21	2	1302.42	240.76	340.25
[M - 2H]²⁻	frag	656.72	2	1313.44	241.96	341.59
[M - 2H]²⁻	frag	679.23	2	1358.45	252.60	352.79
[M - 2H]²⁻	frag	707.24	2	1414.48	254.67	356.04
[M - 2H]²⁻	frag	711.25	2	1422.49	259.88	362.23
[M - 2H]²⁻	frag	715.26	2	1430.52	260.79	360.27
[M - 2H]²⁻	frag	727.27	2	1454.53	259.50	360.18
[M - 2H]²⁻	frag	741.26	2	1482.51	263.14	363.62
[M - 2H]²⁻	frag	755.26	2	1510.52	260.85	363.10
[M - 2H]²⁻	frag	758.26	2	1516.52	267.55	368.25
[M - 2H]²⁻	frag	808.29	2	1616.58	279.40	379.21
[M - 2H]²⁻	frag	849.80	2	1699.61	291.19	393.46
[M - 2H]²⁻	frag	878.32	2	1756.63	292.92	396.43
[M - 2H]²⁻	frag	1011.37	2	2022.74	328.01	434.41

Table 7.5: Absolute ^{DT}CCSs of dextran in positive-ion mode.

Glcₙ	type	m/z	z	MW (Da)	CCS_{He} (Å²)	CCS_{N2} (Å²)
2	[M + Na]⁺	365.11	1	365.11	104.14	179.54
3	[M + Na]⁺	527.16	1	527.16	137.08	215.00
4	[M + Na]⁺	689.21	1	689.21	165.14	243.36
5	[M + Na]⁺	851.26	1	851.26	193.98	273.81
6	[M + Na]⁺	1013.32	1	1013.32	218.85	302.06
7	[M + Na]⁺	1175.37	1	1175.37	243.88	330.94
8	[M + Na]⁺	1337.42	1	1337.42	266.22	355.80
9	[M + Na]⁺	1499.48	1	1499.48	285.99	377.70

Glc$_n$	type	m/z	z	MW (Da)	CCS$_{He}$ (Å^2)	CCS$_{N2}$ (Å^2)
10	[M + Na]$^+$	1661.53	1	1661.53	305.92	397.83
11	[M + Na]$^+$	1823.58	1	1823.58	317.98	412.59
12	[M + Na]$^+$	1985.63	1	1985.63	334.78	425.53
13	[M + Na]$^+$	2147.69	1	2147.69	348.25	-
7	[M + 2Na]$^{2+}$	599.18	2	1198.36	220.16	346.31
8	[M + 2Na]$^{2+}$	680.21	2	1360.41	240.27	365.60
9	[M + 2Na]$^{2+}$	761.23	2	1522.47	264.49	385.24
10	[M + 2Na]$^{2+}$	842.26	2	1684.52	283.52	401.29
11	[M + 2Na]$^{2+}$	923.29	2	1846.57	295.42	409.25
12	[M + 2Na]$^{2+}$	1004.31	2	2008.62	321.83	435.20
13	[M + 2Na]$^{2+}$	1085.34	2	2170.68	332.96	447.36
14	[M + 2Na]$^{2+}$	1166.36	2	2332.73	354.59	467.39
15	[M + 2Na]$^{2+}$	1247.39	2	2494.78	375.00	487.45
16	[M + 2Na]$^{2+}$	1328.42	2	2656.84	391.96	507.44
17	[M + 2Na]$^{2+}$	1409.44	2	2818.89	407.05	525.79
18	[M + 2Na]$^{2+}$	1490.47	2	2980.94	425.99	543.68
19	[M + 2Na]$^{2+}$	1571.50	2	3142.99	442.33	562.36
20	[M + 2Na]$^{2+}$	1652.52	2	3305.05	458.91	578.02
21	[M + 2Na]$^{2+}$	1733.55	2	3467.10	476.60	596.18
22	[M + 2Na]$^{2+}$	1814.58	2	3629.15	490.71	613.29
23	[M + 2Na]$^{2+}$	1895.60	2	3791.21	505.91	629.91
24	[M + 2Na]$^{2+}$	1976.63	2	3953.26	520.73	638.94
25	[M + 2Na]$^{2+}$	2057.66	2	4115.31	535.68	656.94
11	[M + 3Na]$^{3+}$	623.19	3	1869.56	302.41	-
13	[M + 3Na]$^{3+}$	731.22	3	2193.67	332.32	-
14	[M + 3Na]$^{3+}$	785.24	3	2355.72	347.27	508.41
15	[M + 3Na]$^{3+}$	839.26	3	2517.77	360.36	518.99
16	[M + 3Na]$^{3+}$	893.28	3	2679.83	374.82	524.52
17	[M + 3Na]$^{3+}$	947.29	3	2841.88	384.42	543.40
18	[M + 3Na]$^{3+}$	1001.31	3	3003.93	395.48	556.58
19	[M + 3Na]$^{3+}$	1055.33	3	3165.98	418.50	566.19
20	[M + 3Na]$^{3+}$	1109.35	3	3328.04	436.53	584.83
21	[M + 3Na]$^{3+}$	1163.36	3	3490.09	444.57	600.08
22	[M + 3Na]$^{3+}$	1217.38	3	3652.14	470.84	613.48
23	[M + 3Na]$^{3+}$	1271.40	3	3814.19	488.04	627.84
24	[M + 3Na]$^{3+}$	1325.42	3	3976.25	481.14	645.27
25	[M + 3Na]$^{3+}$	1379.43	3	4138.30	515.93	656.41
26	[M + 3Na]$^{3+}$	1433.45	3	4300.35	532.71	671.04
27	[M + 3Na]$^{3+}$	1487.47	3	4462.41	522.66	684.14
28	[M + 3Na]$^{3+}$	1541.49	3	4624.46	561.33	698.65
29	[M + 3Na]$^{3+}$	1595.50	3	4786.51	578.28	713.90
30	[M + 3Na]$^{3+}$	1649.52	3	4948.56	577.61	726.64
31	[M + 3Na]$^{3+}$	1703.54	3	5110.62	604.79	744.03
32	[M + 3Na]$^{3+}$	1757.56	3	5272.67	620.58	756.32
33	[M + 3Na]$^{3+}$	1811.57	3	5434.72	624.77	769.73

Glc$_n$	type	m/z	z	MW (Da)	CCS$_{He}$ (Å^2)	CCS$_{N2}$ (Å^2)
34	[M + 3Na]$^{3+}$	1865.59	3	5596.78	642.19	784.57
35	[M + 3Na]$^{3+}$	1919.61	3	5758.83	656.69	797.75

Table 7.6: Absolute ^{DT}CCSs of dextran and their fragments in positive-ion mode.

Glc$_n$	type	m/z	z	MW (Da)	CCS$_{He}$ (Å^2)	CCS$_{N2}$ (Å^2)
2	[M - H]$^-$	341.11	1	341.11	106.58	174.56
3	A fragment	397.14	1	397.14	137.09	195.68
2	[M + H$_2$PO$_4$]$^-$	439.09	1	439.09	119.60	182.60
3	A fragment	443.14	1	443.14	125.70	190.81
3	[M - H]$^-$	503.16	1	503.16	136.62	202.34
4	[M - H -120]$^-$	545.17	1	545.17	147.32	213.88
3	[M + H$_2$PO$_4$]$^-$	601.14	1	601.14	146.39	212.15
4	[M - H]$^-$	665.21	1	665.21	164.51	233.96
5	[M - H - 120]$^-$	707.23	1	707.23	170.58	244.00
4	[M + H$_2$PO$_4$]$^-$	763.19	1	763.19	171.45	243.76
5	X fragment	767.25	1	767.25	178.58	252.46
5	[M - H]$^-$	827.27	1	827.27	189.91	265.39
6	[M- H - 120]$^-$	869.28	1	869.28	204.11	281.44
6	X frag	899.29	1	899.29	211.35	289.03
5	[M + H$_2$PO$_4$]$^-$	925.24	1	925.24	193.84	271.22
6	[M - H]$^-$	989.32	1	989.32	215.93	296.73
7	[M - H - 120]$^-$	1031.33	1	1031.33	226.84	309.46
7	X fragment	1061.34	1	1061.34	231.28	312.67
6	[M + H$_2$PO$_4$]$^-$	1087.30	1	1087.30	222.35	304.83
7	[M - H]$^-$	1151.37	1	1151.37	235.89	319.21
8	[M - H - 120]$^-$	1193.38	1	1193.38	247.64	332.20
7	[M + H$_2$PO$_4$]$^-$	1249.35	1	1249.35	243.70	327.88
8	[M - H]$^-$	1313.43	1	1313.43	259.58	343.55
9	[M - H - 120]$^-$	1355.44	1	1355.44	274.13	358.79
8	[M + H$_2$PO$_4$]$^-$	1411.40	1	1411.40	261.97	347.78
9	[M - H]$^-$	1475.48	1	1475.48	279.12	365.21
10	[M - H - 120]$^-$	1517.49	1	1517.49	290.90	376.32
9	[M + H$_2$PO$_4$]$^-$	1573.46	1	1573.46	279.64	365.91
11	[M - H - 120]$^-$	1679.54	1	1679.54	309.79	396.71
10	[M + H$_2$PO$_4$]$^-$	1735.51	1	1735.51	298.81	386.51
12	[M - H - 120]$^-$	1841.59	1	1841.59	326.33	413.87
11	[M + H$_2$PO$_4$]$^-$	1897.56	1	1897.56	321.07	408.68
13	[M - H - 120]$^-$	2003.65	1	2003.65	341.21	429.91
8	[M - 2H - 120]$^{2-}$	596.19	2	1192.38	239.17	339.10
9	[M - 2H - 120]$^{2-}$	677.21	2	1354.43	256.63	356.90
10	[M - 2H - 120]$^{2-}$	758.24	2	1516.48	275.06	376.42
9	[M - H + H$_2$PO$_4$]$^{2-}$	786.22	2	1572.45	274.63	374.48

Glc$_n$	type	m/z	z	MW (Da)	CCS$_{He}$ (Å^2)	CCS$_{N2}$ (Å^2)
9	[M + 2H$_2$PO$_4$]$^{2-}$	835.21	2	1670.43	281.74	382.60
11	[M - 2H - 120]$^{2-}$	839.27	2	1678.53	293.70	400.25
10	[M - H + H$_2$PO$_4$]$^{2-}$	867.25	2	1734.50	293.51	392.04
10	[M + 2H$_2$PO$_4$]$^{2-}$	916.24	2	1832.48	298.49	402.89
12	[M - 2H - 120]$^{2-}$	920.29	2	1840.59	310.36	413.37
11	[M - H + H$_2$PO$_4$]$^{2-}$	948.28	2	1896.55	313.01	414.35
11	[M + 2H$_2$PO$_4$]$^{2-}$	997.27	2	1994.53	314.91	417.06
13	[M - 2H - 120]$^{2-}$	1001.32	2	2002.64	333.94	438.76
12	[M - H + H$_2$PO$_4$]$^{2-}$	1029.30	2	2058.61	327.87	430.31
12	[M + 2 H$_2$PO$_4$]$^{2-}$	1078.29	2	2156.58	328.42	441.59
14	[M - 2H - 120]$^{2-}$	1082.35	2	2164.69	350.01	456.27
13	[M - H + H$_2$PO$_4$]$^{2-}$	1110.33	2	2220.66	346.73	450.98
13	[M + 2 H$_2$PO$_4$]$^{2-}$	1159.32	2	2318.64	342.57	448.72
15	[M - 2H -120]$^{2-}$	1163.37	2	2326.75	366.44	471.79
14	[M - H + H$_2$PO$_4$]$^{2-}$	1191.36	2	2382.71	362.70	468.91
15	[M + 2H$_2$PO$_4$]$^{2-}$	1240.34	2	2480.69	380.76	490.38
16	[M - 2H - 120]$^{2-}$	1244.40	2	2488.80	379.81	490.31
15	[M - H + H$_2$PO$_4$]$^{2-}$	1272.38	2	2544.76	381.53	490.71
17	[M - 2H - 120]$^{2-}$	1325.43	2	2650.85	395.43	507.21
16	[M - H + H$_2$PO$_4$]$^{2-}$	1353.41	2	2706.82	398.04	510.82
18	[M - 2H -120]$^{2-}$	1406.45	2	2812.90	407.48	525.98
17	[M - H + H$_2$PO$_4$]$^{2-}$	1434.44	2	2868.87	416.93	531.21
19	[M - 2H - 120]$^{2-}$	1487.48	2	2974.96	424.42	542.86
18	[M - H + H$_2$PO$_4$]$^{2-}$	1515.46	2	3030.92	432.67	550.34
19	[M - H + H$_2$PO$_4$]$^{2-}$	1596.49	2	3192.98	445.72	566.96
20	[M - H + H$_2$PO$_4$]$^{2-}$	1677.51	2	3355.03	460.39	584.25
21	[M - H + H$_2$PO$_4$]$^{2-}$	1758.54	2	3517.08	476.85	600.90
22	[M - H + H$_2$PO$_4$]$^{2-}$	1839.57	2	3679.13	490.08	615.75
23	[M - H + H$_2$PO$_4$]$^{2-}$	1920.59	2	3841.19	504.20	630.23
24	[M - H + H$_2$PO$_4$]$^{2-}$	2001.62	2	4003.24	518.80	645.02
25	[M - H + H$_2$PO$_4$]$^{2-}$	2082.65	2	4165.29	531.55	659.35

Curriculum Vitae

For reasons of data protection, the curriculum vitae is not included in the online version.

List of Publications

1. W. Hoffmann, <u>J. Hofmann</u>, K. Pagel, Energy-resolved ion mobility-mass spectrometry–A concept to improve the separation of isomeric carbohydrates, *J. Am. Soc. Mass Spectrom.* **2014**, *25*, 471-479.

2. <u>J. Hofmann</u>, W. B. Struwe, C. A. Scarff, J. H. Scrivens, D. J. Harvey, K. Pagel, Estimating collision cross sections of negatively charged N-glycans using traveling wave ion mobility-mass spectrometry, *Anal. Chem.* **2014**, *86*, 10789-10795.

3. <u>J. Hofmann</u>[‡], H. S. Hahm[‡], P. H. Seeberger, K. Pagel, Identification of carbohydrate anomers using ion mobility-mass spectrometry, *Nature* **2015**, *526*, 241-244.

4. W. B. Struwe, C. Baldauf, <u>J. Hofmann</u>, P. M. Rudd, K. Pagel, Ion mobility separation of deprotonated oligosaccharide isomers–Evidence for gas-phase charge migration, *Chem. Commun.* **2016**, *52*, 12353-12356.

5. H. Hinneburg[‡], <u>J. Hofmann</u>[‡], W. B. Struwe, A. Thader, F. Altmann, D. Varón Silva, P. H. Seeberger, K. Pagel, D. Kolarich, Distinguishing *N*-acetylneuraminic acid linkage isomers on glycopeptides by ion mobility-mass spectrometry, *Chem. Commun.* **2016**, *52*, 4381-4384.

6. <u>J. Hofmann</u>, A. Stuckmann, D. J. Harvey, K. Pagel, W. B. Struwe, Identification of Lewis and blood group carbohydrate epitopes by ion mobility-tandem-mass spectrometry fingerprinting, *Anal. Chem.* **2017**, *89*, 2318-2325.

7. H. S. Hahm, M. Schlegel, M. Hurevich, S. Eller, F. Schuhmacher, <u>J. Hofmann</u>, K. Pagel, P. H. Seeberger, Automated glycan assembly using the Glyconeer 2.1 synthesizer, *Proc. Natl. Acad. Sci. U.S.A.* **2017**, *114*, E3385-E3389.

8. <u>J. Hofmann</u> and K. Pagel, Glycan analysis by ion mobility-mass spectrometry, *Angew. Chem. Int. Ed.* **2017**, *56*, 8342-8349.

[‡]The authors contributed equally to this work.

Eidesstattliche Erklärung

Hiermit erkläre ich an Eides statt, dass ich die vorliegende Dissertation selbstständig verfasst und keine als die angegebenen Hilfsmittel genutzt habe. Alle wörtlich oder inhaltlich übernommenen Stellen habe ich als solche gekennzeichnet.

Ich versichere außerdem, dass ich die vorliegende Dissertation nur in diesem und keinem anderen Promotionsverfahren eingereicht habe und dass diesem Promotionsverfahren keine endgültig gescheiterten Promotionsverfahren vorausgegangen sind.

Berlin, Juni 2017

_____

Johanna Hofmann